SCUOLA DI DOTTORATO
UNIVERSITÀ DEGLI STUDI DI MILANO-BICOCCA

Dipartimento di / Department of

BIOTECNOLOGIE E BIOSCIENZE

Dottorato di Ricerca/ PhD program in SCIENZE CHIMICHE, GEOLOGICHE E AMBIENTALI... Ciclo / Cycle **XXXI**...

Curriculum in ..Scienze chimiche - 94R – 2..

Glycofunctionalization of Liposomes via Chemoselective Linkers and in-vitro/in-vivo Applications

Cognome / Surname Edwards Nome / Name Rana

Matricola / Registration number 811127

Tutore / Tutor: Francesco Nicotra

Cotutore / Co-tutor: Laura Russo

Coordinatore / Coordinator: Maria Luce Frezzotti

ANNO ACCADEMICO / ACADEMIC YEAR 2018/2019

Index

Preface

The research work presented in this manuscript has been a European Commission project funded by the MARIE SKŁODOWSKA-CURIE ACTIONS **(ITN) Call: H2020-MSCA-ITN-2014** "**NABBA**" under the supervision of NABBA coordinator Prof. Francesco Nicotra and the co-supervision of Dr. Laura Russo.

Chapter 1 describes the strategy of the functionalization of variable mono-/polysaccharides to liposomes based on the development of two short linkers compatible for chemoselective ligation, in addition to characterization and quantification methods. This work has been conducted at the novel cutting-edge research facility U28, Monza in collaboration with Prof. Masserini, Prof. Francesca Re, and Dott. Beatrice Formicola.

Chapter 2 describes an in-vitro cell-uptake (Operetta) and cytotoxicity (MTT) test using Macrophages RAW264.7. This work has been conducted in collaboration with Prof. Masserini, Prof. Francesca Re, Dott. Beatrice Formicola, and Dott. Roberta Dal Magro.

Chapter 3 describes a study conducted at Nerviano Medical Sciences which consisted of three parts: 1) In-vitro HepG2 cell uptake of glycoliposomes, 2) In-vitro MRI analysis of Gd encapsulated liposomes, 3) In-vivo analysis of the Biodistribution of Gd-encapsulated glycoliposomes. This study was conducted in collaboration with Dr. Anna Degrassi.

Riassunto

The role of carbohydrates in cellular communication and biological targeting has been a major topic of study in recent years. Different pathologies, including cancer, tend to overexpress lectin receptors that bind specifically to selected sugar moieties.

Based on this fact, simple and complex glycans have become interesting candidates for specific cellular targeting. This study aimed to find a procedure providing an easy and efficient way to functionalize nanoparticles with simple and complex glycans, exploiting commercial deprotected sugars. In order to do so we developed 6-Carbon linkers displaying an aminooxy- group, or a phenylhydrazine- group, able to spontaneously and chemoselectively attach a reducing sugar. The other end of each linker contains a thiol group that can attach to PEGylated liposomes via maleimide-thiol coupling. The design of the linkers can therefore be considered a straightforward method for the decoration of nanoparticles with an array of simple and complex glycans *Results:* liposomes functionalized with two different linkers, aminooxy- or phenylhydrazine, were each distinctively coupled with multiple simple sugars including glucose, mannose, and galactose as well as a complex sugar *Sialyl Lewis X* and they were fully characterized. Traditional methods of detection and quantification of carbohydrates expressed on the outer surface of the liposome have been modified and optimized to generate new protocols of nanosight based agglutination assay using corresponding lectins, and direct/indirect detection/quantification methods specific to glycoliposomes using the Phenol-Sulfuric assay. Additionally, the relevance of

glycofunctionalization strategies on Nanoparticle-Cell communication and interaction was verified via 1) functionalization of liposomes with glucose or mannose and the testing of cytotoxicity/selectivity of uptake using macrophages, 2) the functionalization of liposomes with galactose or Sialyl Lewis X to target receptors overexpressed in hepatocellular carcinoma for in-vitro/in-vivo studies. Briefly, Macrophages express C-type lectins CD206 (Cluster of differentiation 206) that are specific for mannose. In the first study, glucose functionalized liposomes were directly compared to mannose functionalized liposomes to test for targeting properties via cell-uptake using RAW 264.7 (murine macrophage cell line). Meanwhile, in the second study, Asialoglycoprotein receptor (ASGPR), a hepatic lectin specific for galactose, and selectin, a sialic acid specific receptor overexpressed in proinflammatory tissues, have been used for targeted delivery of MRI compatible liposomes encapsulated with Gadolinium (MRI contrast agent) and Sorafenib (a first line defense drug of hepatocellular carcinoma). In-vitro uptake studies were performed using HepG2, and the cells were further inoculated into nude mice to monitor biodistribution and efficacy via MRI.

Conclusion: This study presents new methods for the glyco-functionalization of liposomes along with novel characterization techniques specific for carbohydrates, thus creating a complete glyco-model with great potential in translational applications and drug delivery displayed by the in-vitro/in-vivo studies conducted.

Introduction

Biological barriers and site-targeting present some of today's biggest challenges in drug delivery. This was the topic of NABBA [**H2020-MSCA-ITN-2014]** that stands for the Design and Development of advanced **NA**nomedicines to overcome **B**iological **BA**rriers and to treat severe diseases. The Marie SKŁODOWSKA-Curie funded project proposed various solutions through a network of European laboratories that focused collaboratively on discovering innovative nanomedicine-based solutions for the specific targeting and/or crossing of biological barriers. Recent studies have revealed dramatic overexpressions of glycan genes, carbohydrate binding proteins, and carbohydrate-mediated interactions in pathological tissues such as tumor microenvironments.

Based on such findings, our research group focused its efforts on the synthesis of non-toxic biodegradable nanoparticles functionalized with glycol-scaffolds for the purpose of designing diagnostic and therapeutic tools. Within the scope of "NABBA", this research project was focused on the (i) design and chemical synthesis of different types of nanocarriers, (ii) development of corresponding techniques of detection and characterization, (iii) strategies of loading , targeting, and delivery of drugs and/or diagnostic probes, (iv) in vitro and in vivo experiments including biodistribution and pharmacodynamics. In this case, carbohydrates were used in the glycofunctionalization of nanoparticles for the specefic targeting of lectins overexpressed in various pathologies. First, a general introduction of carbohydrate binding lectins, various types of nanoparticles, glyco-functionalization methods, characterization methods, and up to date translational applications will be presented.

Carbohydrate-binding lectins

Lectins are genereally grouped within the larger group of GBPs (glycan-binding proteins) and they represent proteins that selectively interact with specific sugar structures. They were first recognized in the 1950s by William C. Boyd, an American immunochemist, in an attempt to distinguish a group proteins that was not produced in response to antigens like antibodies [1]. In terms of interactions with glycomaterials, three types of lectins are most investigated and known for their glycan specificity, cell-specific presentation, and pivotal role in cancer and the immune system.

i. Galectins

Galectins are small soluble proteins with β-galactoside binding sites consisting of 130 amino acids known as carbohydrate recognition domains (CRDs)[2]. They show great affinity for galactose residues even when attached to other organic entities such as lactose [(β-D-Galactosido)-D-glucose], N-acetyl-lactosamine, poly-N-acetyllactosamine, galactomannans, fragments of pectins, etc [3]. Different types of Galectin receptors identified by serial numbers (1-15) and sub letters are distributed in various human tissues. For example, Galectin-8 is widely spread in the liver, kidney, cardiac muscle, lung

[2] Johannes, L., Jacob, R., & Leffler, H. (2018). Galectins at a glance. *Journal of Cell Science*, *131*(9).

[3] Klyosov AA. Galectins as New Therapeutic Targets for Galactose-Containing Polysaccharides. Bull. Georg. Natl. Acad. Sci. 2014;8(1).

and brain[4], while Galectin-3 is prominent in macrophages and epithelial cells [5]. Although galectins research has come a long way, the quantitative aspect of galectin distribution per tissue (density and number of galectin epitopes on cell surface) and the correlation between abundance of galectin receptors and health/diseases is still under investigation with strong evidence indicating a direct rapport between their expression and pathological diseases such as inflammation, fibrosis, and cancer [6]. For the aforementioned reason, significant attention has been placed into the development of galectin-based therapies for the targeted treatment of galectin-related diseases.

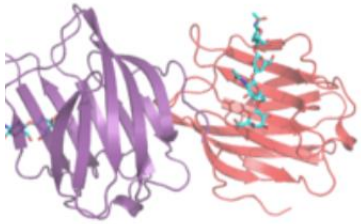

Figure 1. *Structure of human Galectin-3 and Binding site of Carbohydrate*

[4] Froehlich, R., et al. "Galectin fingerprinting detects differences in expression profiles between bovine endometrium and placentomes as well as early and late gestational stages." *Placenta* 33.3 (2012): 195-201.
[5] Elola, M. T., Chiesa, M. E., Alberti, A. F., Mordoh, J., & Fink, N. E. (2005). Galectin-1 receptors in different cell types. *Journal of biomedical science*, *12*(1), 13-29.
[6] Klyosov and Traber; Galectins and Disease Implications for Targeted Therapeutics ACS Symposium Series; American Chemical Society: Washington, DC, 2012.

ii. C-type lectins

This family of lectins, similar to Galectins, contain carbohydrate binding domains (CRDs) that bind to carbohydrate entities in an active calcium dependent manner[7]. They are produced as transmembrane proteins or secreted as soluble proteins[8]. Some examples of the most abundant C-type lectins are: selectins, mannose receptors (MMR family), and the dendritic cell-specific ICAM-3 grabbing non-integrin (DC-SIGN). C-type lectins are overexpressed in macrophages for the recognition and elimination of microbes identified by antigenic fragments[9].

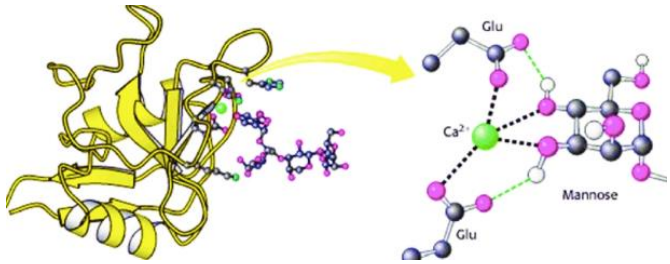

Figure 2 *Structure of an animal C-Type Lectin with a Carbohydrate Binding Domain specific for Mannose*

[7] Cambi, Alessandra, Marjolein Koopman, and Carl G. Figdor. "How C-type lectins detect pathogens." *Cellular microbiology*7.4 (2005): 481-488.
[8] Ley, K., & Kansas, G. S. Selectins in T-cell recruitment to non-lymphoid tissues and sites of inflammation. *Nature Reviews Immunology*, 2004, *4*(5), 325.
[9] Figdor, C. G., van Kooyk, Y., & Adema, G. J. C-type lectin receptors on dendritic cells and Langerhans cells. *Nature Reviews Immunology*, 2002, *2*(2), 77.

iii. Siglecs

Siglecs represent a family of immunoglobulin-like lectins specific for sialic acids. They are thought to be involved in the innate and adaptive immune systems via glycan recognition and in cell-cell communication. The signaling pathways of Siglecs have been an extensive topic of research in attempts to unfold their potential role in triggered endocytosis and pathogen recognition[10]. Accordingly, targeting siglecs with sialic acids has been another strategy used in nanomedicine glycol-targeting of lectins in immune-cell-mediated diseases[11,12].

[10] CROCKER, Paul R.; PAULSON, James C.; VARKI, Ajit. Siglecs and their roles in the immune system. *Nature Reviews Immunology*, 2007, 7.4: 255.
[11] O'REILLY, Mary K.; PAULSON, James C. Siglecs as targets for therapy in immune-cell-mediated disease. *Trends in pharmacological sciences*, 2009, 30.5: 240-248.
[12] JANDUS, Camilla; SIMON, Hans-Uwe; VON GUNTEN, Stephan. Targeting siglecs—a novel pharmacological strategy for immuno-and glycotherapy. *Biochemical pharmacology*, 2011, 82.4: 323-332.

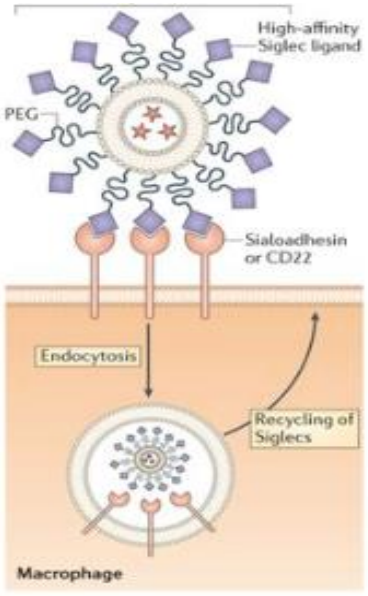

Figure 3: *Display of the mechanism of Siglec mediated Endocytosis*

Nanoparticles and Glyconanoparticles

Nanoparticles are engineered tools with significant applications in disease diagnostics and therapeutics[13]. They are assembled from different building blocks (polymers, lipids, metals, etc) and can be modified in a way to encapsulate hydrophobic drugs or display selected entities on their outer surface for specific targeting. Nanoparticles offer enormous potential specifically in the sector of *pharmaceutical nanotechnology, which* focuses on the optimization of

[13] Couvreur, P.; Nanoparticles in drug delivery: past, present and future. *Adv. Drug Deliv. Rev.*, **2013**, *65*, 21-23.

drug delivery, cell targeting, and efficacy. This field of study is greatly investigated due to the conventional drug delivery profile characterized by poor biodistribution, selectivity, and undesirable side effects. What nanoparticles offer as drug carriers is the potential to design formulations with enhanced bioselectivity, higher solubility, improved bioavailability, a more rapid onset of therapeutic action, and lower cytotoxicity[14]. Another significant application for nanoparticles is the possibility to engineer glycobiomimetics to better investigate carbohydrate-protein interactions involved in a wide array of biological events such as bacterial and viral infections, cancer metastasis, immune response, and cell-signaling pathways. Additionally, the functionalization of nanoparticles with specific carbohydrates has been of great interest in recent years for the active targeting of pathological cells that overexpress carbohydrate-binding proteins (lectins)[15,16]. The study of these interactions with glycofunctionalized nanoparticles is advantageous because they display carbohydrates in a multivalent clustered three-dimensional fashion, which theoretically optimizes the glyco-lectin recognition and targeting[17]. This section will cover different types of glyconanoparticles, functionalization and characterization methods, as well as give an overview of some of the most recent applications in the biomedical field.

---

[14] Bhatia S. Nanoparticles Types, Classification, Characterization, Fabrication Methods and Drug Delivery Applications. In: *Natural Polymer Drug Delivery Systems.* Springer Ed., **2016**, pp. 33-93.

[15] Niemeyer, C. M. Nanoparticles, proteins, and nucleic acids: biotechnology meets materials science. *Angew. Chem. Int. Ed.*, **2001**, *40.22*, 4128-4158.

[16] E. Katz, I. Willner, Integrated nanoparticle-biomolecule hybrid systems: synthesis, properties, and applications, Angew. Chem. Int. Ed. 33 (2004) 6042–6108

[17] Lee, Y. C.; Lee, R. T. Carbohydrate-protein interactions: basis of glycobiology *Acc. Chem. Res.* **1995,** *28*, 321–327.

2.0. Types of Glyconanoparticles

Nanoparticles are defined as a category of particles of a specific size between 1 and 100 nanometers. They vary in chemical and physical properties depending on their building block, structure, shape, and size. This section will give a general overview of three types of glyconanoparticles: liposomes, PLGA/PLA polymer based, and metallic nanoparticles (iron oxide, gold, and silver). The various types share a stable and biocompatible profile, and have been widely used in biomedical applications for targeted drug delivery and non-invasive imaging.

2.1. Liposomes

Liposomes are amphiphilic phospholipids that self-assemble in water forming a closed lipid bilayer vesicle. They are formed by stacking thin lipid films containing mainly phospholipids, followed by film-stack hydration, which causes swelling between the layers, and agitation which results in the self-assembly of the vesicles to shield the hydrocarbon bilayer from interacting with water. The lipid bilayer facilitates fusion with other bilayers such as the cell membrane, thus allowing the delivery of hydrophobic drugs intercalcalated into the bilayer region or hydrophilic drugs encapsulated in the core[18]. The size of the liposomes can be controlled using sonication or extrusion techniques and it can range from 20-100nm for Small Unilamellar Vesicles (SUV).

[18] Marradi M., Chiodo F., Garcia I., Penades S. Glycoliposomes and metallic glyconanoparticles in glycoscience. *Synthesis and Biological Applications of Glycoconjugates*, **2011**, 164-202

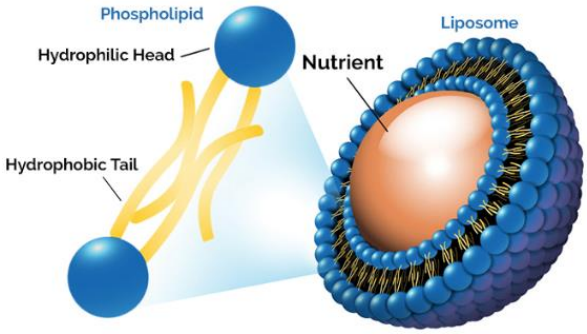

Figure 4 *Structure of the liposome consisting of a lipid bilayer made of cholesterol (hydrophobic tail) and phospholipids constituting the hydrophilic heads*

Liposomes have been widely explored and well-developed, with many FDA approved liposome-based formulations in the market as displayed in table **1**[19].

[19] Bobo D., Robinson K., Islam J., Thurecht K., Corrie, S. Nanoparticle-Based Medicines: A Review of FDA-Approved. Materials and Clinical Trials to Date. *Pharmaceutical research*, **2016 ,** *33*(10), 2373–2387

FDA Approved liposome based Formulations

Name	Material	Year Approved	Indication
Onivyde® (Merrimack)	Liposomal Irinotecan	2015	Pancreatic Cancer
Marqibo® (Onco TCS)	Liposomal Vincristine	2012	Acute-Lymphoblastic Leukemia
AmBisome® (Gilead Sciences)	Liposomal Morphine sulphate	2004	Analgesia (post-operative)
DepoD1ur®(Pacira Pharma)	Liposomal Verteporfin	2000	Macular Degenration; Ocular histoplasmosis
Visudyne® (Bausch&Lomb)			
DepoCyt© (Sigma-Tau)	Liposomal Cytarabine	1996	Lymphomatous Meningitis
DaunoXome® (Galen)	Liposomal Daunorubicin	1996	Karposi's Sarcoma

Table 1 List of FDA Approved liposomal drugs

2.1.1 Glycoliposomes

The incorporation of carbohydrates into liposomes was first achieved in the seventies in Lester's laboratory by mixing suitable proportions of glycolipids (a hydrophobic chain linked to a carbohydrate head) and phospholipids during the lipids film preparation step prior to the assembly of the liposome[20]. One negative aspect of this approach was the difficulty of achieving the full

[20] Hill, M.W.; Lester, R. Mixtures of gangliosides and phosphatidylcholine in aqueous dispersions. Biochim. Biophys. Acta, **1972**, 282, 18-30.

externalization of carbohydrates on the outer surface of the liposome due to the competitive state of encapsulation of sugars into the hydrophilic core. Consequently, another strategy was developed consisting of the functionalization of liposomes post-assembly with glycoconjugates comprising reactive organic functionalities complementary to the functional groups displayed in the outer shell of the liposome. This approach allowed carbohydrates to be exclusively attached to the vesicular surface of the liposome using covalent linking methodologies[21].

Coupling of Carbohydrates to the surface of liposomes

There is a wide range of coupling methods used for the functionalization of liposomes. In this section, the most commonly used types of linkages have been reported.

I. *Thioether linkage* One of the most common types of coupling used in the functionalization of liposomes is the linkage between a thiol function (displayed on a modified carbohydrate) and a maleimide group functionalized to fatty acid anchor chains such as N-(4-(p-Maleimidophenyl) butyryl) phophatidylethanolamine (MPB-PE) or to PEG-Maleimide linkers in the case of PEGylated liposomes [7,22]. This reaction is normally carried out in a phosphate buffer and neutral pH which makes it convenient for biological applications.

[21] Nobs, L.; Buchegger, F.; Gurny, R.; Allémann, E. Current methods for attaching targeting ligands to liposomes and nanoparticles. *J. Pharm. Sci*., **2004**, *93*, 1980-1992.
[22] Derksen JT, Scherphof GL. An improved method for the covalent coupling of proteins to liposomes. *Biochim. Biophys. Acta*, **1985**, *814*, 151–155.

II. *Disulfide linkage* This coupling method is well established and is considered a rapid onset type of reaction. It requires the presence of a thiol function on both the modified carbohydrate and the functionalized phosphatidylethanolamine (PE) such as pyridyldithiopropionate PE-PDP. Although this method was found to be efficient in the coupling process, the stability of this type of linkage suffered under the reductive environment of serum[23]

III. *Amide linkage* The cross linkage occurs between carboxylic acid groups exposed on the surface of the liposome and a primary amine group present on the modified carbohydrate. Carboxylic acid end groups are incorporated into the liposome via anchors' functionalization with PEG-COOH such as distearoyl-N-(3-carboxypropionoyl poly(ethylene glycol) succinyl) phosphatidylethanolamine (DSPE-PEG-COOH). Crosslinking is most efficient at physiological PH in presence of 1-Ethyl-3-(3 in dimethylaminopropyl) carbodiimide (EDC) and NHS. EDC activates the carboxylic acid group by forming an O-acylisourea intermediate stabilized by NHS, which can be easily displaced by the nucleophilic

[23] Martin F.J.; Hubbell, W.L.;, Papahadjopoulos, D. Immunospecific targeting of liposomes to cells: a novel and efficient method for covalent attachment of Fab0 fragments via disulfide bonds. *Biochemistry*, **1981**, 20, 4229–4238.

attack of the primary amine. EDC by-product is then released in the form of soluble urea derivative[24].

IV. *Hydrazone linkage* is a coupling between an aldehyde group of the carbohydrate and a hydrazine group grafted on the surface of the liposome. The carbohydrate can be oxidized using mild oxidizing agents such as sodium (meta)periodate to produce the aldehyde group[25]. In the liposome, the use of a lipid bilayer containing a hydrazide-hydrophobic anchor such as lauric acid hydrazide or a functionalized DSPE-PEG-hydrazine chain allows for the formation of a hydrazone linkage with the carbohydrate's aldehyde group.[26].

V. *Click Chemistry* is a fast regiospecific reaction that has been widely used in the synthesis of novel polymeric delivery systems, dendrimers, and in the cross-linking of micelles and modifications of nanomaterial surfaces. One of the most used types of click chemistry is Cu^{I}-catalyzed Huisgen 1,3-dipolar cycloaddition that occurs between azides present on the outer surface of nanomaterials (or grafted PEG chains) and terminal alkyne group of a modified carbohydrate, forming a 1,2,3-triazoles linkage. The limitation this functionalization method is that it requires the use of

[24] Ishida, O.; Maruyama, K.; Tanahashi, H.; Iwatsuru, M.; Sasaki. K.; Eriguchi, M.; Yanagie, H.. Liposomes bearing polyethyleneglycol-coupled transferrin with intracellular targeting property to the solid tumors in vivo. *Pharm. Res.*, **2001**, *18*, 1042–1048.
[25] Chua, M.M.; Fan, S.T.; Karush, F. Attachment of immunoglobulin to liposomal membrane via protein carbohydrate. *Biochim. Biophys. Acta*, **1984**, *800*, 291–300.
[26] Zalipsky, S.. Synthesis of an end-group functionalized polyethylene glycol-lipid conjugate for preparation of polymer-grafted liposomes. *Bioconjug. Chem.*, **1993**, *4*, 296–299.

copper catalyst, which is unfavored in high quantity in terms of biocompatibility[27]

Chemical coupling of Carbohydrates to Liposome Surface

Method	Carbohydrate	Liposome	Covalent Coupling
Maleimide-Thiol	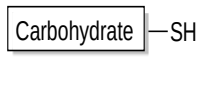	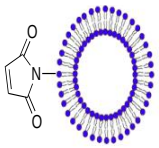	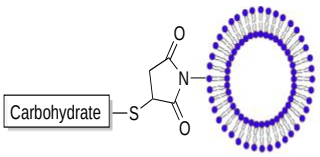
Disulfide	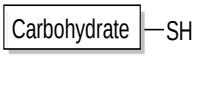	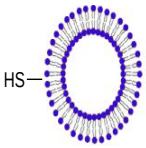	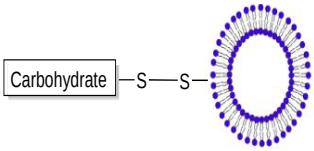
Amide	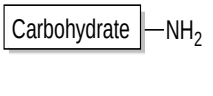	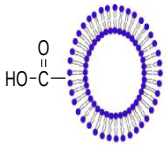	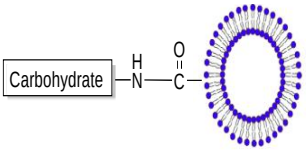
Hydrazone	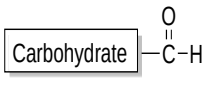	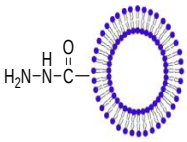	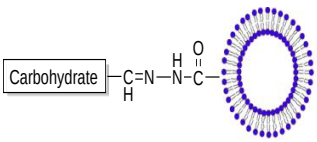
Click Chemistry		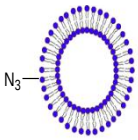	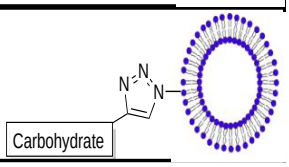

Table 2. Covalent Coupling methods used to attach carbohydrates to Liposomes, polymeric, and metallic Nanoparticles.

[27] Hein, C.D.; Liu, X.M. & Wang, D. Click Chemistry, A Powerful Tool for Pharmaceutical Sciences. *Pharm. Res*., **2008**, *25*, 2216-2230.

Translational applications of glycoliposomes

Glycoliposomes have been widely used in targeted drug delivery especially in tumor cells. In a recent study conducted by L. Mo et al, hyaluronic acid HA (a nonsulfated glycosaminoglycan) was functionalized to PEGylated (PEG) liposomes to target the overexpressed CD44 receptors in breast cancer cells.[28] Sorafenib, a Kinase inhibitor drug that regulates tumor cell growth and angiogenesis, was encapsulated within the liposome to obtain a dual targeted chemotherapeutic effect. It was reported that the liposome functionalized with PEG-HA displayed a higher cellular uptake in MDA-MB-231 cells overexpressing CD44 receptors, a reduction in tumor size in tumor-bearing mice, an improvement in systemic exposure by 3 folds, as well as an increase in half-life by 2 folds. These recent findings shed light on the potential of glycoliposomes to become a competitive platform for targeted drug delivery.

Glycoliposomes have also been used as diagnostic tools by Tian et al., who developed mannose-coated liposomes encapsulated with gadolinium to discriminate between mild and severe acute pancreatitis (AP) by targeting the mannose specific c-lectin receptors overexpressed on macrophages in the tumor microenvironment[29]. Gadolinium-diethylenetriaminepentaacetic (Gd-DTPA) is an FDA approved MRI contrast agent used for the diagnosis of medical conditions. The results showed 85% encapsulation efficiency of Gd-DTPA

[28] Mo, L., Song, J. G., Lee, H., Zhao, M., Kim, H. Y., Lee, Y. J., ... & Han, H. K. PEGylated hyaluronic acid-coated liposome for enhanced in vivo efficacy of sorafenib via active tumor cell targeting and prolonged systemic exposure. *Nanomedicine*, **2018**, *14*, 557–567.

[29] Tian, B., Liu, R., Chen, S., Chen, L., Liu, F., Jia, G. Mannose-coated gadolinium liposomes for improved magnetic resonance imaging in acute pancreatitis. *Int. J. Nanomedicine*, **2017**, *12*, 1127-1141.

within the liposome, and a notable increase in cellular uptake of the mannosylated liposomes in vitro (macrophage cell line) and in vivo (severe acute pancreatitis model). Additionally, glycoliposomes displayed a significantly higher T_1 magnetic resonance imaging signal in severe AP versus mild AP, which indicates that the dual diagnostic/targeting liposomes can be potential tools in the early detection of many macrophage-associated diseases, such as myocardial inflammation, atheroscleosis, and liver tumors[30,31].

Polymeric Nanoparticles

Poly (lactic acid) PLA, poly (glycolic acid) PLGA and their copolymers poly (lactic-co-glycolic acid) have been largely investigated for drug delivery and targeting purposes. Both PLGA and PLA are hydrophobic polymers usually conjugated with PEG for its hydrophilic properties to form amphiphilic building blocks that can be assembled in water into nanoparticle vesicles characterized by a hydrophobic core and a hydrophilic surface. The typology of this carrier allows for the encapsulation of hydrophobic drugs in the core of the nanoparticle at concentrations significantly higher than their intrinsic water solubility. Meanwhile, the hydrophilic outer surface renders the nanoparticle compatible with IV route administration[32]

[30] Moon, H.; Park, H.E.; Kang, J.; Lee, H.; Cheong, C.; Lim, Y.T.; Ihm, S.H.; Seung, K.B.; Jaffer, F.A.; Narula, J.; Chang, K.; Hong, K.S. *Circulation*, **2012**, *125*, 2603-2612.

[31] Dong, Y.; Chen, H.; Chen, C. Polymer-lipid hybrid theranostic nanoparticles co-delivering ultrasmall superparamagnetic iron oxide and paclitaxel for targeted magnetic resonance imaging and therapy in atherosclerotic plaque. *J. Biomed. Nanotechnol,* **2016**, *12*, 1245–1257.

[32] Oerlemans, C., Bult, W., Bos, M., Storm, G., Nijsen, J., Hennink, W. Polymeric micelles in anticancer therapy. Pharm. Res., **2010**, 27, 2569

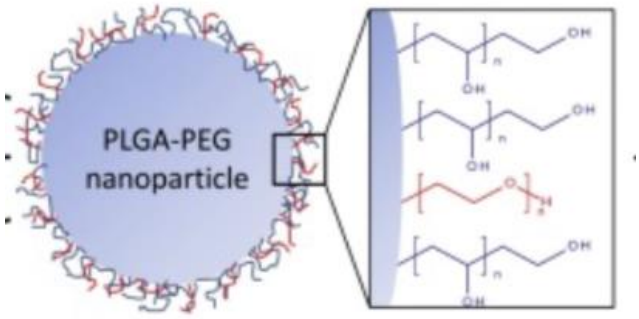

Figure 5: *Structure of the PLGA-PEG nanoparticle consisting of a hydrophobic core (PLGA) and a hydrophilic outer surface (PEG)*

There is a significant amount of polymer formulations that have been approved by the FDA in the last decades as indicated in table **3**.

Polymeric Drug Formulations approved by FDA

Drug	Polymer	Year Approved	Indication
Signifor LAR	PLGA	2014	Acromegaly Treatment
Bydureon	PLGA	2012	Glycemic control Type II diabetes
Ozurdex	PLGA	2009	Macular Edema
Risperdal Consta	PLGA	2003	Schizophrenia and bipolar disorder
Eligard	PLGA	2002	Palliative Treatment-Advanced prostate cancer

Arestin	PLGA	2001	Adult periodontitis
Trelstar	PLGA	2000	Palliative Treatment-Advanced prostate cancer
Atridox	PLA	1998	Chronic Adult periodontitis
Sandostatin LAR	PLGA	1998	Acromegaly Treatment
Lupron	PLGA	1995	Endometriosis
Lupron Depot-PED	PLGA/PLA	1993	Central preocious puberty
Lupron Depot	PLGA/PLA	1989	Palliative Treatment-Advanced prostate cancer
Zoladex	PLGA	1989	Local stage T2b-T4 carcinoma of prostate
Vivitrol	PLGA	1984	Treatment of alcohol dependence

Table 3. FDA Approved polymeric based drug formulation[33]

2.2.i. Methods of Assembly of polymeric nanoparticles

Emulsion-Evaporation

The emulsion – solvent evaporation technique is a useful method for the encapsulation of hydrophobic drugs. It entails the emulsification of an organic

[33] Wang, Y.; Qu, W.; Choi, S. FDA's Regulatory Science Program for Generic PLA/ PLGA-Based Drug Products. *Am. Pharm. Rev.*, **2016,** *19*, 5-9.

solvent containing the dissolved polymers and hydrophobic drug against a surfactant aqueous phase using ultrasonication or miscrofluidization. This leads to the formation of nano-sized organic droplets surrounded by the surfactant aqueous environment. The organic solvent is then evaporated under low pressure and the nanodroplets are left under stirring conditions in the surfactant of choice. Last, the assembled nanoparticles are washed from the surfactant in water using centrifugation techniques [34]. The size and efficiency of encapsulation are variables controlled by the optimization of potency and length of the ultrasound source used, as well as the type and concentration of the surfactant of choice.

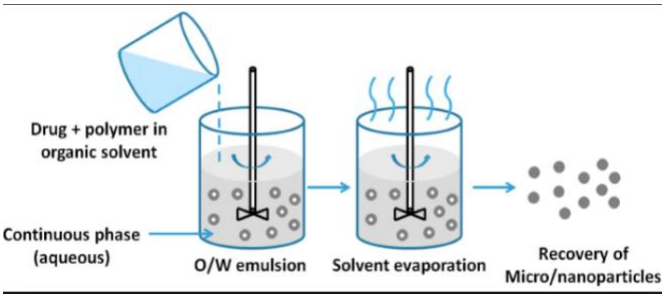

Figure 6 *The Emulsion-Evaporation technique for the assembly of polymeric (PLGA/PLA) nanoparticles*

Nanoprecipitation

The nanoprecipitation technique is based on the selection of two miscible solvents. Ideally, the polymer and the drug selected for encapsulation should dissolve in the first solvent and not in the second. The first solvent containing

[34] Plard, J. P., Bazile, D. Comparison of the safety profiles of PLA50 and Me. PEG-PLA50 nanoparticles after single dose intravenous administration to rat. *Colloid. Surfaces B*, **1999**, *16*, 173-183.

the polymer/drug is added to the second solvent causing a rapid desolvation and the encapsulation of the drug inside the precipitated polymers. The benefit of this technique is the ability to assemble nanoparticles without the use of surfactants. The organic solvents used are eventually removed under low pressure[35].

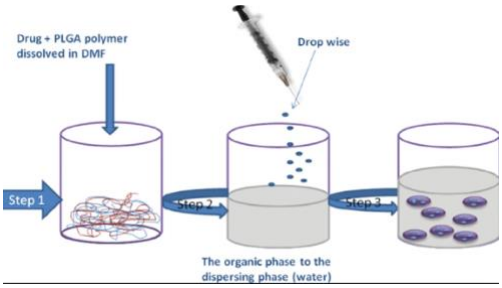

Figure 7: *Nanoprecipitation technique for the assembly of polymeric nanoparticles*

Dialysis

The dialysis technique is based on dissolving polymers/drugs in a water-miscible solvent such as DMF, then placing them into a dialysis tube against distilled water. This method is dictated by the molecular cut-off of the dialysis tube in accordance with the weight of the polymer selected. It is a commonly used technique especially in cases where the avoidance of use of surfactants in the preparation process is favored[36].

[35] Iravani S, Korbekandi H, Mirmohammadi SV, Zolfaghari B. Synthesis of silver nanoparticles: chemical, physical and biological methods. *Res Pharm Sci*. 2014;9(6):385–406.
[36] Nah, J. W., Paek, Y. W., Jeong, Y. I., Kim, D. W., Cho, C. S., Kim, S. H., & Kim, M. Y. Clonazepam release from poly (DL-lactide-co-glycolide) nanoparticles prepared by dialysis method. *Arch. Pharm. Res.*, **1998**, *21*(4), 418-422.

PLGA or PLA based glyconanoparticles

Similarly to liposomes, covalent linkage is mostly used to attach the polymer or polymer-PEG chains containing functional groups complementary to the reactive organic functionalities comprised in the carbohydrate of interest. The functionalization of carbohydrates to the polymer can occur before the assembly of the nanoparticle leading to the externalization of the hydrophilic sugar entities on the outer surface as the nanoparticle is assembled. Alternatively, the assembly of the PLGA/PLA polymers with or without grafted PEG chains can be performed first, followed by the functionalization of carbohydrates directly to the outer surface of the nanoparticle in the aqueous medium.

Applications

Polymeric nanoparticles have been used in multiple FDA approved formulations (*Table 3)* and continue to be used to improve the water solubility of several drugs. Accordingly, Kang et al. encapsulated the anti-cancer agent albendazole (ABZ) in PLGA nanoparticles functionalized with chiostan to enhance mucoadhesiveness and colloidal stability. The in vitro results showed that nanoparticles exhibited lower cytotoxicity and superior mucoadhesion when tested with mucin of the intestinal surface, which can enhance oral

bioavailability[37]. In another study, Dong et al. designed a galactose-decorated biodegradable poloxamer 188-PLGA diblock copolymer nanoparticle encapsulated with resibufogenin (RGB) to target asialoglycoprotein receptors overexpressed in liver cancer. In vitro, the cellular uptake of galactose-NP in HepG2 cell line was superior due to active liver targeting. The ratio of apoptotic cells was increased, and the nanoparticles were found to be non-toxic and biocompatible. In vivo, the therapeutic effects of the nanoparticles were assessed in a hepatocarcinogenic mouse model. The results showed a higher internalization and concentration of RGB in the liver, and a notable improvement in the therapeutic index. On that account, polymeric nanoparticles decorated with carbohydrates can be considered a highly promising platform of drug delivery since they have been FDA approved for multiple drug formulations, and can be functionalized for additive targeting properties[38].

Metallic nanoparticles

Metallic contrast agents including magnetic, gold, and silver nanoparticles started emerging and advancing with the development of diagnostic imaging devices such as MRI, CT, PET, ultrasound, SERS, and optical imaging. These

[37] Kang, B. S., Choi, J. S., Lee, S. E., Lee, J. K., Kim, T. H., Jang, W. S., Park, J. S. Enhancing the in vitro anticancer activity of albendazole incorporated into chitosan-coated PLGA nanoparticles. *Carbohydr. Polym.*, **2017,** *159*, 39-47.

[38] Dong, H., Tian, L., Gao, M., Xu, H., Zhang, C., Lv, L., Ma, X. Promising galactose-decorated biodegradable poloxamer 188-PLGA diblock copolymer nanoparticles of resibufogenin for enhancing liver cancer therapy. *Drug deliv.* **2017**, *24*, 1302-1316.

nanoparticles can be modified with various chemical functional groups, which allow them to be conjugated with antibodies, ligands, drugs of interest, as well as carbohydrates. The functionalization with carbohydrates occurs on the outer surface of the nanoparticle using the same linkage techniques described in table 2. By doing so, the metallic nanoparticles have shown to be a great asset in both diagnostic imaging and targeted delivery, making them frontline candidates in the field of theragnostic.

Types of metallic nanoparticles

I. **Magnetic nanoparticles (Iron NPs)** Iron oxide (Fe_2O_3) is an inorganic paramagnetic compound characterized by its ultrafine size, biocompatibility, and unique magnetic properties which induces a decrease in the T1 and T2 relaxation times of the water protons surrounding a tissue thereby manipulating the signal intensity of the images collected.

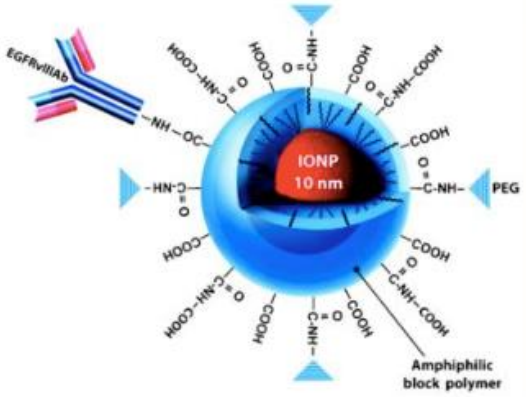

Figure 8: *Structure of the Iron Oxide Nanoparticle*

Multiple superparamagnetic nanoparticles have been approved by the FDA for clinical use as displayed in table 4[39].

FDA Approved Oxide Nanoparticles

Name	Application	Formulation
Feridex	MRI - Focal hepatic lesions	Superparamagtic iron oxide coated with Dextran
Gastromark	MRI- Gastrointestinal lumen imaging	Silicone-coated superparamagnetic iron oxide nanoparticle
Feraheme	MRI; Iron replacement therapy	Nonstoichiometric superparamagnetic iron oxide coated with polyglucose sorbitol carboxymethylether

Table 4. FDA-approved iron oxide nanoparticles[40].

[39] Hildebrandt, N., Hermsdorf, D., Signorell, R., Schmitz, S. A., & Diederichsen, U. Superparamagnetic iron oxide nanoparticles functionalized with peptides by electrostatic interactions. *Arkivoc*, **2007**, 5, 79-90.

[40] Bobo, D., Robinson, K. J., Islam, J., Thurecht, K. J., & Corrie, S. R. Nanoparticle-based medicines: a review of FDA-approved materials and clinical trials to date. *Pharm. Res.*, **2016**, *33*, 2373-2387.

Synthesis of Fe_2O_3 Nanoparticles

Co-precipitation from aqueous solutions is one of the most frequently used methods for the synthesis of magnetic nanoparticles. The reaction consists of the addition of Fe(II) salt in aqueous solution to a base in the presence of a mild oxidant to produce spherical NPs ranging in size between 30-100nm[41].

Applications

Magnetic nanoparticles offer multiple possibilities for biomedical applications. In a study conducted by Moskvin et al., magnetic nanoparticles were synthesized and coated by biocompatible polymers or carbohydrates such as l-ascorbic acid, D-galactose, D-mannose, and sucrose in order to develop novel theranostic tool for colon cancer[42]. It was shown that glycosylated nanoparticle did enhance both biocompatibility and uptake by Caco-2, HT-29, and SW-480 epithelial colorectal adenocarcinoma cell lines. The mechanism of action of the cellular uptake was studied and demonstrated to be dependent on lectin-mediated membrane transport[43]. D-mannose coated particles were further tested and displayed a reduction of colon cancer cell viability by 20%. In addition to

[41] Wu, S., Sun. A., Zhai, F., Wang, J., Xu, W., Zhang, Q., Volinsky, A.A.,. Fe_3O_4magnetic nanoparticles synthesis from tailings by ultrasonic chemical co-precipitation. Mat Lett. **2011**, 65(12), 1882–1884.

[42] Moskvin, M.; Babič, M.; Reis, S.; Cruz, M.M.; Ferreira, L.P.; Carvalho, M.D.; Lima, S.A.C.; Horák, D. Biological evaluation of surface-modified magnetic nanoparticles as a platform for colon cancer cell theranostics. Colloids Surf. B. *Biointerfaces*, **2018**, 161, 35-41.

[43] Horák, D.; Babič, M.; Jendelová, P.; Herynek, V.; Trchová, M.; Likavčanová, K.; Syková, E. Effect of different magnetic nanoparticle coatings on the efficiency of stem cell labeling. *J. Magn. Magn. Mater*., **2009**, *321*(10), 1539-1547.

targeting, the property of magnetic induction was evaluated, and the particles coated with biocompatible polymers were able to enhance heating efficiency, which is a promising result with respect to treatment via magnetic hyperthermia[29]. Another study conducted by Kania et al. used superparamagnetic iron oxide nanoparticles (SPION) coated with cationic or anionic chiostan derivatives to test them in vivo as contrast agents for magnetic reasonance imaging[44]. BALB/c mouse models were used and the nanoparticles uptaken by the liver displayed an enhancement in MRI contrast for up to 7 days. The overall results indicated that SPION coated with ionic chiostan derivatives could serve as T2 contrast agents for organ imaging and specifically in the diagnosis of liver disease.

II. **Gold nanoparticles (AuNPs)**

The modern scientific evaluation of colloidal gold began with Michael Faraday's work in the 1850s, when he observed that the colloidal gold solutions have unique optical properties that differ from the bulk gold[45]. In the presence of an oscillating electromagnetic field of light, it was discovered that the free electrons of the metal oscillate at a particular frequency, then decay radiatively in the form of light scattering or non-radiatively in the form of heat. These unique properties generated a great interest in the use of gold nanoparticles in

[44] Kania, G.; Sternak, M.; Jasztal, A; Chlopicki, S; Błażejczyk, A.; Nasulewicz-Goldeman, A.; Wietrzyk, J.; Jasiński, K.; Skórka, T.; Zapotoczny, S.; Nowakowska, M. Uptake and bioreactivity of charged chitosan-coated superparamagnetic nanoparticles as promising contrast agents for magnetic resonance imaging. *Nanomedicine*, **2018**, *14*, 131-140.

[45] Edwards, P.P., Thomas, J.M. Gold in a metallic divided state--from Faraday to present-day nanoscience. *Angew. Chem. Int. Ed. Engl.*, **2007**, 46(29), 5480-6.

multiple imaging techniques such as dark-field imaging, surface-enhanced Raman spectroscopy, and optical imaging for the diagnosis of various diseases[46].

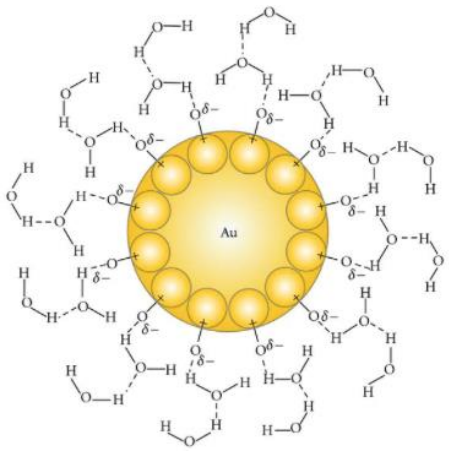

Figure 9: *Structure of the Gold Nanoparticle*

Synthesis of AuNPs

Gold salts ($HAuCl_4$) are reduced by reducing agents such as citrate to produce spherical particles in the range of 10-20nm[47]. Other methods were reported to produce larger nanoparticles reaching 100nm in size by seeding Au^{3+} with hydroxylamine[48].

Applications

[46] El-Sayed, I. H., Huang, X., & El-Sayed, M. A. Surface plasmon resonance scattering and absorption of anti-EGFR antibody conjugated gold nanoparticles in cancer diagnostics: applications in oral cancer. *Nano letters*, **2005**, *5*(5), 829-834.
[47] Frens, G. Controlled nulceation for the regulation of particle size in monodisperse gold suspensions. Na Phys Sci. **1973**, 241, 20–22.
[48] Brown, K.R., Natan, M.J. Hydroxylamine seeding of colloidal Au nanoparticles in solution and on surfaces. Langmuir, 1998, 14(4), 726–728.

Chiodo et al introduced gold glyconanoparticles as a new multifunctional drug-delivery system for highly active antiretroviral therapy (HAART) against HIV. The glucose-coated gold nanoparticles were functionalized via thiol-thiol linkage with modified derivatives of nucleoside reverse transcriptase inhibitors abacavir and lamivudine (figure).

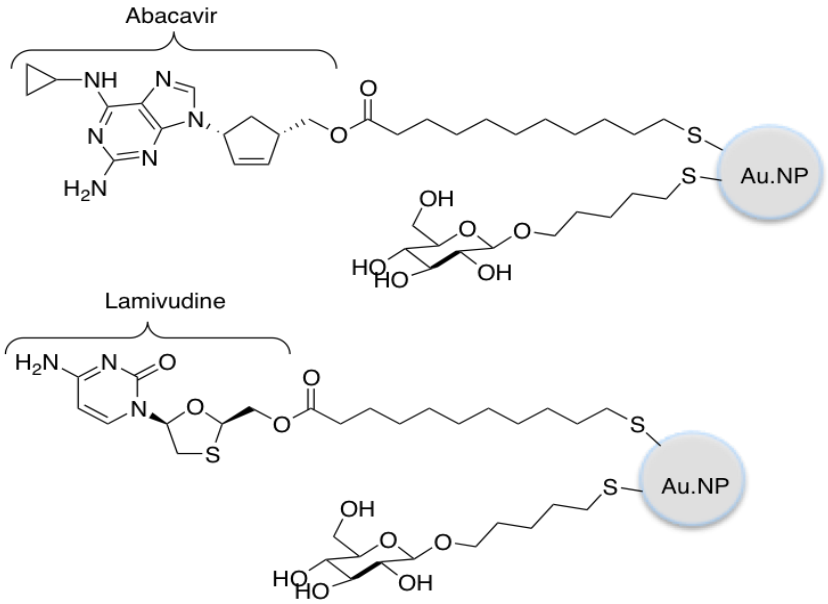

Figure 10: Glyconanoparticles bearing anti-HIV pro-drugs lamivudine and abacavir.

Glucose was selected to coat the nanomaterial to enhance the biocompatibility of the carrier and optimize cellular uptake[49]. Antiviral activity was then tested by evaluating the replication of HIV-1 virus (NL4-3 strain) in TZM-bl infected cells (derived HeLa-cell immortalized cell line). The results showed that under

[49] Murray, R. A., Qiu, Y., Chiodo, F., Marradi, M., Penadés, S., & Moya, S. E. A Quantitative Study of the Intracellular Dynamics of Fluorescently Labelled Glyco-Gold Nanoparticles via Fluorescence Correlation Spectroscopy. *Small*, **2014**, *10*, 2602-2610.

acidic conditions, the drugs were cleaved from the gold nanoparticle and were able to inhibit viral replication in cellular assays with IC50 values similar to the free drugs[50]. These findings highlight the biocompatibility and multiple drug loading properties of the nanoparticle that can be highly beneficial in the design of HAART treatments against HIV. Another study conducted by Calavia et al. reported that the functionalization of phthalocyanine Gold nanoparticles with lactose led to the production of water-dispersible nanoparticles capable of generating singlet oxygens and cause cell death upon irradiation in photodynamic therapy[51]. The decoration of the nanoparticle with lactose served as a stabilizing agent in the aqueous solution and for the targeting of carbohydrate-binding receptors overexpressed in breast cancer cells. The in vitro photodynamic therapy showed a promising 97% cell-death in SK-BR-3 cell line targeted by lactose-C3Pc-AuNPs versus 75% cell-death with non-targeted C3Pc sPEG-AuNPs. This report therefore presents a competitive candidate for the development of targeted photodynamic therapy devices.

III. Silver nanoparticles

The unique physiochemical properties of silver nanoparticles including surface plasmon reasonance and large effective scattering per cross-section

[50] Chiodo, F.; Marradi, M.; Calvo, J.; Yuste, E.; Penadés, S. Glycosystems in nanotechnology: Gold glyconanoparticles as carrier for anti-HIV prodrugs. *Beilstein J. Org. Chem.* **2014,** *10,* 1339–1346.

[51] Calavia, P. G., Chambrier, I., Cook, M. J., Haines, A. H., Field, R. A., & Russell, D. A. Targeted photodynamic therapy of breast cancer cells using lactose-phthalocyanine functionalized gold nanoparticles. *J. Colloid Interface Sci.*, **2018**, *512*, 249-259.

made them ideal candidates for surface- enhanced Raman scattering imaging as well as molecular labeling[52].

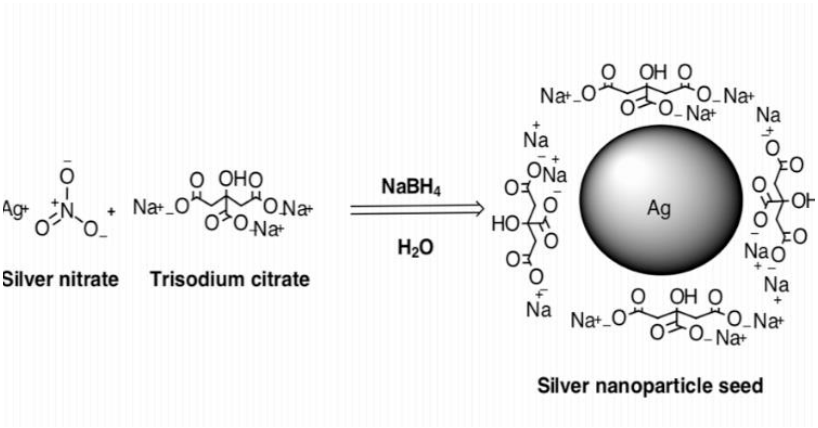

Figure 11: *Assembly of Silver Nanoparticle*

Synthesis of silver NPs

Silver salt is reduced in the presence of a colloidal stabilizer such as polyvinyl alcohol or bovine serum albumin. Other methods use β-d-glucose as a reducing sugar and starch as a stabilizer[53].

Applications

The antibacterial activity of silver has long been known and widely used in the prophylactic treatment of burns and water disinfection[54]. This unique

[52] Schultz, S., Smith, D. R., Mock, J. J., & Schultz, D. A. Single-target molecule detection with nonbleaching multicolor optical immunolabels. *Proceedings of the National Academy of Sciences*, **2000**, *97*(3), 996-1001.
[53] Stepanov, A.L., Popok, V.N., Hole, D.E. Formation of Metallic Nanoparticles in Silicate Glass through Ion Implantation. Glass. Phy. Chem., **2002**, 28, 90–5.

[54]Clement, J. L., & Jarrett, P. S. Antibacterial silver. Metal-based drugs, **1994**, 1, 467-482.

application was further investigated with the additional properties that a silver nanoparticle system offers.

In a recent study, Chen et al. designed a Konjac glucomannan/silver nanoparticle composite sponge with antibacterial properties for wound dressing and healing. Konjac glucomannan (KGM) is a hemicellulosic plant cell-wall polysaccharide containing glucose and mannose. It was used in the functionalization of silver nanoparticles to attract and retain water molecules via hydrogen bonding and to enhance biocompatibility, thus improving the overall wound healing properties of the novel biomaterial[55]. Silver nanoparticles were prepared using green deoxidizer egg whites, followed by the addition of Konjac glucomannan powder, vigorous stirring, and freeze-drying. The antimicrobial effect of different compositions of the final product (KGM/Ag) was tested in vitro using *E. coli* and *S. aureus,* and inhibition zones were displayed in the assay, indicating an active antibacterial profile. In-vivo experiments also showed that the wound dressings shortened the healing time of the infected-wound animal groups, which demonstrate the potential application of the new polyglycosilver composite sponges in wound treatment[56].

Characterization methods of glyconanoparticles

The size and morphology of a nanoparticle can significantly impact its behavior in vivo in terms of circulation time and biodistribution. There are well-established methods designed for the study of glyconanoparticles such

[55] Zhang, C., & Yang, F. Q. Konjac glucomannan, a promising polysaccharide for OCDDS. *Carbohydr. Polym.*, **2014**, *104*, 175-181.

[56] Chen, H.; Lan, G.; Ran, L.; Xiao, Y.; Yu, K.; Lu, B.; Dai, F.; Wu, D.; Lu, F. A novel wound dressing based on a Konjac glucomannan/silver nanoparticle composite sponge effectively kills bacteria and accelerates wound healing. *Carbohydr. Polym.*, **2018**, *183*, 70-80

as: dynamic light scattering, electrophoretic light scattering, nanoparticle tracking analysis, transmission electron microscopy, surface plasmon resonance, and binding affinity.

Dynamic Light Scattering (DLS)

DLS measures the intensity fluctuations of light, at an angle, scattered by the dispersed particles suspended in solution that are in a state of constant motion (Brownian motion). Based on the Stokes-Einstein equation, a correlation function is used to determine the hydrodynamic diameter (average particle size) of the nanoparticle in nanometers. DLS is also used to monitor the stability of nanoparticles over time by detecting diameter size and size distribution changes over time[57].

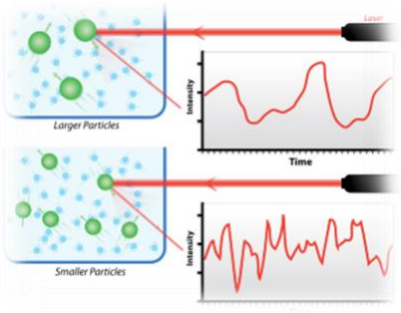

Figure 12: *Dynamic Light Scattering System for the determination of hydrodynamic nanoparticle size.*

[57] Bhattacharjee, S. DLS and zeta potential – What they are and what they are not? Journal of Controlled Release, **2016**, 235, 337–351.

Electrophoretic light scattering (ELS)

ELS measures the zeta potential, which is the magnitude of the electrostatic attraction/repulsion between the surface of nanoparticles and the bulk of the voltage-conducting water particles. The measured charge can be in the positive or negative range depending on the functional groups exposed on the outer surface of the nanoparticle. Zeta potential can also be an indicator of the stability of the nanoparticle where emulsions with higher values tend to be more electrically stable in comparison to emulsions with lower values, which aggregate faster due to their poor physical stability[58].

[58] Lu, G., Gao, P. Emulsions and Microemulsions for Topical and Transdermal Drug Delivery. Handbook of non-invasive drug delivery systems, **2010**, 59–94.

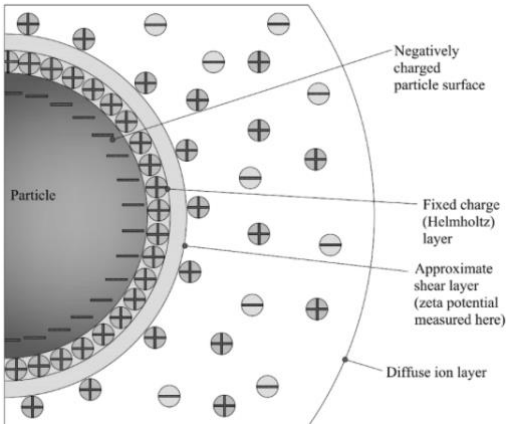

Figure 13: *Display of the Approximate sheer layer in a nanoparticle, at which Zeta Potential is measured*

Nanoparticle tracking analysis (NTA) This light scattering technique similarly to DLS detects the hydrodynamic diameter produced by Brownian motion. The advantage is that it provides an image analysis of the nanoparticles and the size detection is performed on a particle-by particle basis, which gives a more precise measurement in the case of polydispersed samples displaying a range of particle sizes. Some instruments also contain a laser source that can be used to characterize fluorescently labeled nanoparticles by detecting the fluorescence signal emitted by the particles[59].

[59] Filipe, V., Hawe, A., Jiskoot, W. Critical evaluation of nanoparticle tracking analysis by nanosight for the measurement of nanoparticles and protein aggregates. Pharm Res, **2010**, 27(5), 796-810.

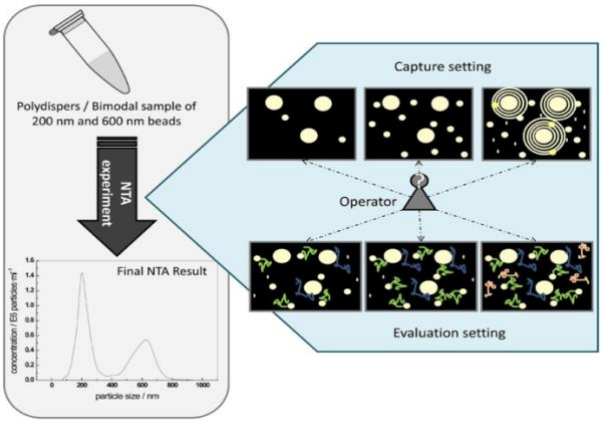

Figure 14: *Nanoparticle Tracking Analysis System (NTA)*

Scanning/Transmission Electron Microscopy (SEM/TEM)

This type of microscopy is a visualization technique used to detect the shape, morphology, and surface topography of the nanoparticle. It consists of a finely focused beam of electron that transmits through the sample which results in the emission of electronic signals, that then gets collected to be processed and translated into pixels to form an image of the 3-dimensional structure of the nanoparticle[60].

[60] Singh, A. Experimental methodologies for the characterization of nanoparticles. Engineered nanoparticles, **2016**,4, 125-170.

Figure 15: *Scanning Electron Microscopy SEM system displaying the microscope and software for the detection of morphology and topology of nanoparticle surface*

Surface Plasmon Resonance (SPR)

SPR is an optical biosensing technology used to measure the adsorption of materials on metal nanoparticles (magnetic, silver, gold). When the surface plasmon wave interacts with the surface of a metal nanoparticle or an irregularity, part of the energy is re-emitted as light, and the variation in absorption wavelength is detected by imaging sensors to produce a high contrast image[61].

[61] Amendola, V., Pilot, R., Frasconi, M., Latì, M. A., Maragò, O. Surface plasmon resonance in gold nanoparticles: a review. J. Phys: Condens. Matter, **2017**, 29, 20.

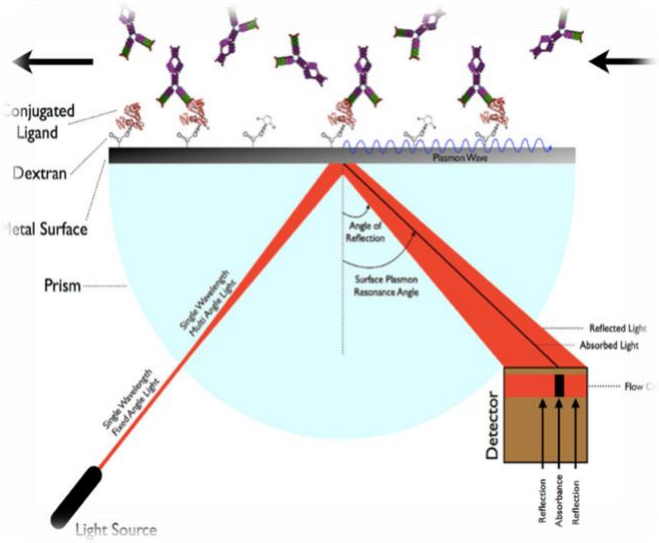

Figure 16: *Display of the mechanism of Surface Plasmon Resonance in the detection of nanoparticle outer surface glycans*

Binding affinity

Glyconanoparticles are designed to target the sugar-binding proteins expressed by a large number of mammalian cells. In order to mimic this process and confirm the presence of carbohydrates on the outer surface of the nanoparticle, fluorescent lectin assays can be used. Glyconanoparticles and the corresponding carbohydrate-specific lectin are incubated, and the binding

affinity is measured based on the fluorescence intensity detected by the spectrofluorometer device[62,63].

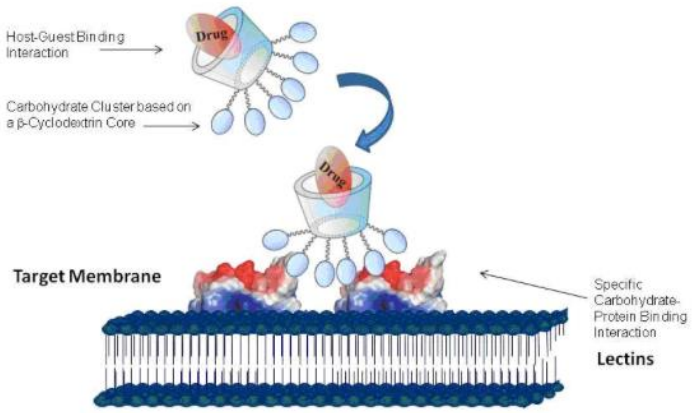

Figure 17: *Display of the mechanism of Lectin targeting via glycofunctionalized nanoparticles*

The introduction highlighted the framework of this research project that involved: 1) the design of a glycofunctionalization method that can be well-adapted to different types of glycans and nanoparticles, 2) the characterization of glycofunctionalized nanoparticles including the detection and quantification of outer-surface glycans, 3) In-vitro and in-vivo experiments to test the effect of glyco-targeting to corresponding receptors. Chapter 1 includes the synthesis of two chemoselective linkers that were concurrently

[62] Wang, X., Ramström, O., Yan, M. Quantitative Analysis of Multivalent Ligand Presentation on Gold Glyconanoparticles and the Impact on Lectin Binding. *Analytical Chemistry*, 2010, *82*(21), 10.
[63] Yilmaz, G., Becer, C.R. Glyconanoparticles and their interactions with lectins. Polym. Chem., **2015**, 6, 5503-5514.

used and compared for the glycofunctionalization of liposomes with two simple glycans: D-glucose and α-D-Mannose and one complex sugar: Sialyl Lewis X. Chapter 2 covers the in-vitro testing of liposomes (Blank, Glucose, Mannose) for cytotoxicity as well as targeting of RAW 264.7 macrophages. Chapter 3 covers the glycofunctionalization of liposomes with D-Galactose (simple glycan) and Sialyl Lewis X (complex glycan), followed by in-vitro testing of cell HepG2 uptake (FACS) and MRI in-vivo study of Gd-labeled glycoliposomes for the targeting of glyco-receptors overexpressed in hepatocellular carcinoma.

Chapter 1:
Chemoselective ligation linkers and liposome glycofunctionalization

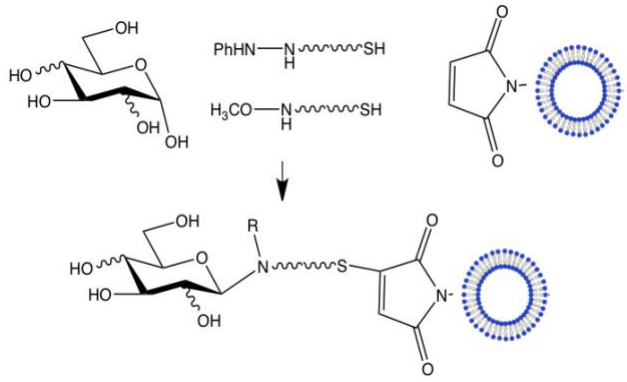

Abstract

Carbohydrates, some of the most abundant biomolecules in nature, have recently experienced a significant upsurge in nanomaterials research. Their wide range of functions as leading regulators in cell signaling, post-translational modifications, tumor genesis, metastasis, infections, and immune responses make them optimal candidates for translational applications. The obstacle that often limits extensive investigations of their biological impact in the nanoresearch field is the difficulty to engineer standardized functionalization, detection, and quantification procedures compatible with a wide range of mono-/polysaccharides and materials. For instance, most methods used for the glycofunctionalization of liposomes or nanoparticles require the presence of a synthetically modified carbohydrate comprising functional groups complementary to the reactive organic groups exposed on the outer surface of the nanomaterial. The drawback to this approach is the necessary synthetic modifications of the sugar that require multiple steps of synthesis and can be challenging depending on the complexity of the glycan. This approach limits many carbohydrate enthusiasts from further exploiting its implications in a multitude of research fields. In an attempt to address the gap presented, our lab developed new strategies of functionalization, detection, and quantification of unmodified mono-/polysaccharides to facilitate the design of glyconanomaterials. Liposomes were selected as the initial model to display the glycofunctionalization strategy due to its biocompatible nature

(FDA approved). The strategy of the functionalization of variable mono-/polysaccharides was based on the development of two short linkers compatible for chemoselective ligation as follow; First, two 6-carbon linkers were synthesized; the first being a thiol-Oxyamino and the second being a thiol-PhenylHydrazine. The thiol ends of the linkers are used for the linkage with the maleimide groups exposed on the outer surface of the liposomes as the end-chain of the grafted PEG in a traditional click-chemistry reaction. On the other end, one of two functional groups was present on each linker: linker 1 displayed an aminooxy group, widely used in oxime chemistry, while linker 2 contained Phenylhydrazine, a functional group tested for the first time, to the best of our knowledge, for chemoselective ligation.

The mechanism of the reaction entails the presence of unmodified carbohydrates (mono-/polysaccharides) with reducing chain ends that can form stable conjugates when exposed to the nucleophilic entities of (oxyamino, phenylhydrazine) in a one-step reaction. Since the reactions have been conducted on the outer surface of liposomes, the occurrence of the reaction has been tested in chemically non-traditional ways. Dynamic light scattering and Zetasizer have been used to evaluate the variation in size and Z-potential indicative of modification manifestations. Additionally, an agglutination assay was conducted using nanosight in a particle-by-particle tracking analysis to confirm the detection of carbohydrates on the outer surface. Last, a traditional Phenol-sulfuric assay was modified to deliver a direct detection method and an indirect quantitative method of the outer-surface glycans. As a proof of concept of the versatility and validity of the newly developed methods, liposomes were functionalized with a more

complex sugar Sialyl Lewis X (polysaccharide), and the aforementioned characterization/detection/and quantification methods were applied.

Chemistry of Conjugation of Unprotected Carbohydrates to Liposomes Surface

Due to the great involvement of mono-, poly-, and oligo-saccharides in various biological and pathological processes, there has been a growing interest in the development of (neo)glycoconjugates for applications for biomedical and pharmaceutical applications[64]. In this chapter chemoselective ligation was the selected method for the conjugation of unprotected, commercial sugars to the outer surface of liposomes. The chemical principle of the reaction relies on the presence of highly nucleophilic groups such O-amino or aminooxy ($-ONH_2$), or phenylhydrazine ($-NHNH_2$). These chemical groups share the ability to readily react with activated esters, aldehydes, or ketones of unprotected sugars leading to the formation of a stable C=N double bond-mediated bioconjugation[65]. Using this strategy, the immobilization of glycans through oxyamine linkers and a novel phenylhydrazine linker was investigated. Extensive work on this area of study has been reported by Chen et Al.[66] in a thorough review covering N-O linkage in carbohydrates and glycoconjugates. Similar applications to our experimental design were presented in the review as displayed in the following figure.

---

[64] Chen, N., Xie, J. N-O linkage in Carbohydrates and glycoconjugates. *Organic and Biomolecular Chemistry*. 14.47, **2016**, 11028-11047.
[65] Kalia, J., Raines, R. "Hydrolytic stability of hydrazones and oximes." *Angewandte Chemie International Edition* 47.39, **2008**, 7523-7526.
[66] Chen, N., Xie, J. N-O linkage in Carbohydrates and glycoconjugates. *Organic and Biomolecular Chemistry*. 14.47, **2016**, 11028-11047.

Conjugation of unprotected carbohydrates to microarrays and Gold NPs

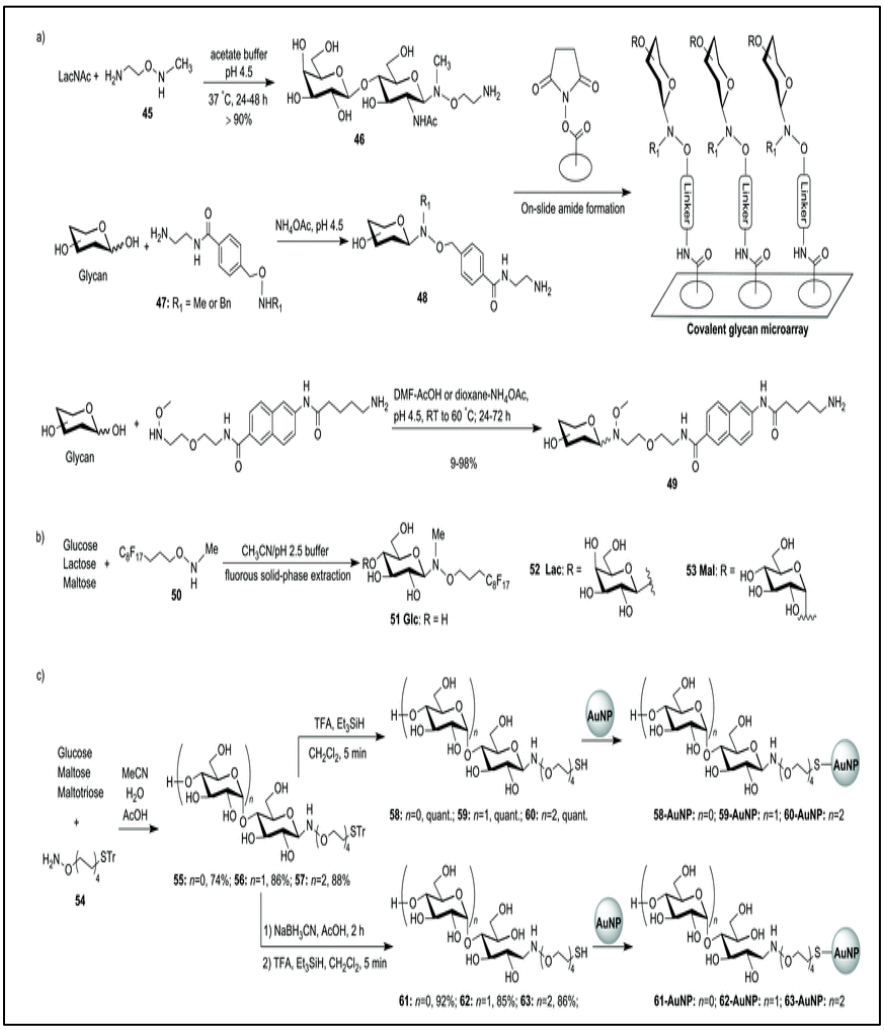

Scheme 13 – Immobilization of glycan through Oxyamine linkers[67].

[67] Chen, N., Xie, J. N-O linkage in Carbohydrates and glycoconjugates. *Organic and Biomolecular Chemistry*. 14.47, **2016**, 11028-11047.

Experimental Design of the Conjugation of Unprotected Carbohydrates to the surface of Liposomes

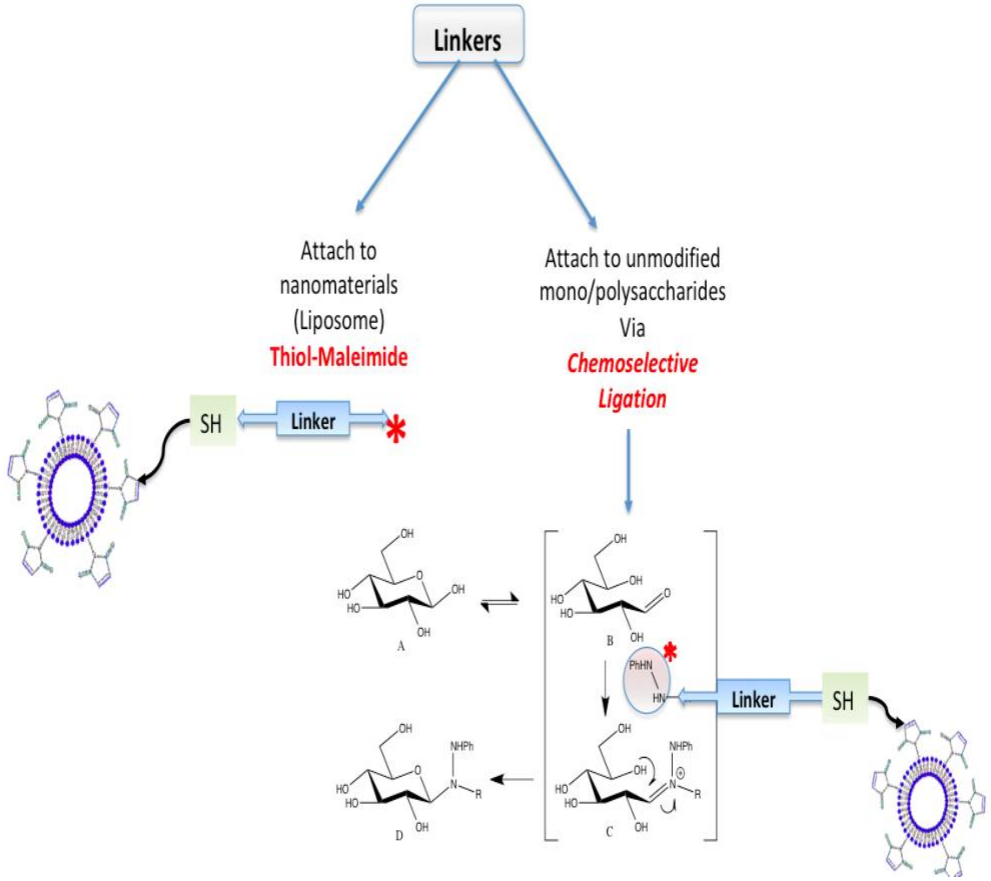

Briefly, Nucleophilic linkers were designed to attach to unprotected commercial mono-,poli-, oligo- saccharides via chemoselective ligation on one end and to be linked to the surface of liposomes via (Thiol-Maleimide linkage) from the other end. Further details will be covered throughout the chapter.

Results and Discussion

Three- step One-Pot synthesis of thiol-functionalized linkers. The use of oxyamines in the strategy of chemoselective ligation was first reported by our lab in the context of preparation of neoglycopeptides and neoglycolipids [68,69,70]. This approach has since been widely used in an array of oxime applications including neoglycorandomization of drugs and the synthesis of glycans, glycolipids, and glyco-amino acid analogs. Amongst these applications, the synthesis of methoxyamine linker in a one-pot strategy has been reported by Munneke et al, using acrolein as a bifunctional reagent and propane-1,3-dithiol to generate a thiol-functionalized short linker[71]. This strategy was adopted and expanded upon by substituting the methoxyamine group with phenyl hydrazine, to introduce a new linker with similar function as the initially discovered oxime group. Briefly, both linkers were synthesized by the same three-step one-pot strategy. Step one is the addition of acrolein and propane-1,3-dithiol to form the backbone of the 6-carbon linker, followed by the addition of methoxyamine hydrochloride for the first linker or phenylhydrazine for the second linker. Last, the reduction of imine using sodium cyanoborohydride affording both linkers in 82% and 85% yield respectively.

---

[68] Peri, F.; Deutman, A.; La Ferla, B.; La Nicotra, F. *Chem. Commun.* **2002**, 1504– 1505
[69] Peri, F.; Cipolla, L.; La Ferla, B.; Nicotra, F. *C. R. Chim.* **2003**, 6, 635– 644
[70] Peri, F.; Jiménez-Barbero, J.; García-Aparicio, V.; Tvaroska, I.; Nicotra, F. *Chem-Eur. J.* **2004**, 10, 1433– 1444
[71] Munneke S., Prevost J. R. C.,Painter G. P.,Stocker B. L. ,Timmer M. S. *Organic Letters* **2015,** *17* (3), 624-627.

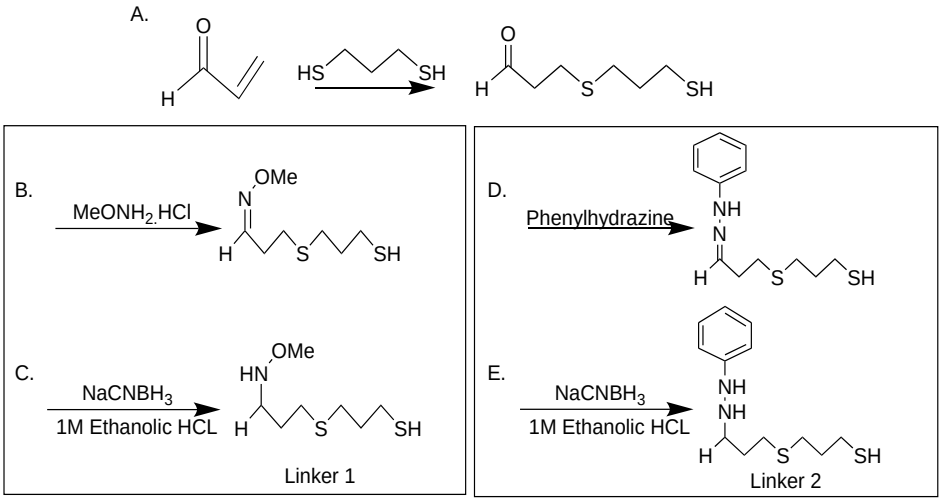

Figure1: The synthesis of two short thiol linkers labeled as linker1 and linker2 in a one-pot synthetic scheme a) addition of acrolein to propanedithiol to form a 6-carbon backbone, b) for the formation of linker 1, methoxyamine hydrochloride was added to the crude, as for linker 2 c) PhenylHydrazine was added to the crude. Last, the imine reduction was carried out in both products using sodium cyanoborohydride. The final products hence represent linker 1 (NOMe) and linker 2 (PhHyd).

Liposomes

Assembly The liposomes used in the study are a matrix of 1:1 ratio of sphingomyelin: cholesterol in addition to a 2.5% of the total molar ratio of DSPE-PEG-Maleimide. The three components were dissolved in chloroform/methanol 2:1, followed by the evaporation of the organic solvents. The lipid film was rehydrated in PBS buffer for a final molarity of 5mM, vortexed, and extruded 10 times at 55°C through a stack of two polycarbonic 100 nm filters under 20 bar nitrogen pressure. Liposomes produced were characterized in terms of size, polydispersity index, and Zeta potential. Additionally, the final concentration of sphingomyelin (μg/mL) per sample

was determined using the Stewart assay protocol in order to calculate the percent yield and equivalence for the following reaction[72].

***Figure 2**: Liposome membrane extruder (Avanti Polar Lipids)*

[72] Stewart, J.C.M. Colorimetric determination of phospholipids with ammonium ferrothiocyanate. (1980). Anal Biochem. 1980;104(1):10-4.

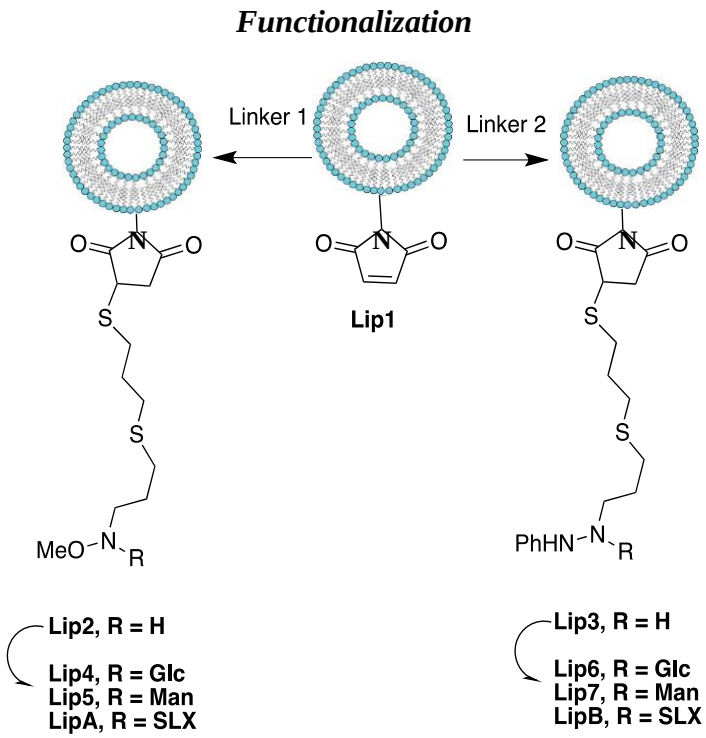

Figure 3: The two steps functionalization of glycoliposomes.
Step one is the addition of linkers 1 and 2 to the assembled liposome functionalized with maleimide **(Lip1)** at pH 7.4 in PBS to generate **Lip2** (Lip-NOMe) and **Lip3** (Lip-PhHyd). **Step two** consists of the reaction of Lip2 and Lip3 with glucose (Glc), mannose (Man) and sialyl Lewis X (SLX) at pH 4.5 to generate the glycosylated liposomes: (**Lip4**-NOMe-Glc), (**Lip5**-NOMe-Man), (**Lip5**-PhHyd-Glc), and (**Lip7**-PhHyd-Man) in addition to complex sugar liposomes : (**LipA**-NOMe-SLX), and (**LipB**-PhHyd-SLX).

The first step of the functionalization is the maleimide-thiol crosslinking reaction conducted at pH=7.4 in PBS. Maleimide groups were exposed on the outer surface of the liposome as the chain-ends of the embedded DSPE-PEG, thus maximizing the contact the thiol groups of the methoxyamino linker (linker 1) producing liposome 2 (Lip2-NOMe) and the Phenylhydrazine linker (linker 2) producing liposome 3 (Lip3-PhHyd).

The second step of the functionalization is the chemoselective ligation between the nucleophilic group of linkers 1 and 2, and the reducing end of the selected glycan. Liposome 2 (lip2-NOMe) and liposome 3 (lip3-PhHyd) were both functionalized with 2 different commercial monosaccharides: D-glucose and α-D-Mannose to produce: liposome 4 (lip4-NOMe-Glc), liposome 5 (lip5-NOMe-Man), liposome 6 (lip6-PhHyd-Glc), liposome7 (lip7-PhHyd-Man). Additionally, as a proof of concept, linkers 1 and 2 were each functionalized with a complex glycan, sialyl lewis X, using the same conditions and producing liposome A (Lip-NOMe-SLX) and liposome B (Lip-PhHyd-SLX). The reaction was conducted at pH 4.5 over 48 hours at room temperature.

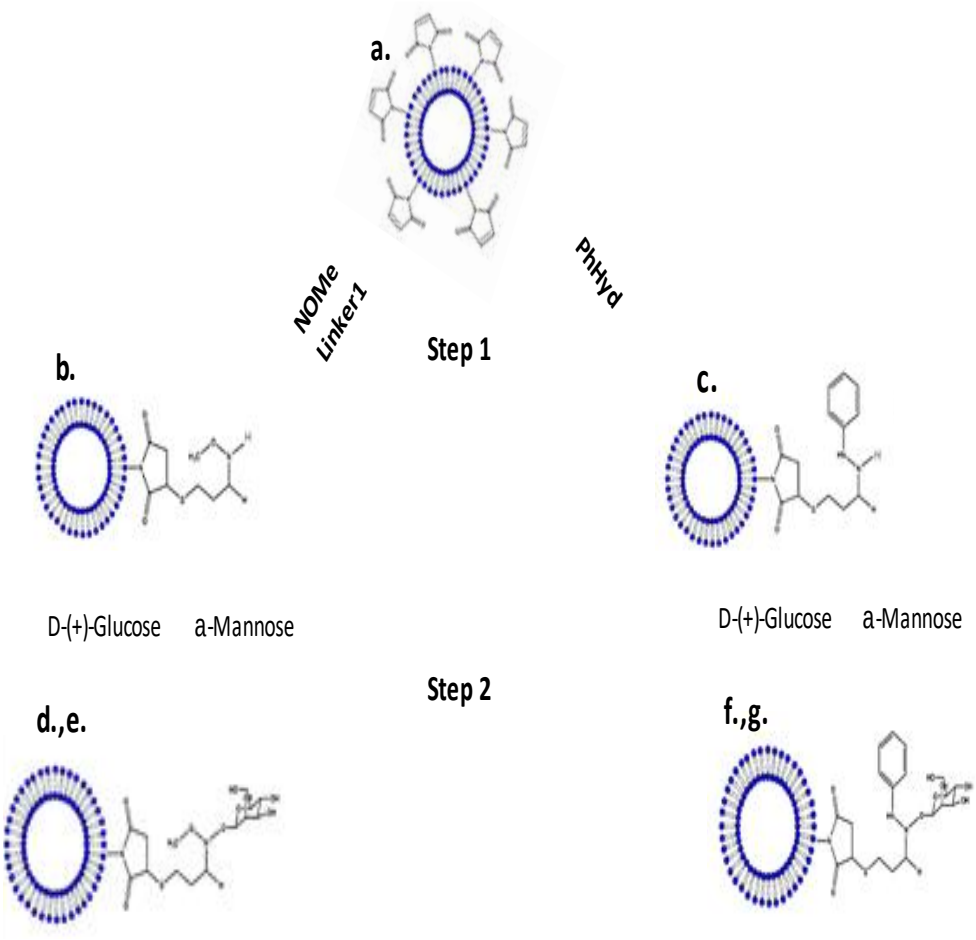

Figure 4: The two steps functionalization of glycoliposomes.

Characterization of Liposomes

The occurrence of reactions on the outer surface of liposomes has been monitored via: 1) Stewart Assay, 2)size variation, 3) Z-potential, 4) Agglutination assay, and 5) Phenol-Sulfuric assay.

1) Stewart Assay

The quantitative assay was first published by J. M. Stewart in 1980[73]. It is based on the ability of phospholipids to form a complex with ferrocyanate, detectable at 485nm. The ferrocyanate reagent (dark red solution) was prepared following the published procedure[74] and a calibration curve of sphingomyelin was established. In a glass tube, 10μL of liposome sample, followed by 2 mL of chloroform/2 mL ferrocyanate reagent were added in the aforementioned order and vortexed for 90 seconds. The solution was left to settle for 5 minutes and the clear bottom layer was separated using a Pasteur pipet. The optical density of the solutions was detected at λ=490nm and their corresponding concentrations of sphingomyelin was extrapolated from calibration curves in (μg/μl). This quantification method was used to normalize all the samples used in further reactions/assays.

[73] Stewart, J.C.M. Colorimetric determination of phospholipids with ammonium ferrothiocyanate. (1980). *Anal Biochem. 1980;104(1):10-4.*

[74] Stewart, J.C.M. Colorimetric determination of phospholipids with ammonium ferrothiocyanate. (1980). *Anal Biochem. 1980;104(1):10-4.*

1- **Particle size and polydispersity** of the 7 liposomes was detected via dynamic light scattering (DLS). There was a notable and consistent increase in size (nm) following *step 1* with linkers and *step 2* with carbohydrates, indicative of the occurrence of functionalization.

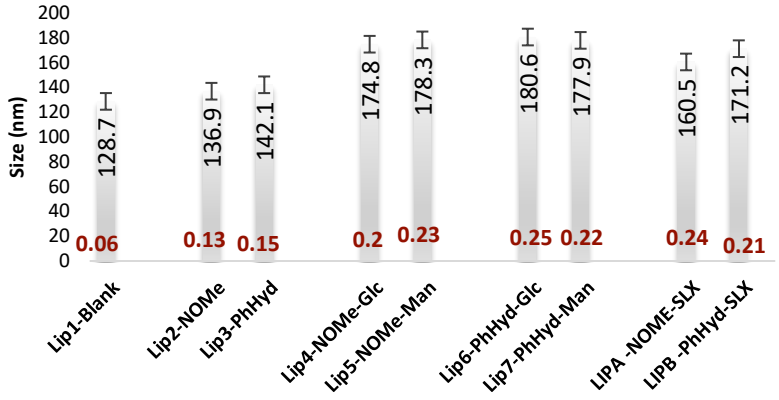

Figure 5: The size of liposomes (1-7)+(A/B) in nm tested using DLS. Data in red indicate the polydispersity index of each population of liposomes per sample. The 9 samples tested are: **Lip1**-Blank, **Lip2**-NOMe, **Lip3**-PhHyd, **Lip4**-NOMe-Glc, **Lip5**-NOMe-Man, **Lip5**-PhHyd-Glc, **Lip7**-PhHyd-Man, **LipA**-NOMe-SLX, and **LipB**-PhHyd-SLX. The bars represent ± SD, n=3.

As displayed in *table*, the size increased by increments of 10-15nm with the addition of linkers 1 and 2, followed by an additional increase of 20-40nm with the addition of the carbohydrates (Glucose, Mannose, Sialyl Lewis X). This size variation corresponds to the results obtained by Zhang et al.[75] and

[75] ZHANG, Hailong; MA, Yong; SUN, Xue-Long. Chemically-selective surface glyco-functionalization of liposomes through Staudinger ligation. *Chemical Communications*, **2009**, 21: 3032-3034.

Liu et al.[76], and others. The polydispersity also increased to a maximum value of 0.25. The uniformity of population size was verified via Nanosight using a particle-by-particle tracking analysis, with consistent results.

Zeta potential (mV) was tested using Zetasizer (Nano-Z Malvern instruments, UK) in order to monitor the surface modifications in terms of charge (mV) at a physiological PH. Initially, *blank liposome 1* contained PEG-Maleimide on its outer surface and displayed a negative zeta potential of -3.69 mV. With the addition of linkers 1 and 2, the charges of liposomes 2 and 3 shifted into a low positive range in mV, indicating the shielding of the negative surface with neutral molecules. The final steps of glycofunctionalization were monitored with a slight increase in positive zeta potential representing a larger coverage of the surface area with neutral carbohydrates. However, with the addition of Sialyl Lewis X which carries a negative charge at physiological pH, the outer charge of liposomes A and B shifted to a negative range as displayed in *figure*. The results correspond to the work of Moros at al[77], Liu et al[78], as well as Wattendorf et al[79]

---

[76] Liu, W., Chaix, A., Gary-Bobo, M., Angeletti, B., Masion, A., Da Silva, A., El Cheikh, K.. Stealth Biocompatible Si-Based Nanoparticles for Biomedical Applications. *Nanomaterials*, **2017,** *7*(10), 288.

[77] *María Moros, Bruno Hernáez, Elina Garet, Jorge T. Dias, Berta Sáez, Valeria Grazú, África González-Fernández, Covadonga Alonso, and Jesús M. de la Fuente. Monosaccharides versus PEG-Functionalized NPs: Influence in the Cellular Uptake.* ACS Nano, ***2012,*** 6, *(2), 1565-1577.*

[78]Liu, W., Chaix, A., Gary-Bobo, M., Angeletti, B., Masion, A., Da Silva, A., El Cheikh, K.. Stealth Biocompatible Si-Based Nanoparticles for Biomedical Applications. *Nanomaterials*, **2017,** *7*(10), 288

[79] Wattendorf, U., Coullerez, G., Vörös, J., Textor, M., & Merkle, H. P. (2008). Mannose-based molecular patterns on stealth microspheres for receptor-specific targeting of human antigen-presenting cells. *Langmuir*, *24*(20), 11790-11802.

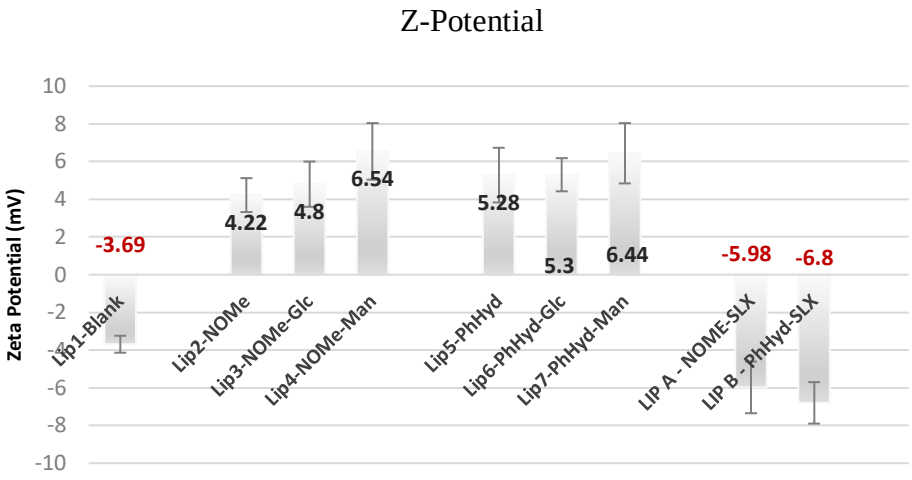

Figure 6: Zeta potential measurements (mV) performed at PH= 7.4 The 9 liposome samples tested are: **Lip1**-blank, **Lip2**-NOMe, **Lip3**-PhHyd, **Lip4**-NOMe-Glc, **Lip5**-NOMe-Man, **Lip5**-PhHyd-Glc, **Lip7**-PhHyd-Man, **LipA**-NOMe-SLX, and **LipB**-PhHyd-SLX. The bars represent ± SD, n=3

Liposome Characterization DLS and Zetasizer

Liposomes	DLS nm	PDI	Z potential
Lip1-Blank	128.7 ± 3.8	0.06	-3.69 ± 0.31
Lip2 -NOMe	136.9 ± 2.7	0.13	4.22 ± 0.36
Lip3 -PhHyd	142.1 ± 2.9	0.15	4.8 ± 0.8
Lip4 -NOMe-Glc	174.8 ± 8.3	0.2	6.54 ± 0.35
Lip5-NOMe-Man	178.3 ± 6.9	0.23	5.28 ± 0.77
Lip6-PhHyd-Glc	180.6 ± 9.6	0.25	5.3 ± 0.39
Lip7-PhHyd-Man	177.9 ± 7.7	0.22	6.44 ± 0.25
*LIPA-NOME-SLX	165.5 ± 5.1	0.24	-5.98 ± 0.37

*LIPB-PhHyd-SLX	171.2 ± 4.8	0.21	-6.8 ± 0.45

Table 1 *:* Characterization of 9 liposomes via DLS (size nm, polydispersity Index) and Zetasizer (ζ-potential mV).

Detection and quantification of carbohydrates

Agglutination Assay

Concavalin A (ConA), a carbohydrate binding protein (lectin) specific to D-glucose and α-Mannose, was used for the detection of glycans on the outer surface of liposomes. The lectin was incubated with 7 samples (Liposomes 1-7) in DPBS to evaluate the occurrence of cross-linkage between the tetramer protein and the carbohydrates on the outer surface. Cross-linkage would cause aggregate formation and consequent turbidity in the solution detectable via spectrophotometry. This method of glycan detection has been a standard used procedure and successfully tested by Villalva et al[80], Zhang et al[81], and others.

[80] Villalva, D. G., Giansanti, L., Mauceri, A., Ceccacci, F., & Mancini, G. (2017). Influence of the state of phase of lipid bilayer on the exposure of glucose residues on the surface of liposomes. *Colloids and Surfaces B: Biointerfaces*, **2017**, *159*, 557-563.

[81] Zhang, H., Ma, Y., & Sun, X. L. Chemically-selective surface glyco-functionalization of liposomes through Staudinger ligation. *Chemical Communications*, 2009, (21), 3032-3034.

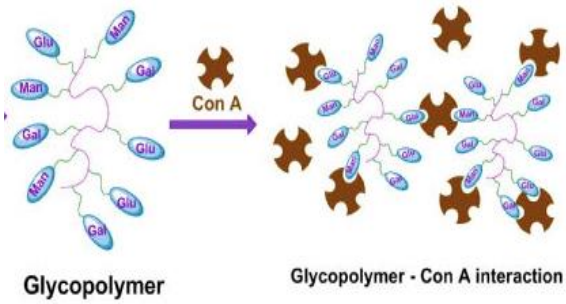

Figure 7: Specific interaction of the tetramer lectin protein Concavalin A with liposome outer surface glycans D-glucose and α-D-Mannose

A new supporting protocol was developed by our lab to concurrently analyze the aggregate formation using the imaging feature of Nanosight tracking analysis. In this two parts experiments: 1) the optimal time of incubation of samples (1-7) with ConA was analyzed by testing the absorbance at 6 timepoints from 30-1500 minutes at 495 nm using Spectrostar nanoabsorbance microplate reader (BMG LABTECH). Liposomes were prepared in DPBS (0.1mM), and the concentration values were normalized using the Stewart assay via quantification of sphingomyelin[82]. Concavalin A was prepared in DPBS (0.1M) containing $MgCl_2$ + $CaCl_2$, necessary for the activation of the lectin. Then, 100μL of Con A stock was added to 900μL of each liposome sample. Samples were analyzed after 24 hours incubation with the lectin by pipetting 270μL of each sample in a microplate.

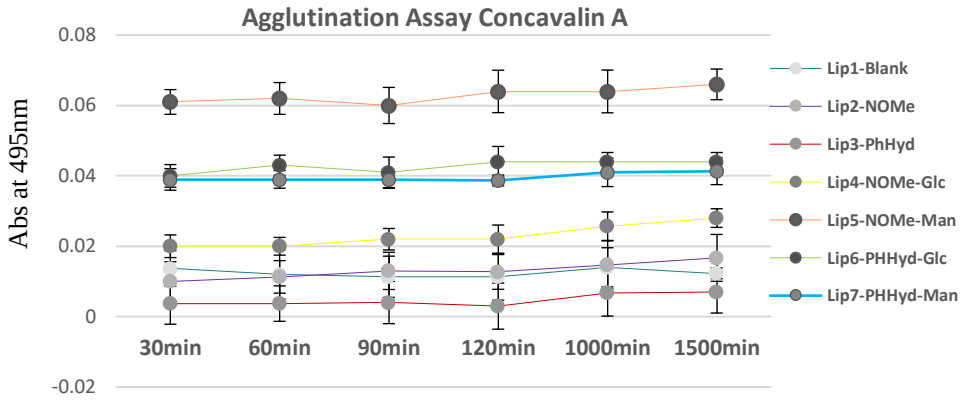

Figure 8: Agglutination assay using Concavalin A for the detection of carbohydrates functionalized. To the outer surface of liposomes. The 7 color coded samples tested are 1) Blank liposome, 2) Liposome-Aminooxy Linker, 3) Liposome – PhenylHydrazine Linker, 4) Liposome- Aminooxy linker – Glucose, 5) Liposome – Aminooxy Linker- Mannose, 6) Liposome- PhenylHydrazine linker- Glucose, 7) Liposome- PhenylHydrazine linker – Mannose. Data are expressed as the absorbance of each sample against the blank over 6 time points (30min, 60min, 90min, 120min, 1000min, 1500min). The bars represent ± SD, n=3.

The glycosylated samples (4-7) displayed a higher absorbance from the initial time point (30 minutes). Over time, absorbance values seemed to plateau, with minimal variations (*figure 4).* The results offer an initial indication to the presence of outer surface glycans that crosslink with ConA to form aggregates. The following part of the aggregation experiment is 2) Nanosight based aggregation analysis.

Previous works reported agglutination in terms of size increase of the liposome (nm) due to carbohydrate/lectin binding[83]. In this study, Nanosight was used to track aggregates formation/size variation with light scattering and microscope imaging.

[83] Zhang, H., Ma, Y., & Sun, X. L. Chemically-selective surface glyco-functionalization of liposomes through Staudinger ligation. *Chemical Communications*, 2009, (21), 3032-3034.

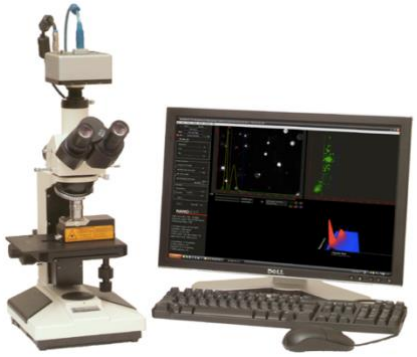

Figure 9: Nanosight instrument for the detection of size (nm) and aggregation

Similarly to the previous protocol, liposomes were prepared in DPBS (0.1mM), and the concentration values were normalized using the Stewart assay. Concavalin A was prepared in DPBS (0.1M) containing $MgCl_2$ + $CaCl_2$, and 100µL was added to 900µL of each liposome sample. Samples were analyzed after 24 hours incubation with the lectin.

Agglutination Assay Nanosight Results

1- **Nanosight 20x magnification microscope/Camera for Agglutination Assay Analysis**

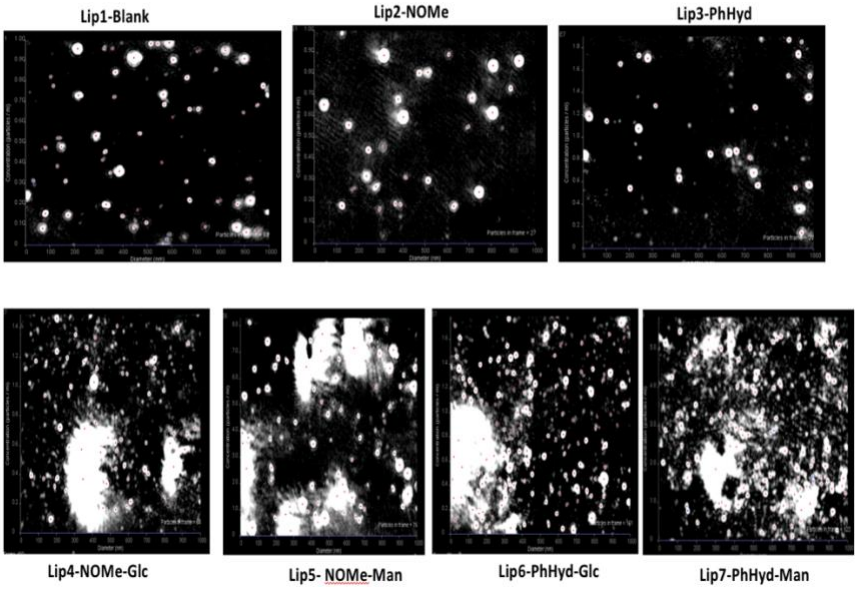

Figure 10 : Nanosight images display the aggregation of glycoliposome samples with the addition of Concavalin A, a carbohydrate-binding lectin protein. The top 3 figures represent 1)Lip-Blank, 2)Lip-NOMe, 3)Lip-PhHyd. Meanwhile, the bottom 4 pictures represent the 4 glycosylated liposomes interacting with Con A: 4) Lip-NOMe-Glc, 5) Lip-NOMe-Man, 6) Lip-PhHyd-Glc, 7) Lip-PhHyd-Man.

The samples tested are as follow: **Lip1**-Blank, **Lip2**-NOMe, **Lip3**-PhHyd, **Lip4**-NOMe-Glucose, **Lip5**-NOMe-Mannose, **Lip5**-PhHyd-Glucose, **Lip7**-PhHyd-Mannose. Samples (1-3) did not display any aggregate formation, on the contrary to glycoliposomes (4-7) that formed a notable level of aggregation when incubated with Concavalin A. These results indicate the presence of glycans on the outer surface of liposomes functionalized with chemoselective linkers.

As displayed in *figure 10* , the images portray the difference in behavior between the non-glycosylated samples (1-3) and the glycofunctionalized

liposomes (4-7) when incubated with Concavalin A. In the latter samples, there is a clear aggregate formation that can be attributed to the formation of multi-binding aggregates between the tetramer Con A protein and the glycofunctionalized samples. The protein-glycoliposome cross-binding phenomenon was also studied by Moratz et al. using a thioether exchange technique[84].

Agglutination Assay Nanosight Results

2- **Size variation detection using Nanosight Particle-By-Particle Tracking analysis**

[84] Moratz, J., Klepel, F. and Ravoo, B.J., 2017. Dynamic glycosylation of liposomes by thioester exchange. *Organic & biomolecular chemistry*, **2017,** *15*(23), p.5089-5094.

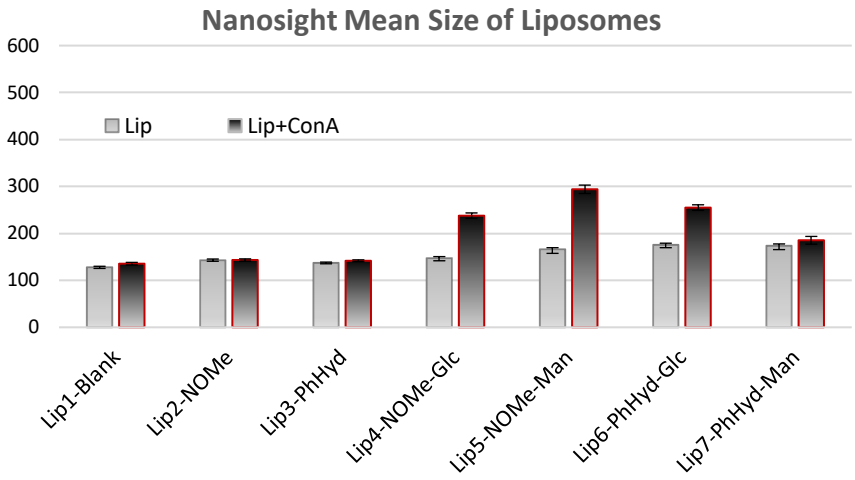

Figure 11: Nanosight Mean size of liposome samples: **Lip1**-Blank, **Lip2**-NOMe, **Lip3**-PhHyd, **Lip4**-NOMe-Glucose, **Lip5**-NOMe-Mannose, **Lip6**-PhHyd-Glucose, **Lip7**-PhHyd-Mannose, before Con A incubation (light gray columns) and Post-incubation (Black columns). The bars represent ± SD, n=3.

An increase in the mean size of the liposomes was noted in samples (4-7) attributed to the formation of ConA/ glycoliposomes aggregates. Meanwhile, samples (1-3) did not display any significant variation.

The variation in size samples (4-7) presented: 61.2% increase **in Lip4**-NOMe-Glucose

76.7% increase **in Lip5**- NOMe-Mannose

45.2% increase in **Lip6**-PhHyd-Glucose

6.7% increase in **Lip7**-PhHyd-Mannose

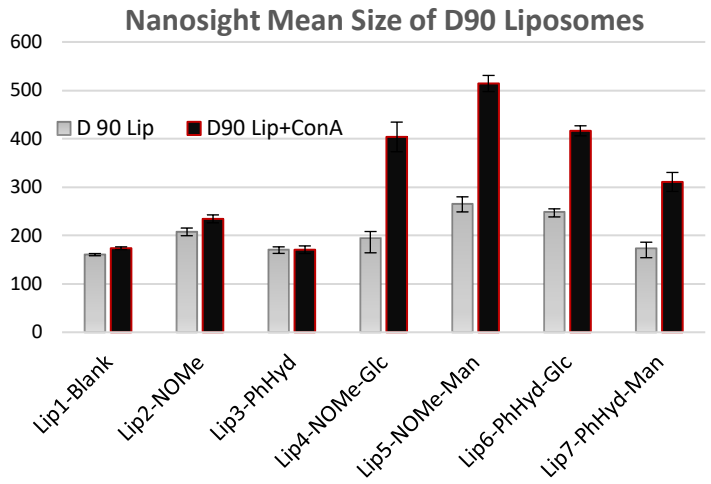

Figure 12: Nanosight Mean size of D90 (largest 10% of population) Particle-by-particle tracking analysis. Liposome samples: **Lip1**-Blank, **Lip2**-NOMe, **Lip3**-PhHyd, **Lip4**-NOMe-Glucose, **Lip5**-NOMe-Mannose, **Lip6**-PhHyd-Glucose, **Lip7**-PhHyd-Mannose, before Con A incubation (light gray columns) and Post-incubation (Black columns). The bars represent ± SD, n=3. The largest 10% of the population represent the biggest aggregates formed due to ConA/glycoliposomes interactions. Therefore, the variation in size is much more significant in the D90 population and can be noted by:

107.7% increase **in Lip4**-NOMe-Glucose

93.8% increase **in Lip5**- NOMe-Mannose

67.4% increase in **Lip6**-PhHyd-Glucose

78.9% increase in **Lip7**-PhHyd-Mannose

Nanosight Tracking Analysis

Through the nanoparticle Tracking Analysis feature of Nanosight, liposomes used in the agglutination study were tracked and sized. Results are displayed as frequency distribution graphs demonstrated by the figures below. Each sample run consists of pre-Con A incubation (Top of the chart) versus Post-Con A incubation (Bottom of the chart).

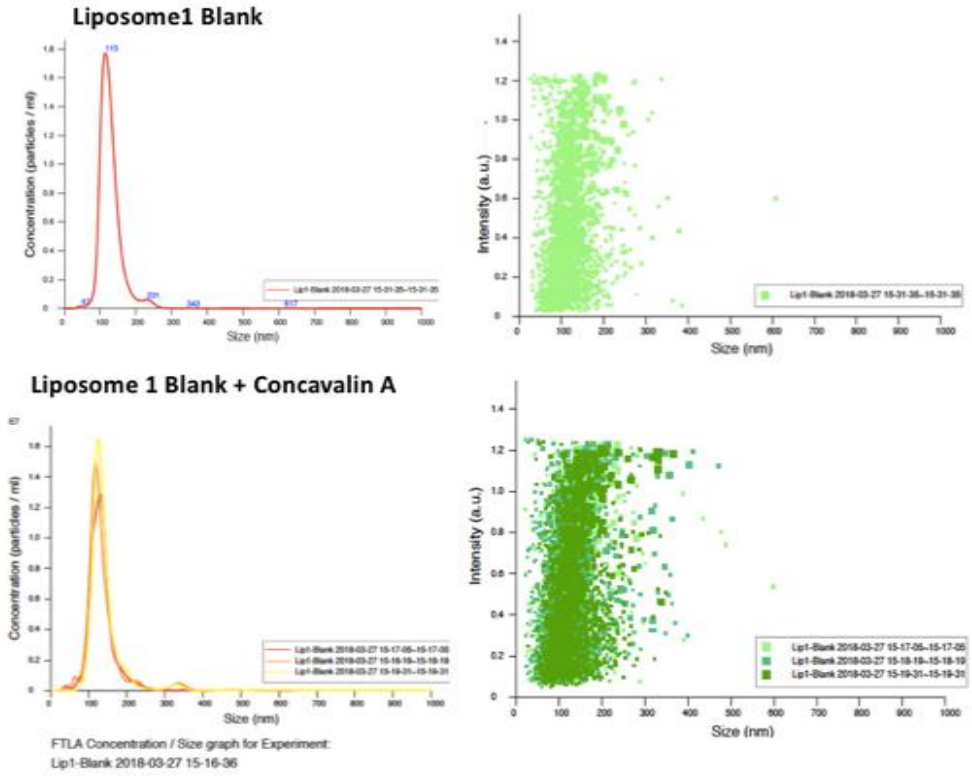

Figure 13: Nanoparticle Tracking Analysis of Sample 1- Blank liposome. No major variation in the particle-by-particle frequency distribution graphs of before/after Con A incubation noted.

Nanosight Tracking Analysis

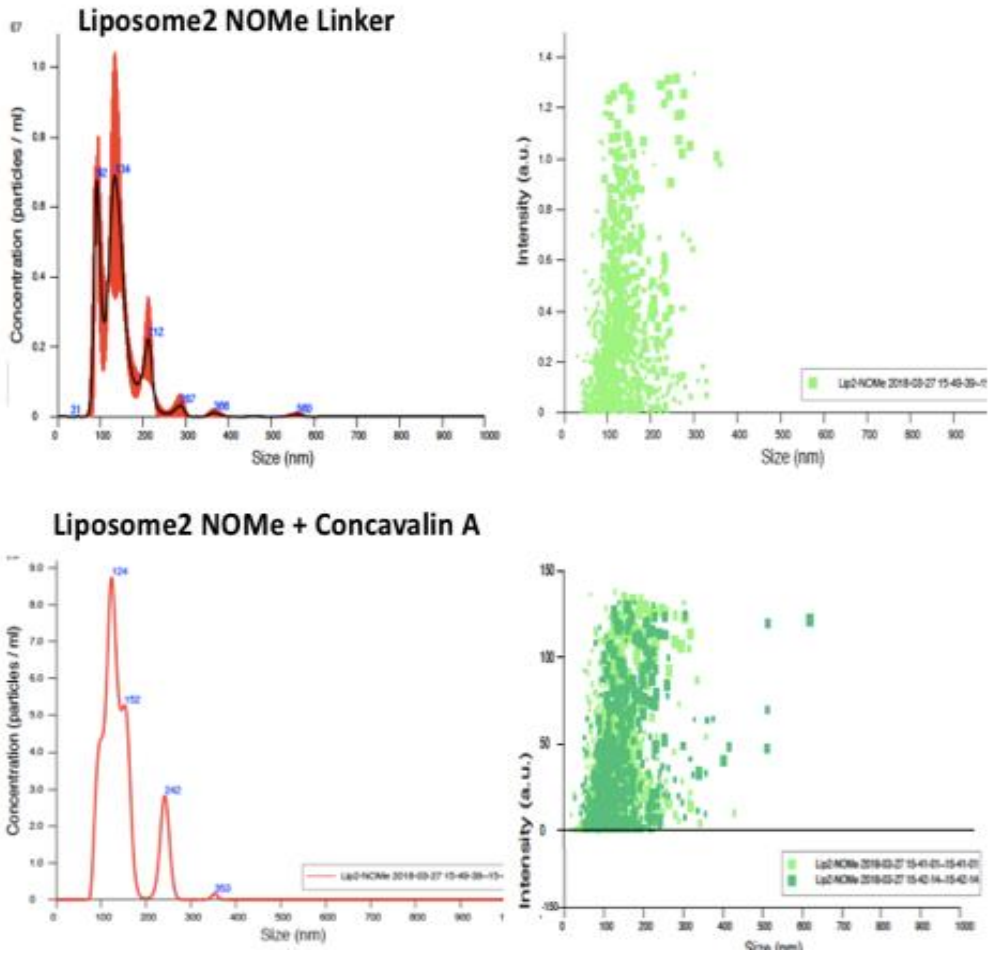

Figure 14: Nanoparticle Tracking Analysis of Sample 2- Liposome-NOMe. No major variation in the particle-by-particle frequency distribution graphs of before/after Con A incubation noted.

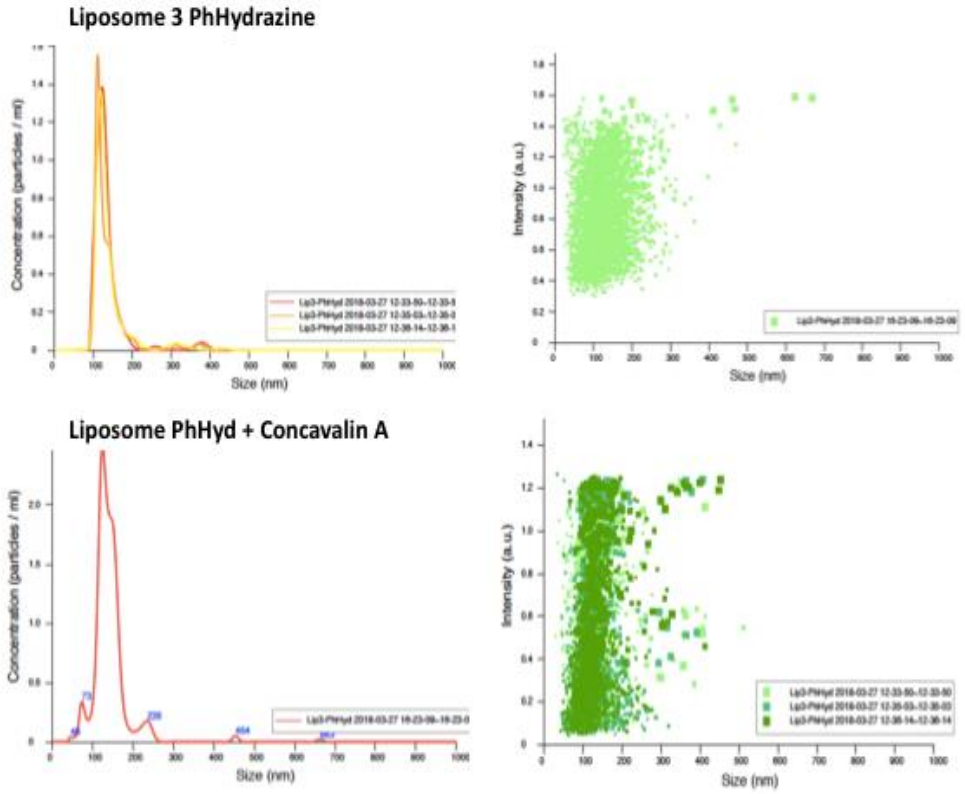

Figure 15: Nanoparticle Tracking Analysis of Sample 3- Liposome-PhHyd. No major variation in the particle-by-particle frequency distribution graphs of before/after Con A incubation noted.

Nanosight Tracking Analysis

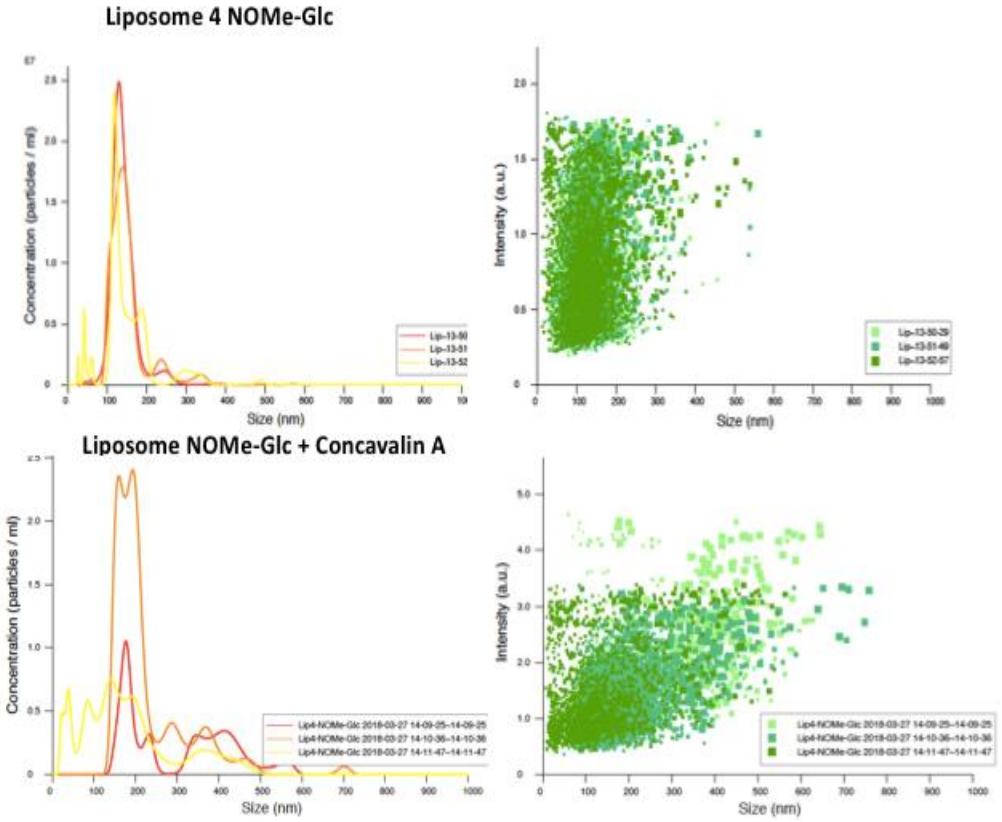

Figure 16: Nanoparticle Tracking Analysis of Sample 4- Liposome-NOMe-Glucose. A notable variation in the particle-by-particle frequency distribution graphs of before/after Con A incubation was evident. The bottom graph representing Lip4+ConA significantly shifted to the right, indicating a large increase in the mean size of the liposomes due to the presence of large aggregates versus pre-incubated sample in the top graph. The distribution of the liposomes shifted from

the range of [100-300 nm] pre-incubation to the range of [100-700 nm] post-incubation.

Nanosight Tracking Analysis

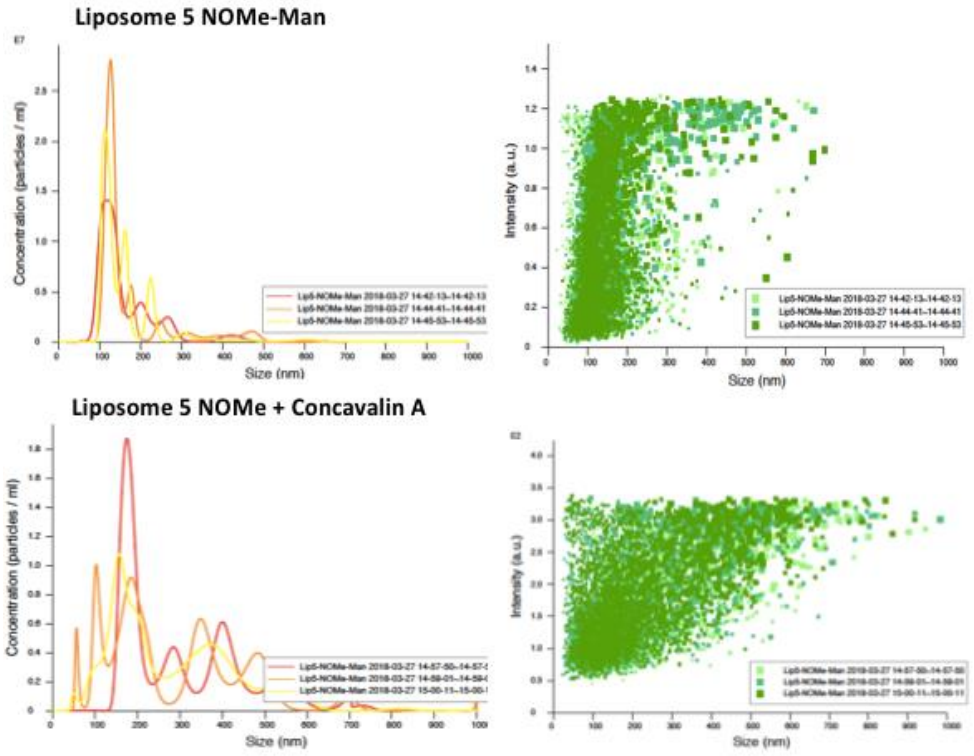

Figure 17: Nanoparticle Tracking Analysis of Sample 5- Liposome-NOMe-Mannose. A notable variation in the particle-by-particle frequency distribution graphs of before/after Con A incubation was evident. The bottom graph representing Lip4+ConA significantly shifted to the right, indicating a large increase in the mean size of the liposomes due to the presence of large aggregates versus pre-incubated

sample in the top graph. The distribution of the liposomes shifted from the range of [100-500 nm] pre-incubation to the range of [100-1000 nm] post-incubation.

Nanosight Tracking Analysis

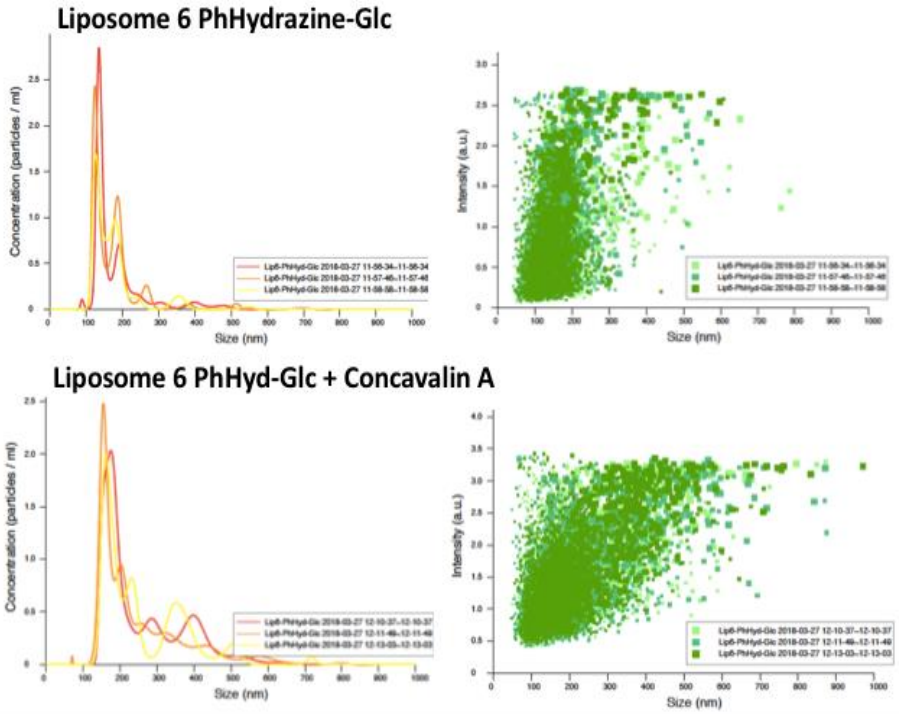

Figure 18: Nanoparticle Tracking Analysis of Sample 6- Liposome-PhHyd-Glucose. A notable variation in the particle-by-particle frequency distribution graphs of before/after Con A incubation was evident. The bottom graph representing Lip4+ConA significantly shifted to the right, indicating a large increase in the mean size of the liposomes due to the presence of large

aggregates versus pre-incubated sample in the top graph. The distribution of the liposomes shifted from the range of [100-300 nm] pre-incubation to the range of [100-800 nm] post-incubation.

Nanosight Tracking Analysis

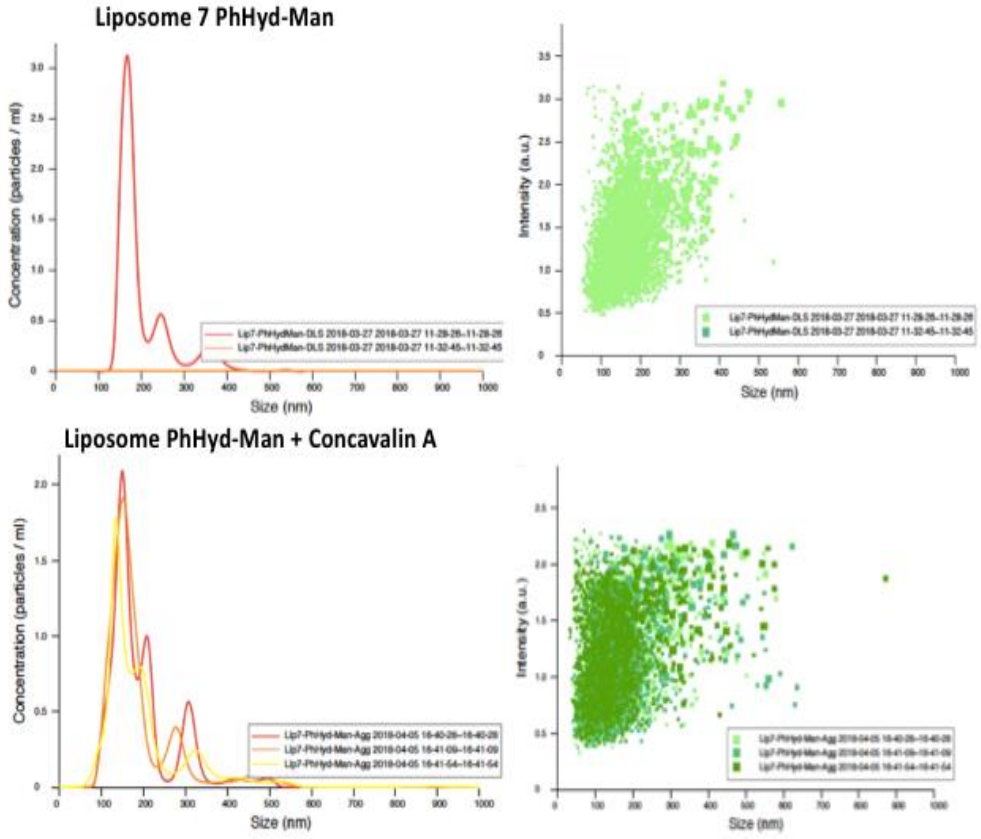

Figure 19: Nanoparticle Tracking Analysis of Sample 7- Liposome-PhHyd-Mannose. A notable variation in the particle-by-particle frequency distribution graphs of before/after Con A incubation was evident. The bottom graph representing Lip4+ConA significantly shifted to the right, indicating a large

increase in the mean size of the liposomes due to the presence of large aggregates versus pre-incubated sample in the top graph. The distribution of the liposomes shifted from the range of [100-300 nm] pre-incubation to the range of [100-600 nm] post-incubation.

In summary, the agglutination assay performed in our lab for the identification of liposomes' outer surface glycans consisted of two steps:

1) Detection of Absorbance λ=495nm to check for turbidity caused by lectin/glycoliposome interaction → aggregate formation
2) Detection of size variation due to aggregate formation (lectin/glycoliposome interaction) using Nanosight.

The results of both steps supported aggregate formation in the glycosylated liposomes (4-7) versus non-glycosylated liposomes (1-3).

As a proof of concept of the universality of the nanosight approach, the agglutination assay was tested on LipA (NOMe-SLX) and LipB (PhHyd-SLX using Wheat Germ Agglutinin (WGA), a carbohydrate-binding lectin protein specific for Sialic Acid.

Agglutination Assay Size variation Tested via Nanosight

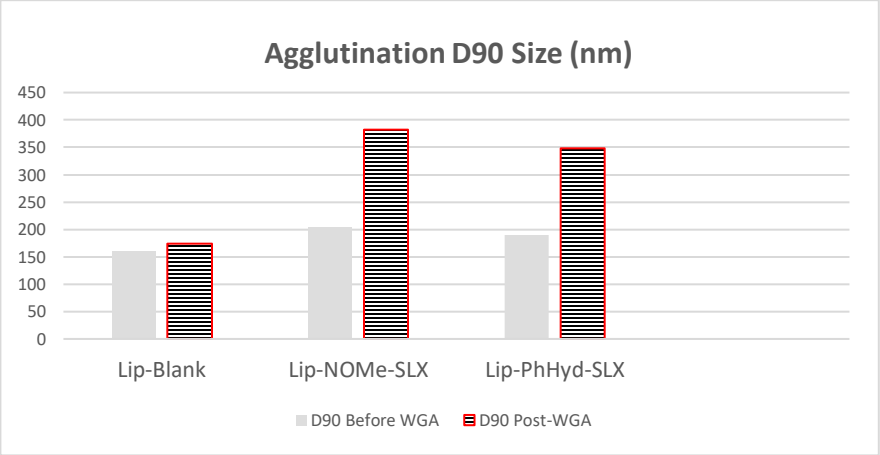

Figure 20: Nanosight Mean size of D90 (largest 10% of population) Pre/Post incubation with WGA (lectin specific for sialic acid). Samples:**Lip-Blank**, **LipA**-NOMe-SLX ,and **LipB**-PhHyd-SLX.

8.02% increase in Lip-Blank

87.25% increase in LipA-NOMe-SLX

83.04% increase in LipB-PhHyd-SLX

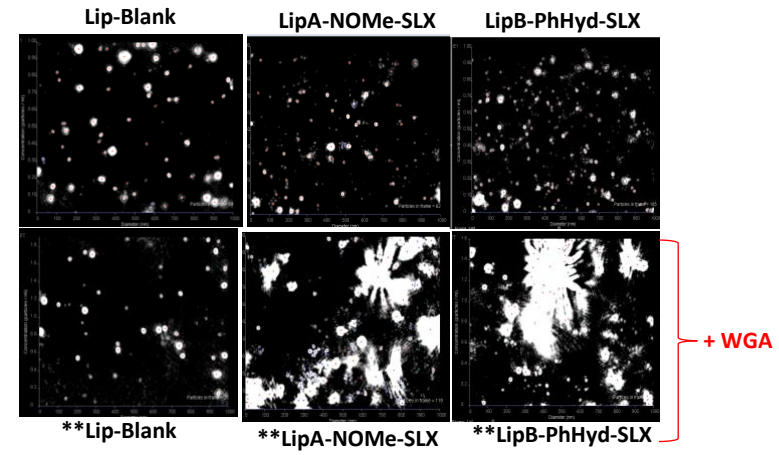

Figure 21 : Nanosight images display the aggregation of glycoliposome samples with the addition of WGA, a Sialic Acid specific lectin protein.
The samples tested are as follow: **Lip1-**Blank, **LipA-**NOMe-SLX, **LipB-**PhHyd-SLX. The blank liposome did not display any aggregate formation while liposomes A/B formed large aggregates following incubation with WGA.

These results are preliminary studies that indicate the advantage of the Nanosight-based aggregation assay. It provides a simple, straight forward method to analyze size variation in 1) the traditional way (size variation

Pre/Post Lectin incubation) through light scattering in addition to 2) tracking analysis that display the particles shift in size through scattered plot graphs, and 3) imaging which gives an instantaneous prediction of the glycofunctionalized surface through aggregate formation.

Phenol-Sulfuric Assay

This calorimetric assay is a direct and rapid method for the detection and quantification of carbohydrates[85,86]. Virtually, the assay can be adapted to all classes of carbohydrates, including mono-, di-, oligo-, and polysaccharides. The method was first described by Dubois et al.[87] in 1951 and found great applications mostly in the food chemistry industry[88]. It entails the hydrolysis of carbohydrates via concentrated sulfuric acid to produce byproducts (furfural derivatives) detectable via visible light absorption as a yellow complex when reacted with phenol. Therefore, the concentration of carbohydrates can reliably be quantified by extrapolating corresponding values from set calibration curves of each carbohydrate tested. Subsequent efforts have been focused on the optimization of the assay to reduce the volumes used, standardize the procedures for high throughput screening, or use it in wider range applications for the quantification of glycoproteins,

[85] X. Wang, O. Ramstrom and M. Yan, J. Mater. Chem., 2009, 19, 8944–8949
[86] . Durka, K. Buffet, J. Iehl, M. Holler, J. F. Nierengarten, J. Taganna, J. Bouckaert and S. P. Vincent, Chem. Commun., 2011, 47, 1321–1323.
[87] Dubois M, Gilles K, Hamilton J, Rebers P, Smith F. A colorimetric method for determination of sugars. Nature 1951;4265, 167.
[88] Brummer, Yolanda & Cui, Steve. (2005). Understanding Carbohydrate Analysis. Food Carbohydrates: Chemistry, Physical Properties, and Applications.

glycomaterials, etc[89,90, 91,92]. This study focused on generating a standard method for the detection and quantification of carbohydrates functionalized on the outer surface of liposomes or nanoparticles. The method has been optimized to detect micromolar range of carbohydrate concentration, using small volumes, no heat requirement, and a 96 wells microplate for high efficiency screening.

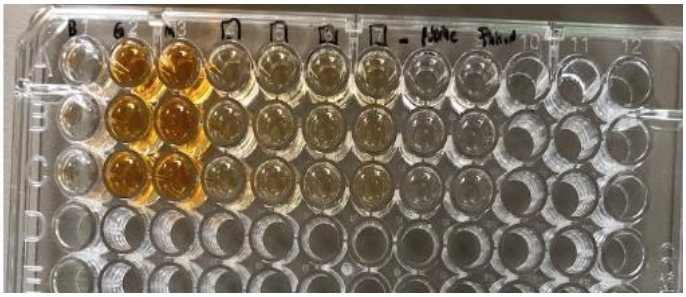

Figure 22: A microplate displaying the layout of a phenol-sulfuric assay. The darker orange color is indicative of a higher sugar concentration.

Direct detection of outer surface glycans

[89] Saha SK, Brewer CF. Determinations of the concentration of oligosaccharides, complex type carbohydrates, and glycoproteins using the phenol sulfuric-acid method. Carbohydr Res 1994;254:157–67.
[90] Masuko T, Minami A, Iwasaki N, Majima T, Nishimura S-I, Lee YC. Carbohydrate analysis by a phenol-sulfuric acid method in microplate format. Anal Biochem 2005;339(April (1)):69–72.
[91] Agbenorhevi JK, Kontogiorgos V. Polysaccharide determination in pro- tein/polysaccharide mixtures for phase-diagram construction. Carbohydr Polym Elsevier Ltd 2010;81(4):849–54.
[92] Noyes, A., Godavarti, R., & Titchener-hooker, N. (2014). Quantitative high throughput analytics to support polysaccharide production process development Quantitative high throughput analytics to support polysaccharide production process development. *Vaccine*, *32*(24), 2819–2828.

In sum, 30μL of 0.1 mM liposome (normalized via Stewart Assay) was pipetted into a microwell plate, followed by the addition of 50μL of 5 wt% phenol solution, and 200 μL of concentrated sulfuric Acid in the indicated order. The assay is photosensitive therefore the microplate was left under shaking *in the dark* for 15 minutes at room temperature and the maximum absorbance was detected at 485 nm using Spectrostar nanoabsorbance microplate reader (BMG LABTECH). Absorbance was collected for 9 samples against a blank over 6 time points (30min, 60min, 90min, 120min, 1000min, 1500min) to evaluate the behavior of the assay.

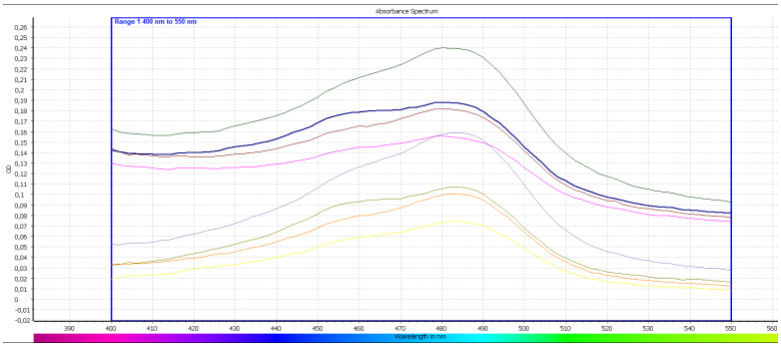

Figure 23: Detection of the Maximum Absorbance of the control and 7 liposome samples in Phenol-Sulfuric Acid Assay**.**

The direct assay was initially intended for the quantification of outer surface glycans. In order to do so, a calibration curve of the corresponding carbohydrate had to be constructed and used to extrapolate glycan the concentration. However, as displayed in *figure* , an increase in absorbance was noted in all samples (1-7) at 485nm, attributed to the lipidic content of the liposome which absorbs in the same range. Although a higher absorbance was noted in glycofunctionalized samples versus non-glycosylated samples, the accuracy of quantification was hindered due to the overlapping effect.

Another drawback of the direct assay was manifested at the time-point study, which revealed a consistent increase in absorbance over time especially in glycofunctionalized samples *(figure)*

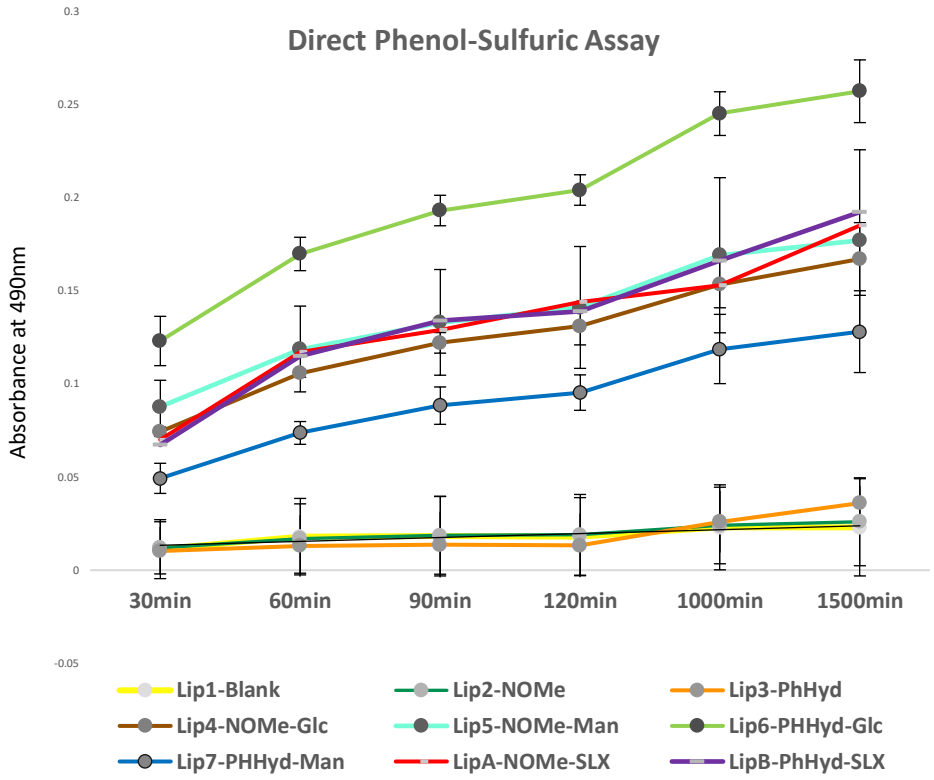

Figure 24: Phenol-Sulfuric Acid Assay for the detection of carbohydrates functionalized on the outer surface of liposomes. The 9 color coded samples tested are: 1) Blank lip,
2) Lip-NOMe, 3) Lip – PhHyd, 4) Lip- NOMe– Glucose,
5) Lip –NOMe- Mannose, 6) Lip- PhHyd - Glucose,
7) Lip- PhHyd– Mannose, A) Lip A-NOMe- SLX, B) Lip B-PhHyd-SLX. Data are expressed as the absorbance of each sample against the blank over 6 time points (30min, 60min, 90min, 120min, 1000min, 1500min). The bars represent ± SD, n=3.

In sum, there were multiple drawbacks to the use of the Direct Phenol-Sulfuric Assay as a Quantitative method:

1) The assay required the use of a large quantity of sample and is a destructive sampling method, therefore, non-efficient for large-scale screening.
2) The assay is photosensitive and must be handled in the dark to ensure that results are uncompromised.
3) The lipids component of liposomes displayed an overlapping absorbance between the blank and the samples, which hindered the accuracy of quantification of outer surface glycans.
4) Last, the time-point study of the assay revealed a consistent increase in absorbance over time especially in glycofunctionalized samples.

Following the aforementioned drawbacks, the assay applied directly on liposomes has proven to be a good general detection method for the presence of outer surface glycans but lacks in *validation* as an accurate quantitative method and in *efficiency* of screening.

Indirect quantification of outer surface glycans

To address the drawbacks of the direct method, an improved indirect quantification method was developed by our lab using a modified Phenol-Sulfuric assay procedure. Following a similar protocol to the new method developed by Zhou et al. for the evaluation of drug release kinetics of

nanoparticles inside a dialysis device[93], an indirect Phenol-Sulfuric method was developed and validated.

Figure 25: Indirect Phenol-Sulfuric Method using Vivaspin Concentrators for the detection/Quantification of outer-surface glycans functionalized to liposomes.

This method entails the use of Vivaspin centrifugal concentrators to remove carbohydrates that are non-bound to the outer surface of the liposome. Subsequently, the phenol-sulfuric assay was used directly on the filtrate containing non-bound carbohydrates, thus eliminating the overlapping effect of the blank liposome absorbance and avoiding the destruction of liposome samples. The degree of functionalization was *indirectly* determined by calculating the difference between the initial amount of carbohydrates used in the reaction and the non-bound amount of carbohydrate. Calibration curves had to be set concurrently at the same time point as the assay (30 minutes) to eliminate variation in absorbance over time, as displayed by the previous time-point study (*figure*). The amount of D- glucose and α-mannose

[93] ZHOU, Yousheng, et al. A new method for evaluating actual drug release kinetics of nanoparticles inside dialysis devices via numerical deconvolution. *Journal of Controlled Release*, 2016, 243: 11-20.

functionalized on the outer surface of liposomes (4-7) was calculated and found to be in the range of 4.6 – 4.8 μg per mmol liposome, while Sialyl Lewis X (A-B) was ranging between 3.8-4.2 μg per mmol liposome.

Phenol Sulfuric Assay Calibration Curves

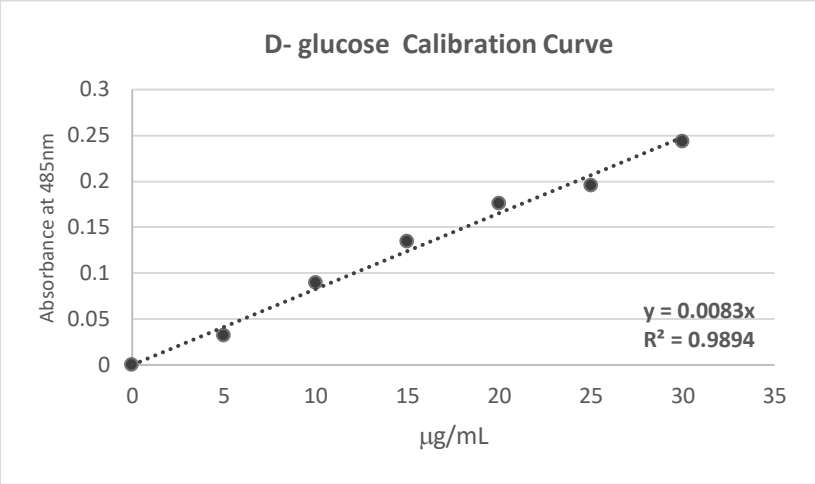

Figure 26 : Calibration curve of D-Glucose, representing the concentration-dependent absorbance of the Phenol-sulfuric assay at a (0-30) micromolar range; 30 minutes time-point. Absorbance was detected at 485nm wavelength. The linear equation is used for the extrapolation of the concentration values (μg/mL) corresponding to the absorbances detected of the unknown samples. N=5. *Calibration curves were constructed concurrently with the samples tested.

Phenol Sulfuric Assay Calibration Curves

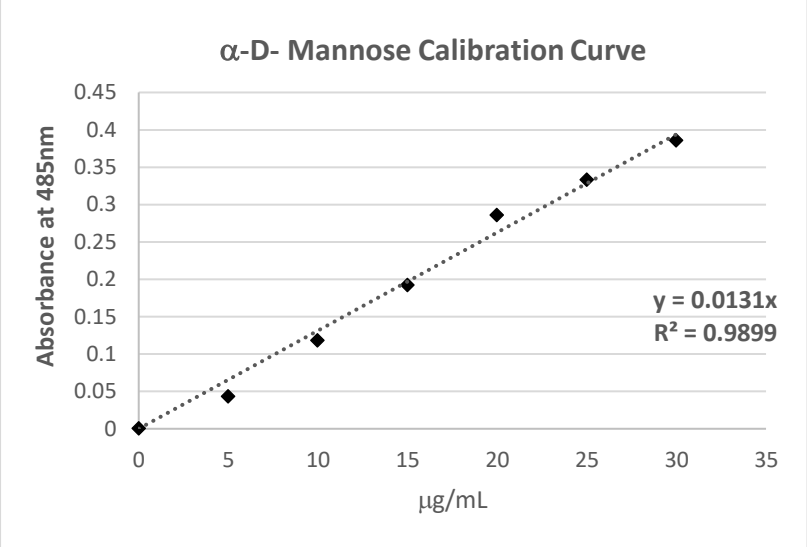

Figure 27 : Calibration curve of α-Mannose, representing the concentration-dependent absorbance of the Phenol-sulfuric assay at a (0-30) micromolar range; 30 minutes time-point. Absorbance was detected at 485nm wavelength. The linear equation is used for the extrapolation of the concentration values (µg/mL) corresponding to the absorbances detected of the unknown samples. N=5. *Calibration curves were constructed concurrently with the samples tested.

Phenol Sulfuric Assay Calibration Curves

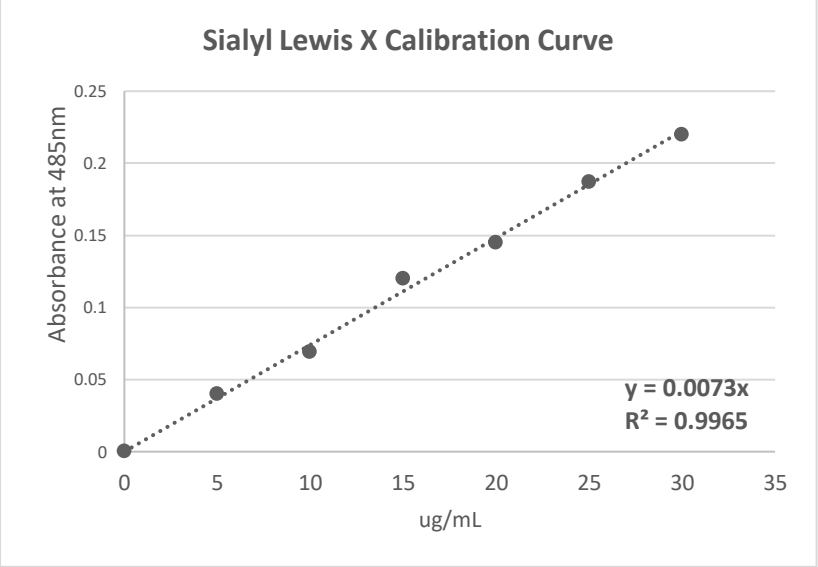

Figure 28 : Calibration curve of Sialyl Lewis X, representing the concentration-dependent absorbance of the Phenol-sulfuric assay at a (0-30) micromolar range; 30 minutes time-point. Absorbance was detected at 485nm wavelength. The linear equation is used for the extrapolation of the concentration values (μg/mL) corresponding to the absorbances detected of the unknown samples. N=5. *Calibration curves were constructed concurrently with the samples tested.

Experimentally, Vivaspin500 centrifugal concentrators (Membrane: 3000 MWCO PES for Glucose/Mannose and Membrane:5000 for Sialyl Lewis X) were used for the ultrafiltration of glycoliposomes. Calibration curves for D-

glucose and α-D-Mannose were constructed at concentrations (0-40 μg/mL) following the same Phenol-Sulfuric Assay procedure previously described, at 30 minutes time point. The parameters of ultrafiltration were calibrated and optimized using 150μL solutions of 1 μmol/mL of D-glucose and α-D-Mannose, separately, in order to mimic the conditions of the passage of unbound carbohydrates through the vivaspin500 filter. The collected filtrate was tested using the Phenol-Sulfuric assay at 30 minutes time-point (*figure)*, and the concentration values were extrapolated from the corresponding calibration curves.

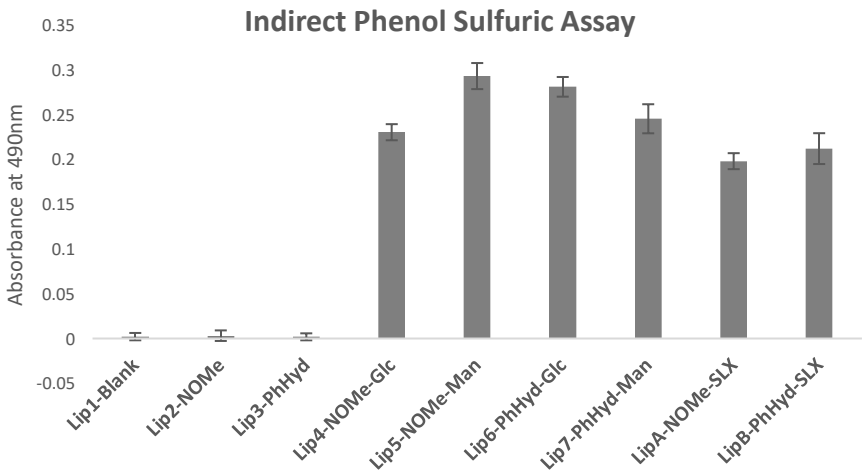

Figure 29: Indirect Phenol-Sulfuric Assay at 30-minutes time-point for the detection of carbohydrates unbound to the glycosylated liposome. Samples tested correspond to the filtrate separated via vivaspin500 centrifugal concentrators, reflecting the absorbance of unbound sugars per sample. Data are expressed as the absorbance of each sample against the blank. The bars represent ± SD, n=3.

As displayed in *figure,* insignificant values of absorbance were detected in samples (1-3). Meanwhile, samples (4-7 and A/B) displayed absorbance in 0.2-0.3 range. It is noteworthy to observe that the absorbance of mannose (liposomes 5 and 7) were slightly higher than glucose (liposomes 4 and 6). This phenomenon is well explained by the calibration curves that reflect that mannose has a slightly higher absorbance range in the phenol-sulfuric assay in comparison to glucose. All samples and corresponding calibration curves were assayed simultaneously to avoid the increase in absorbance over time. The concentration values corresponding to absorbances, extrapolated from the calibration curves in μg/mL were adjusted to the final volume of the filtrate (V_f), and corresponded to the amount of un-bound carbohydrates. The amount of carbohydrates functionalized on the outer-surface of liposomes was *indirectly* calculated by subtracting the un-bound amount from the initial amount of carbohydrate added to the reaction. The amount of D- glucose and α-mannose functionalized on the outer surface of liposomes (4-7) was found to be in the range of 4.6 – 4.8 μg per mmol liposome, while sialyl lewis X (A-B) was ranging between 3.8-4.2 μg per mmol liposome.

Advantages of the indirect Phenol-Sulfuric Assay for the Quantification of liposome outer surface glycans

The indirect Phenol-sulfuric method was found to be advantageous in many aspects; the method is replicable, sensitive to micromolar range, efficient for high throughput screening (using 96-well microplate), inexpensive, non-destructive to samples, and proven to be compatible with simple and complex

sugars. The assay was further used to test the kinetics of the glycofunctionalization reaction.

Kinetics of glycofunctionalization via chemoselective linkers

The indirect quantification method enabled the design of analytical studies of the glycofunctionalization reaction step directly on the surface of the liposome. This application was first tested in the analysis of the kinetics of the reaction. The rational for studying the glycofunctionalization kinetics was: 1) to study the behavior of the chemoselective reaction (optimal time, temperature, pH, sonication conditions,..), 2) to study the behavior of linker 1 versus linker 2 and determine if one displays a favorable profile.

Therefore, the rate of functionalization of the liposome with Sialyl Lewis X (SLX) was tested using linker 1 and linker 2 at room temperature versus conditions of applied heat/sonication over a 48h time frame. Indirect quantification was used to calculate the concentration of SLX on the outer surface of the liposome at each time point. Both linkers displayed similar kinetics, where glycofunctionalization occurred at the 24h-48h window. The effect of high temperature/sonication on the Kinetics of the reaction was slightly more evident in the rate of functionalization of linker 2 (PhHyd).

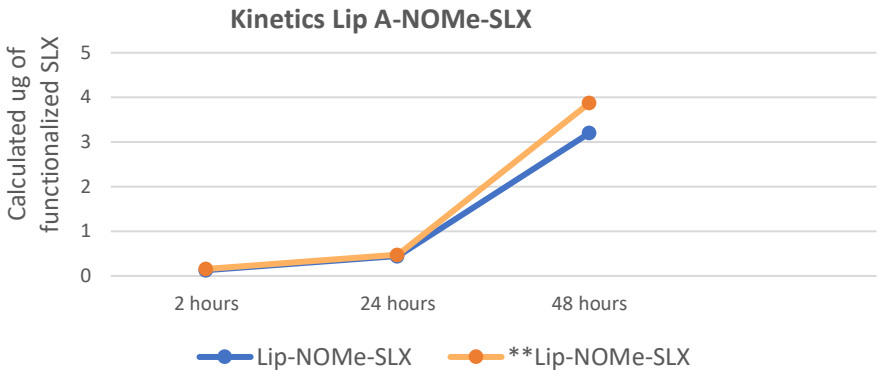

Figure 30: Indirect Phenol-Sulfuric Assay at time-points 2 hrs, 24 hrs, and 48 hrs for the analysis glycofunctionalization kinetics of Sialyl Lewis X with linker 1 (NOMe). Samples tested correspond to the filtrate separated via vivaspin500 (MW=5000) centrifugal concentrators, and values displayed correspond to the calculated amount of SLX in µg at each time point (A) Liposome A (Lip-NOMe-SLX) at RT (blue) versus heat/sonication (orange). (B) Lip B (Lip-PhHyd-SLX) at RT (blue) versus heat/sonication (orange). Both linkers display the same pattern with most of the functionalization occurring at the 24h-48h window**.**

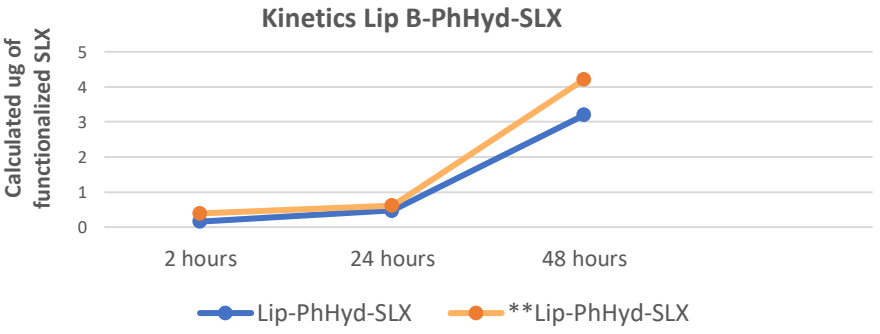

Figure 31: Indirect Phenol-Sulfuric Assay at time-points 2 hrs, 24 hrs, and 48 hrs for the analysis glycofunctionalization kinetics of Sialyl Lewis X with linker

2 (PhHyd). Samples tested correspond to the filtrate separated via vivaspin500 (MW=5000) centrifugal concentrators, and values displayed correspond to the calculated amount of SLX in μg at each time point (A) Liposome A (Lip-NOMe-SLX) at RT (blue) versus heat/sonication (orange). (B) Lip B (Lip-PhHyd-SLX) at RT (blue) versus heat/sonication (orange). Both linkers display the same pattern with most of the functionalization occurring at the 24h-48h window**.**

This preliminary study showed great potential in tracking the glycofunctionalization step in real-time in a similar approach to the use of Thin Layer Chromatography, and it could have wide applications in the instant characterization and optimization of chemoselective reactions used on the outer surface of nanoparticles.

Conclusion

In conclusion, liposomes were glycofunctionalized with unprotected glycans (Glucose, Mannose, Sialyl Lewis X) to exploit and implement the proposed chemoselective method via linkers (RNH-OMe and RNHNHPh). A complimentary agglutination assay using Nanosight was developed. Additionally, a Phenol-Sulfuric quantification assay, economic, efficient, compatible with all classes of glycans was and can thereof be used in a multitude of applications was designed. Future work will be aimed at engineering glycoliposomes as drug carriers to target overexpressed lectins in various pathologies.

Chapter 1: Experimental Section

One-Pot synthesis of thiol-functionalized linkers[94]

Linker 1

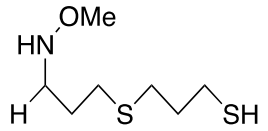

Chemical Formula: $C_7H_{17}NOS_2$
Exact Mass: 195.08
Molecular Weight: 195.34
m/z: 195.08 (100.0%), 197.07 (9.0%), 196.08 (7.6%), 196.07 (1.6%)
Elemental Analysis: C, 43.04; H, 8.77; N, 7.17; O, 8.19; S, 32.82

Step1

A.

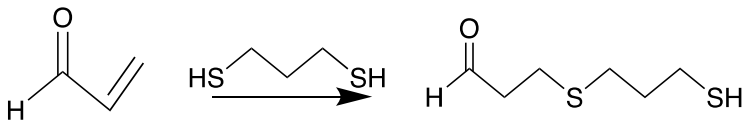

Reagents	MW	Mmol	Mass	Eq	Volume	Density
Acrolein	56.06	2.99	-	1	0.2 mL	0.839
Propane Dithiol	108.23	15	-	5	1.5 mL	1.08

- Acrolein added dropwise to 1,3 propanedithiol
- Reaction stirred for 2 hours at RT
- TLC 7:3 PtEt : AcOEt

[94] Munneke S., Prevost J. R. C.,Painter G. P.,Stocker B. L. ,Timmer M. S. The rapid and facile synthesis of Oxyamine linkers for the preparation of hydrolytically stable glycoconjugates. *Organic Letters* **2015,** *17* (3), 624-627.

Step2

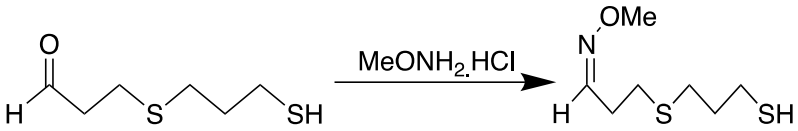

Reagents	MW	Mmol	Mass	Eq	Vol
Crude		3		1	
MethoxyAmineHCl	108.14	3.5	300 mg	1.2	
Sodium Acetate	82.03	6	492 mg	2	
EtOH					5mL

- Dissolve crude in EtOH Then add the other reagents
- Reaction stirred overnight at RT
- TLC 7:3 PtEt : AcOEt

Step 3

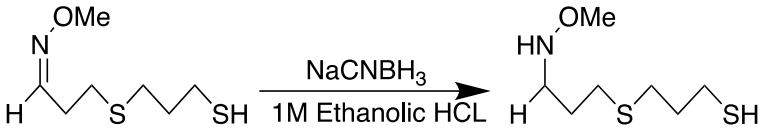

Reagents	MW	Mmol	Mass	Eq	Volume
Crude		1		1	
$NaBH_3CN$	62.84	4.5	282mg	4.5	
EtOH.HCl Dry					5mL

- Sodium cyanoborohydride added to the crude, followed by the dropwise addition of 1.25 M hydrogen chloride – ethanol solution (Reaction under inert condition – Argon)
- Reaction stirred for 1 hour at RT
- TLC 7:3 PtEt : AcOEt

Extraction

1- Product neutralized with sodium carbonate
2- Extracted with dichloromethane 3X
3- Dried over Na_2SO_4

Purification Silica gel column 20-30% ethyl acetate in petroleum ether
Product: Colorless cloudy oil with potent sulfide odor (Photosensitive)

Linker 1

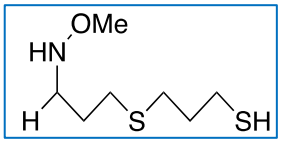

Linker 1: 3-(3-(Methoxyamino) propylthio) propane-1-thiol

Acrolein (0.2 mL, 2.99 mmol) was added dropwise to 1,3 propanedithiol (1.5 mL, 15 mmol), stirred at room temperature for 2 hours. The crude was dissolved in 5 mL EtOH, followed by the addition of methoxyamine hydrochloride (0.3g, 3.5mmol) and sodium acetate (0.492g, 6mmol). The mixture was stirred at room temperature for 16 hours. Last, sodium cyanoborohydride (0.282g, 4.5mmol) was added to the crude, followed by the dropwise addition of 1.25 M hydrogen chloride – ethanol solution (5 mL) at room temperature for 1 hour. The product was neutralized with sodium carbonate, extracted with CH_2Cl_2, and dried over Na_2SO_4. Purification via silica gel column (30% ethyl acetate in petroleum ether) yielded *methoxyamine linker 1* (82%) as a colorless cloudy oil with potent odor. R_f = 0.55 (30% ethyl acetate in petroleum ether). ^{1}H NMR (400 MHz, $CDCl_3$) δ 3.52 (s, 3H, OCH_3), δ 3.00 (t, 2H, $J_{1,2}$ = 6.8 Hz, CH_2-1), δ 2.63 (m, J= 7.1 Hz, 4H, CH_2-4, CH_2-6), δ 1.98 (t, J = 7.1 Hz, 2H, CH_2-3), δ 1.89 (p, J = 7.0 Hz, 2H, CH_2-5), δ 1.84 (p, J = 7.0 Hz, 2H, CH_2-2), δ 1.36 (t, J = 6.0 Hz, 1H, SH).^{13}C NMR ($CDCl_3$) δ 62.0 (OCH_3), 51.0 (C-1), 33.5 (C-5), 32.0 (C-4), 30.5 (C-3), 29.5 (C-2), 26.8 (C-6). MS $[M+H]^+$ m/z calcd: 196. 0801

Linker 2

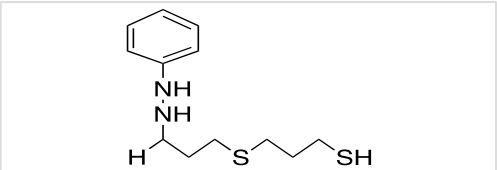

Chemical Formula: $C_{12}H_{20}N_2S_2$
Exact Mass: 256.11
Molecular Weight: 256.43
m/z: 256.11 (100.0%), 257.11 (13.0%), 258.10 (9.0%), 257.11 (1.6%)
Elemental Analysis: C, 56.21; H, 7.86; N, 10.92; S, 25.01

Step1

A.

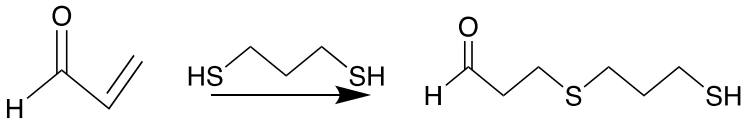

Reagents	MW	Mmol	Mass	Eq	Vol	Density
Acrolein	56.06	2.99	-	1	0.2 mL	0.839
Propane Dithiol	108.23	15	-	5	1.5 mL	1.08

- Acrolein added dropwise to 1,3 propanedithiol
- Reaction stirred for 2 hours at RT
- TLC 7:3 PtEt : AcOEt

Step2

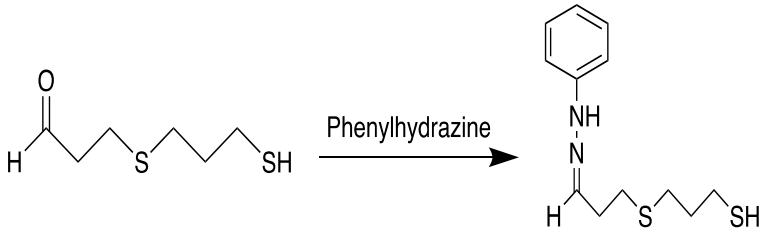

Reagents	**MW**	**Mmol**	**Mass**	**Eq**	**Vol**	**σ**

Crude		3		1		
Phenyl Hydrazine		3.5	378.49 mg	1.2	0.35mL	1.10
Sodium Acetate	82.03	6	492 mg	2		
EtOH					5mL	

- Dissolve crude in EtOH Then add the other reagents
- Reaction stirred overnight at RT
- TLC 7:3 PtEt : AcOE

Step3

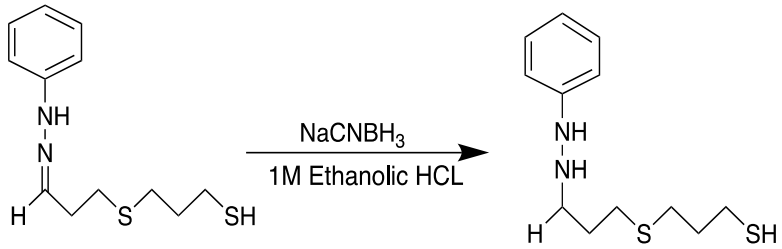

Reagents	**MW**	**Mmol**	**Mass**	**Eq**	**Vol**
Crude		1		1	
$NaBH_3CN$	62.84	4.5	282mg	4.5	
EtOH.HCl Dry					5mL

- Sodium cyanoborohydride added to the crude, followed by the dropwise addition of 1.25 M hydrogen chloride – ethanol solution (Reaction under inert atmosphere – Argon)
- Reaction stirred for 1 hour at RT
- TLC 7:3 PtEt : AcOEt

Extraction

4- Product neutralized with sodium carbonate
5- Extracted with dichloromethane 3X
6- Dried over Na_2SO_4

Purification Silica gel column 20-30% ethyl acetate in petroleum ether
Product: Yellow oil with potent sulfide odor (Photosensitive)

Linker 2

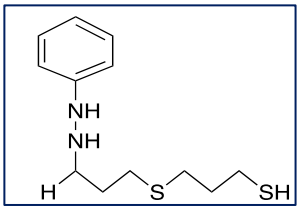

Linker 2: 3-(3-(phenylhydrazine) propylthio) propane-1-thiol

Acrolein (0.2 mL, 2.99 mmol) was added dropwise to 1,3 propanedithiol (1.5 mL, 15 mmol), stirred at room temperature for 2 hours. The crude was dissolved in 5 mL EtOH, followed by the addition of phenylhydrazine (0.35 mL, 5mmol) and sodium acetate (0.492g, 6mmol). The mixture was stirred at room temperature for 16 hours. Last, sodium cyanoborohydride (0.282g, 4.5mmol) was added to the crude, followed by the dropwise addition of 1.25 M hydrogen chloride – ethanol solution (5 mL) at room temperature for 1 hour. The product was neutralized with sodium carbonate, extracted with CH_2Cl_2, and dried over Na_2SO_4. Purification via silica gel column (30% ethyl acetate in petroleum ether) yielded *phenylhydrazine linker 2* (84%) as a yellow oil with potent odor. R_f = 0.51 (30% ethyl acetate in petroleum ether). ^{1}H NMR (400 MHz, $CDCl_3$) δ 7.2-6.8 (m, 5H, Aromatic-CH), δ 2.95 (t, 2H, $J_{1,2}$ = 6.6 Hz, CH_2-1), δ 2.65-2.55 (m, J= 7.1 Hz, 6H, CH_2-4, CH_2-6, CH_2-3), δ 1.95 (p, J = 7.1 Hz, 2H, CH_2-5), δ 1.79 (p, J = 7.1 Hz, 2H, CH_2-2), δ 1.28 (t, J = 6.0 Hz, 1H, SH).^{13}C NMR ($CDCl_3$) δ 128.04 (C-7), δ 122.3 (C-10), δ 118.01-118.9 (C-9), δ 112.1 (C-8), δ 51.2 (C-1), 33.07 (C-5), 30.0 (C-4), 29.5 (C-3), 28.02 (C-2), 27.5 (C-6). MS $[M+H]^+$ m/z calcd: 257.110.

(^{1}H NMR, $CDCl_3$, 400MHz)

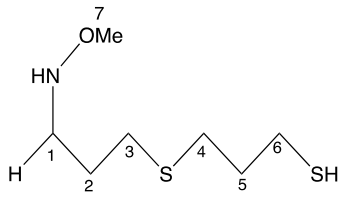

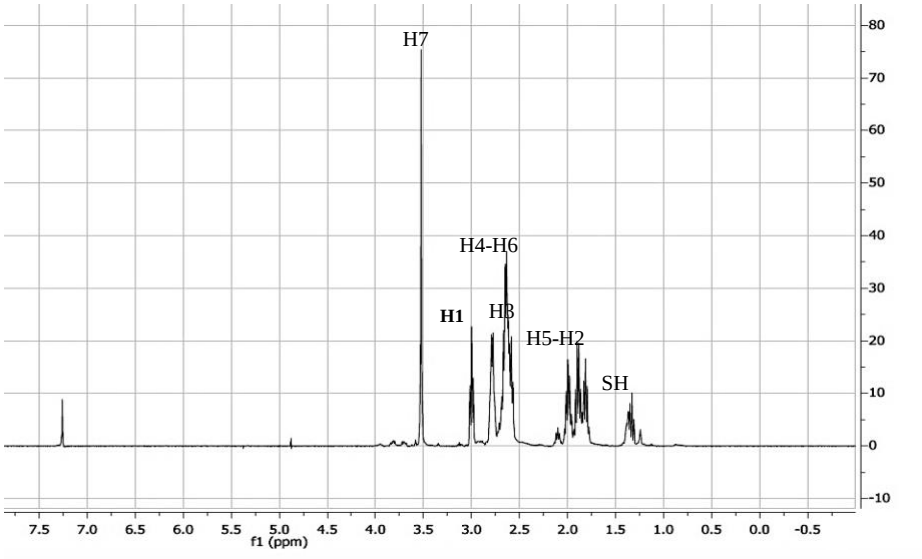

^{13}C NMR ($CDCL_3$, 400MHz)

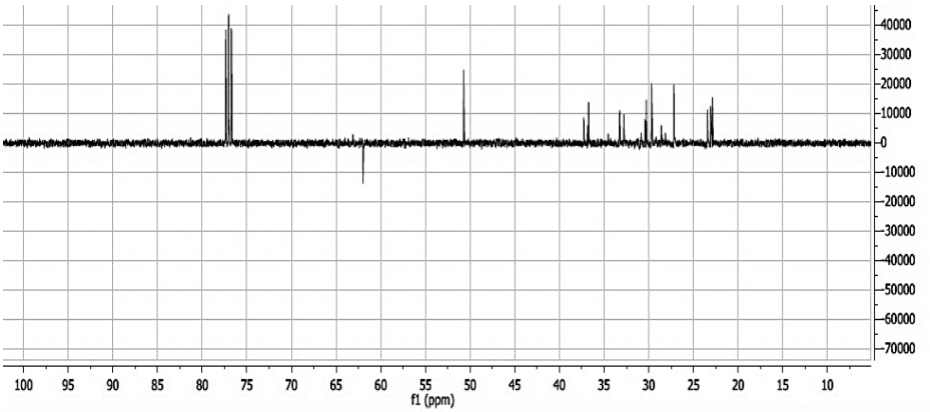

(^{1}H NMR, $CDCl_3$, 400MHz)

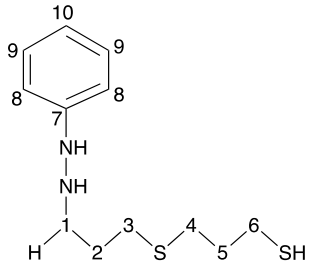

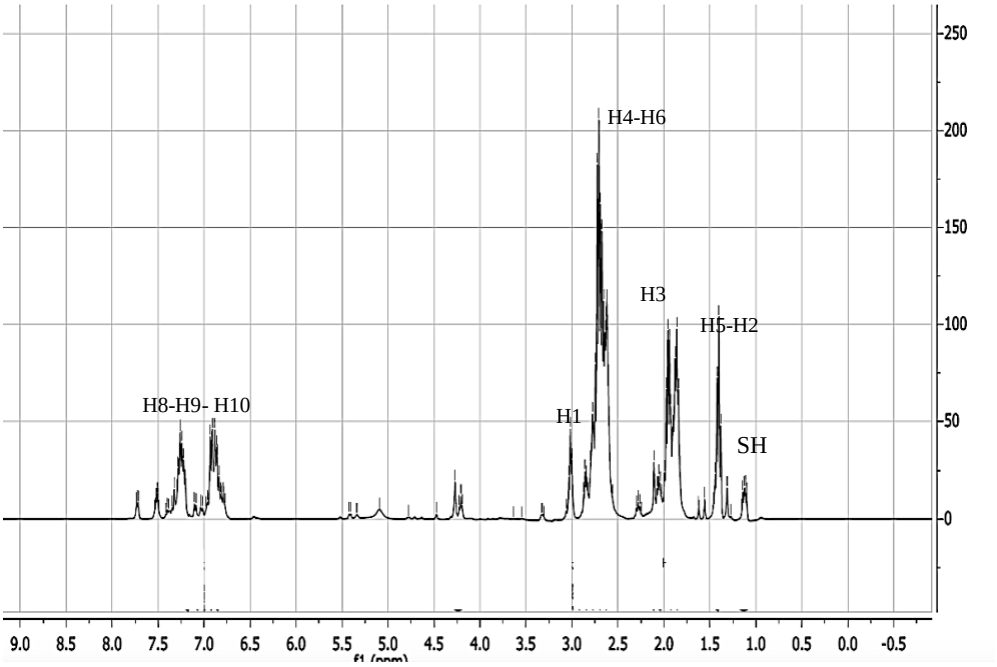

gCOSY ($CDCL_3$, 400MHz)

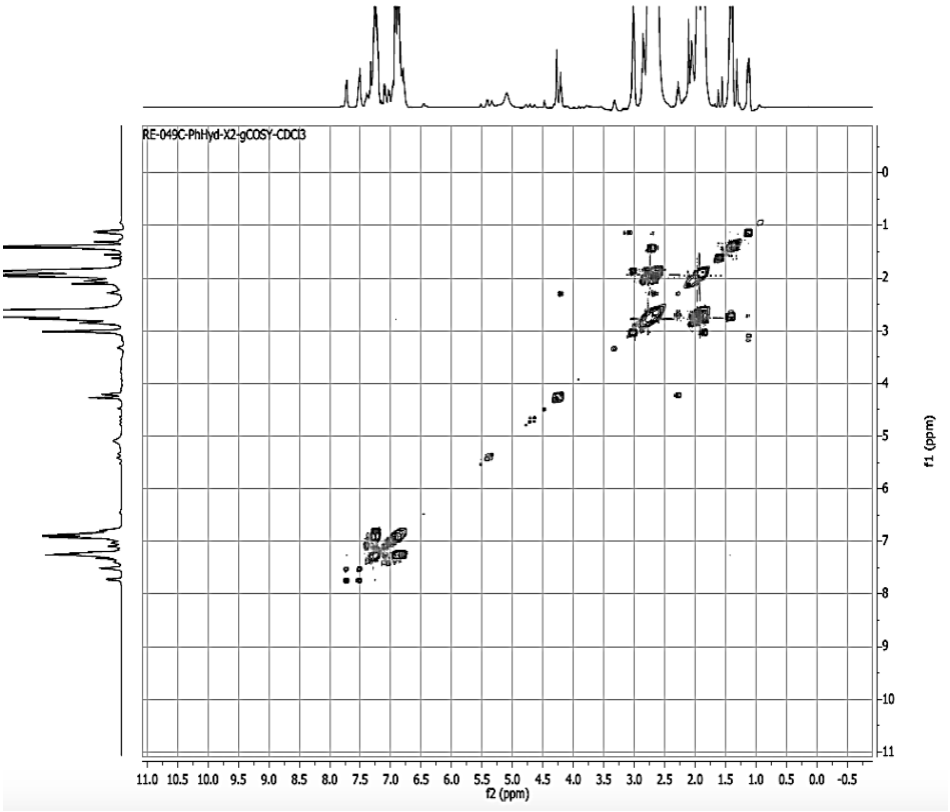

^{13}C NMR ($CDCL_3$, 400MHz)

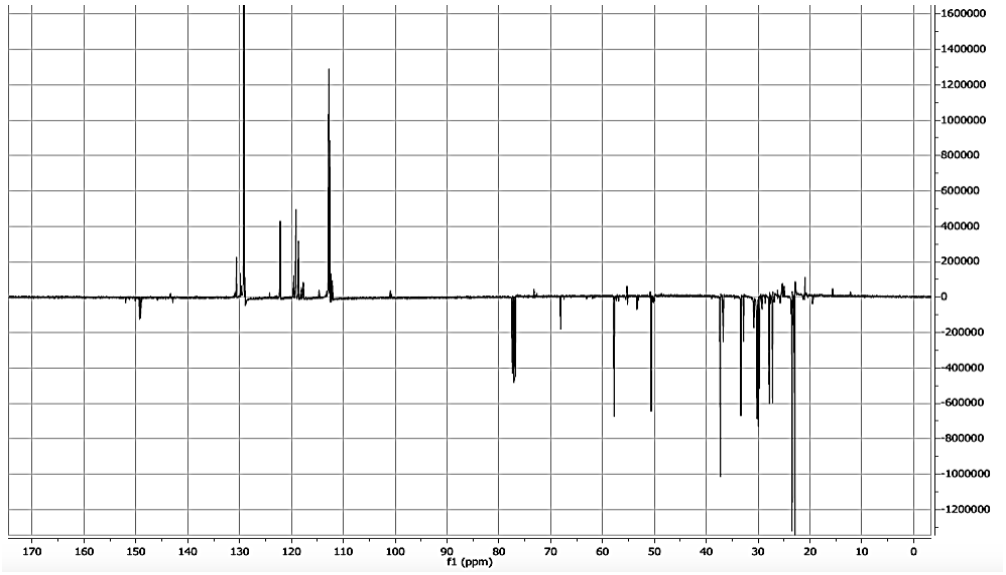

HSQC ($CDCL_3$, 400MHz)

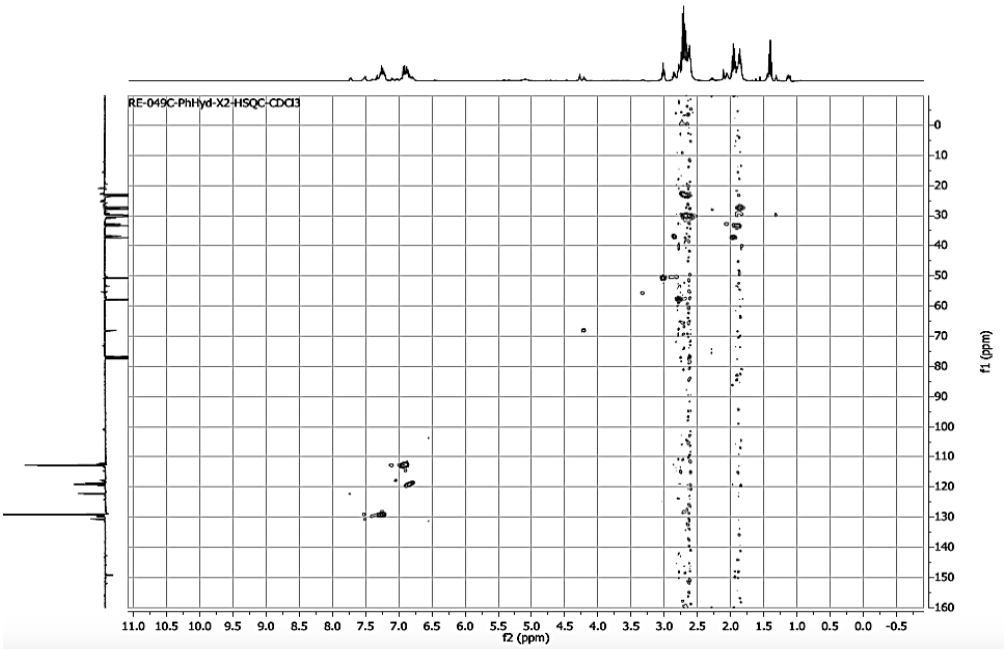

Liposomes functionalization

Assembly

The liposomes used in the study are a matrix of 1:1 ratio of sphingomyelin: cholesterol in addition to a 2.5% of the total ratio of DSPE-PEG-Maleimide. The three components were dissolved in chloroform/methanol 2:1, followed by the evaporation of the organic solvents. The lipid film was rehydrated in PBS buffer for a final molarity of 5mM, vortexed, and extruded 10 times at 55°C through a stack of two polycarbonic 100 nm filters under 20 bar nitrogen pressure.

Liposome Biofilm	MW
Cholesterol	386.7
Sphingomyelin	731
DSPE-PEG-Maleimide	2941.6

**Stock prepared in 2:1 Chloroform/MeOH solution

Cholesterol Stock (100mg/mL)	Sphingomyelin Stock (50mg/mL)	DSPE-PEG-Maleimide Stock (10mg/mL)
48.75%	48.75%	2.5%
1.88mg	3.5mg	735µg
18.8µL	70µL	73.5µL

Procedure

1) All layers added in a glass tube
2) Nitrogen flux used to evaporate solvent and dry out the biofilm
   **Biofilm must appear white as an indication that organic solvent is completely evaporated → to avoid damaging the filter of the extruder
3) Add 2 mL of PBS + vortex to obtain

$$\text{Molarity} = \frac{10\ uM\ of\ Lipids}{2mL\ PBS} = 5mM$$

4) Solution vortexed – soaked in 60C bath – vortexed repeatedly until It becomes a cloudy white solution

5) Extruder is calibrated with PBS, the biofilm suspended in PBS
   Is extruded 10X through a 100nm filter to produce uniform
   Liposomes size range 100-150nm.

6) 10uL of liposomes is suspended in 1mL of milliQ water to prepare
   Sample for DLS analysis (Blank liposome size ranges between 130-140nm in size)

Figure 31: extruder used for the formation of uniform liposomes

STEWART ASSAY

Stuart assay[95] is used to quantify the liposomes. The [Fe] group in the Stuart reagent couples with the phospholipid groups of the sphingomyelins → visible in UV range at an Absorbance = 485

Sample Preparation:

1. Add 2mL of Chloroform to 10uL of sample to break the liposomes
2. Add 2mL of Stuart reagent (dark red) to the solution
3. Vortex for 90 seconds
4. Let the solution rest for 5 minutes to separate into 2 layers
5. Top layer → dark red (removed using a vacuum pipette)
6. Bottom layer → placed in a glass cuvette to measure the absorbance (UV Spectrometer = 485λ) versus blank (chloroform)
7. The concentration of phosphate was determined using the following equation $y = 0.005x$

Example: Sample (A) absorbance = 0.0639 (y-value)

Using the equation x = 12.78 μg/10uL
(concentration of phospholipids per 10uL)

Therefore, x = 2556 μg per 2mL

Initial Amount of Sphingomyelin in the solution was 3500 μg

[95] Stewart, J.C.M. Colorimetric determination of phospholipids with ammonium ferrothiocyanate. (1980). *Anal Biochem. 1980;104(1):10-4.*

Therefore, % Yield $= \frac{2556}{3500} = 73\%$

The percent yield is used to calculate μmoles of Maleimide, used for the following functionalization step as follows:

2.5% DSPE-PEG-Maleimide of 10uM lipids = 0.25% μmoles
73% of 0.25% μmoles = 0.1825 μmoles

Functionalization of Linkers

The first step of the functionalization is the maleimide-thiol crosslinking reaction conducted at pH=7.4 in PBS. Maleimide groups were exposed on the outer surface of the liposome as the chain-ends of the embedded DSPE-PEG, thus maximizing the contact the thiol groups of the methoxyamino linker (linker 1) producing liposome 2 (Lip2-NOMe) and the phenylhydrazine linker (linker 2) producing liposome 3 (Lip3-PhHyd).

- **Functionalization Example**

Linker 1:

Reagents	MW	μmol	Mass	Eq	Vol
DSPE-PEG-Mal	2941.6	0.1825	-	1	
NOMe-Link1	195.34	0.365	71.2μg	2	

*Mass adjusted to PBS volume recovered from extrusion

Linker 2:

Reagents	MW	μmol	Mass	Eq	Vol
DSPE-PEG-Mal	2941.6	0.1825	-	1	
PhHyd-Link2	256.43	0.365	93.6μg	2	

*Mass adjusted to PBS volume recovered from extrusion

The second step of the functionalization is the chemoselective ligation between the nucleophilic group of linkers 1 and 2, and the reducing end of the selected glycan. Liposome 2 (lip2-NOMe) and liposome 3 (lip3-PhHyd) were both functionalized with 2 different commercial monosaccharides: D-glucose and α-D-Mannose to produce: liposome 4 (lip4-NOMe-Glc), liposome 5 (lip5-NOMe-Man), liposome 6 (lip6-PhHyd-Glc), liposome7 (lip7-PhHyd-Man). Additionally, as a proof of concept, linkers 1 and 2 were each functionalized with a complex glycan, Sialyl Lewis X, using the same conditions and producing liposome A (Lip-NOMe-SLX) and liposome B (Lip-PhHyd-SLX). The reaction was conducted at pH 4.5 (PH adjusted using 0.1 mM HCL solution and checked with Litmus indicator) over 48 hours at room temperature. Samples were purified via 24 hours dialysis against MilliQ water gradient.

- **Glycofunctionalization Example**

Linker 1:

Reagents	MW	μmol	Mass	Eq	Vol
NOMe-Link1	195.34	0.1825		1	
Glucose	180.156	0.9125	164.39μg	5	

*Mass adjusted to the selected volume of the reaction

Reagents	MW	μmol	Mass	Eq	Vol
NOMe-Link1	195.34	0.1825		1	
Mannose	180.156	0.9125	164.39μg	5	

*Mass adjusted to the selected volume of the reaction

Reagents	MW	μmol	Mass	Eq	Vol
NOMe-Link1	195.34	0.1825		1	
Sialyl Lewis X	820.744	0.9125	748.9μg	5	

*Mass adjusted to the selected volume of the reaction

Linker 2:

Reagents	MW	μmol	Mass	Eq	Vol
PhHyd-Link2	256.43	0.1825		1	
Glucose	180.156	0.9125	164.39μg	5	

*Mass adjusted to the selected volume of the reaction

Reagents	MW	μmol	Mass	Eq	Vol
PhHyd-Link2	256.43	0.1825		1	
Mannose	180.156	0.9125	164.39μg	5	

*Mass adjusted to the selected volume of the reaction

Reagents	MW	μmol	Mass	Eq	Vol
PhHyd-Link2	256.43	0.1825		1	
Sialyl Lewis X	820.744	0.9125	748.9μg	5	

*Mass adjusted to the selected volume of the reaction

Liposome characterization

- **Agglutination Assay**

- **Part I: Turbidity**

  Liposomes were prepared in Dulbecco's PBS (0.1mM), and the concentration values were normalized using the Stewart assay via quantification of sphingomyelin[96]. Concavalin A was prepared in Dulbecco's PBS (0.1M) containing $MgCl_2$ + $CaCl_2$, necessary for the activation of the lectin. Then, 100μL of Con A stock was added to 900μL of each liposome sample. Samples were analyzed after 24 hours incubation with the lectin by pipetting 270μL of each sample in

a microplate, absorbance measured via spectrophotometer at λ=495nm.

- **Part II: Nanosight (Tracking analysis for Size and Imaging)**
  The same procedure was followed. Liposomes were prepared in Dulbecco's PBS (0.1mM), and the concentration values were normalized using the Stewart assay via quantification of sphingomyelin[97]. Concavalin A was prepared in Dulbecco's PBS (0.1M) containing $MgCl_2$ + $CaCl_2$, necessary for the activation of the lectin. Then, 100μL of Con A stock was added to 900μL of each liposome sample. Samples were analyzed after 24 hours incubation with the lectin by preparing 10μL of (24h sample+ConA) + 990μL of MilliQ water. Each final sample was injected into the nanosight to produce tracking analysis and imaging data as previously displayed.

- **Sulfuric Assay**

  1) Direct Assay

Using a microplate, items were pipetted in the following order

1. 30μL of 0.1 mM liposome (Normalized via Stewart Assay)
2. 50μL of 5 WT% Phenol solution
3. 200 μL of Concentrated Sulfuric Acid
4. The microplate was left under shaking for 15 minutes at room temperature and the maximum absorbance was detected at 485 nm using Spectrostar nanoabsorbance microplate reader (BMG LABTECH).

5. Absorbance was collected for all samples against a blank (5% Phenol + Sulfuric Acid)

---

2) INDIRECT Assay

Using a microplate, items were pipetted in the following order

1- 30μL of Vivaspin Filtrate of free unbound carbohydrates (indicated in the figure below)*******The concentration values were adjusted to the volume of sample used in vivaspin.*

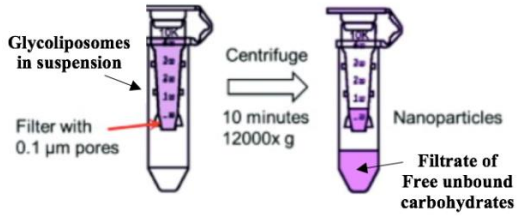

Figure 32: *Vivaspin filtrate used for the separation of unbound carbohydrates*

2- 50μL of 5 WT% Phenol solution

3- 200 μL of Concentrated Sulfuric Acid

4- The microplate was left under shaking for 15 minutes at room temperature and the maximum absorbance was detected at 485 nm using Spectrostar nanoabsorbance microplate reader (BMG LABTECH).

5- The concentration values were extrapolated from the calibration curves corresponding to each sugar (dilutions/sample quantity used in the analysis were factored in).

CHAPTER 2

In vitro cytotoxicity assay and cell uptake Using macrophages RAW 264.7

The relevance of glycofunctionalization strategies on nanoparticle-cell interaction was tested using RAW 264.7 (murine macrophage cell line). Macrophages express C-type lectins CD206 (Cluster of differentiation 206) that are specific for mannose. The strategy of targeting Mannose-specific CD206 lectins has been widely studied for various purposes.

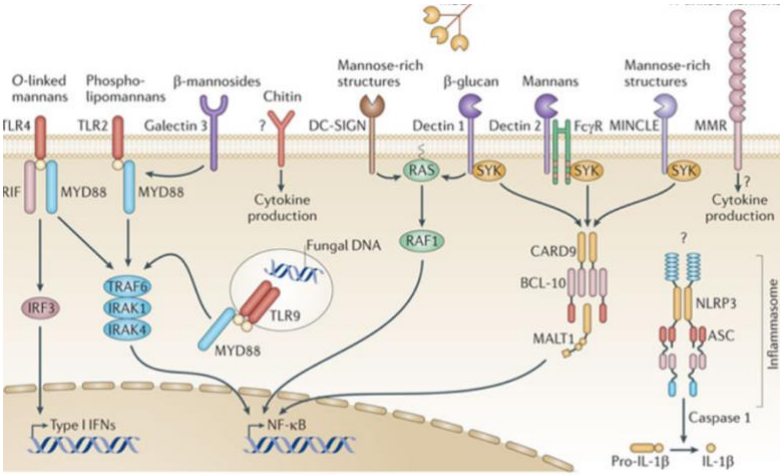

Figure 1: Receptors displayed on the outer surface of macrophages

Most recently, Hagimori et al.[98] designed mannose-grafted lipids to produce liposomes able to target the macrophages of invasive tumors microenvironment. Meanwhile, Filatova et al. [99,] used mannose-liposomes for the targeted delivery of anti-tuberculosis drugs to macrophages. Other studies used the targeting property for the downregulation of NFKB pathway involved in cancer metastasis signaling[100], or to design mannose receptor-targeted Vaccines [101]. In this study, since our strategy was the design of a glycofunctionalization method compatible with all commercially unmodified sugars bearing a reducing end (-OH), Glucose and Mannose functionalized liposomes were directly compared and tested for macrophages targeted cell-uptake. Images were collected using **Operetta high-content imaging system (PerkinElmer)** and the uptake was studied using the analysis software in the form of intensity of FITC-labeled liposomes per number of nuclei/sample. Additionally, The toxicity of the liposomes (1-7) was verified via MTT assay using the same cell line due to its high sensitivity to nanoparticles[102].

---

[98] Hagimori, Masayori, et al. "Synthesis of high functionality and quality mannose-grafted lipids to produce macrophage-targeted liposomes." *European Journal of Pharmaceutical Sciences* 123 (2018): 153-161.

[99] Filatova, L. Yu, Natalya L. Klyachko, and Elena V. Kudryashova. "Targeted delivery of anti-tuberculosis drugs to macrophages: targeting mannose receptors." *Russian Chemical Reviews* 87.4 (2018): 374.

[100] Neog, Manoj Kumar, Farhath Sultana, and Mahaboobkhan Rasool. "Targeting RAW 264.7 macrophages (M1 type) with Withaferin-A decorated mannosylated liposomes induces repolarization via downregulation of NF-κB and controlled elevation of STAT-3." *International immunopharmacology* 61 (2018): 64-73.

[101] Keler, Tibor, Venky Ramakrishna, and Michael W. Fanger. "Mannose receptor-targeted vaccines." *Expert opinion on biological therapy* 4.12 (2004): 1953-1962.

**The following two experiments (Cell uptake and MTT assay) were performed in the laboratory of Prof. M. Masserini and Prof. F. Re in Collaboration with Dott .B. Formicola and Dott. R. Dal Magro at the department of Medicine and Surgery, Vedano al Lambro, MB, UNIMIB.*

In vitro cytotoxicity Assay
Macrophages RAW 264.7

The toxicity of liposomes (1-7) was verified via MTT assay using RAW 264.7 cell line. Experimentally, the concentration of 0.01 mM liposome (Normalized via Stewart Assay) was used in the MTT assay at time points 3 hours and 24 hours. As displayed in the figure below, the samples displayed no significant toxicity at the 3-hour time-point with a % viability ranging between 98%-107%.

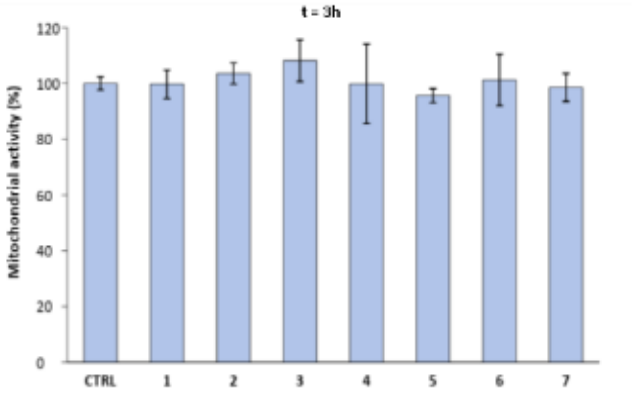

[102] M. Moros, B. Hernáez, E. Garet, J. T. Dias, B. Sàez, V. Grazù, Gonzalez-Fernandez, C. Alonso, J. M. de la Fuente. Monosaccharides versus PEG-functionalized NPs: influence in the cellular uptake. ACS Nano 2012, 6, 2, 1565-1577.

Figure 2 : MTT cytotoxicity assay performed on RAW 264.7 cells (murine macrophages cell line) at 3 hours. The 7 samples tested are labeled as follows: 1) Blank liposome, 2) Liposome-Aminooxy Linker, 3) Liposome – PhenylHydrazine Linker, 4) Liposome- Aminooxy linker – Glucose, 5) Liposome – Aminooxy Linker- Mannose, 6) Liposome-PhenylHydrazine linker- Glucose, 7) Liposome- PhenylHydrazine linker –Mannose. Data are expressed as the absorbance of each sample against the blank. The bars represent ± SD.

At 24 hours, **Lip1-Blank**>**Lip3-PhHyd**>**Lip2-NOMe** had low percent viability in the indicated magnitude. This finding is likely due to the toxic nature of maleimide exposed on the outer surface of the blank Lip1 as the end chain of the embedded DSPE-PEG-Maleimide. In fact, the liposomes functionalized with linkers 1 and 2 displayed an improvement in the cytotoxicity profile which could be attributed to the partial coverage of the liposomes with linkers, followed by the glycofunctionalization step that shielded the toxic liposome chain-ends with non-toxic outer surface glycans. Therefore, as displayed in *figure* glyco-liposomes (4-7) display 100% cell viability. This test was repeated to n=3 (LDH and MTT) with similar results, which highlights another valid aspect to the glycofunctionalization strategy; the improvement of cytotoxicity profile of drug carriers. These results also display that consistency in results between liposomes (4-7) thus indicating that they share a similar nature and topology post-glycofunctionalization step.

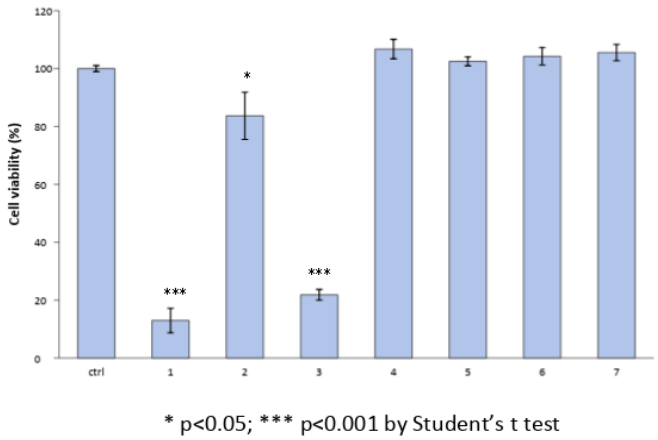

Figure 3 : MTT cytotoxicity assay performed on RAW 264.7 cells (murine macrophages cell line) for 24 hours. The 7 samples tested are labeled as follows: 1) Blank liposome, 2) Liposome-Aminooxy Linker, 3) Liposome – PhenylHydrazine Linker, 4) Liposome- Aminooxy linker – Glucose, 5) Liposome – Aminooxy Linker- Mannose, 6) Liposome- PhenylHydrazine linker- Glucose, 7) Liposome- PhenylHydrazine linker –Mannose. Data are expressed as the absorbance of each sample against the blank. The bars represent ± SD.

Cell Uptake RAW 264.7

For the cell-uptake study, Liposomes were prepared following the same procedure indicated in the previous experimental section with the addition of 0.5% fluorescent dye BODIPY (boron-dipyrromethene) sphingomyelin. Liposomes used in the study are: **Lip1**-Blank, **Lip4**-NOMe-Glucose, **Lip5**-NOMe-Mannose, **Lip6**-PhHyd-Glc, **Lip7**-PhHyd-Man. A concentration of 0.01 mM liposome (Normalized via Stewart Assay) was used in the assay at a 3-hour time point. Images were collected using **Operetta high-content imaging system (PerkinElmer)** and the uptake was detected using the analysis software in the form of intensity of FITC-labeled liposomes per number of nuclei/sample.

Figure 4: Operetta high-content imaging system (PerkinElmer)

Cell Uptake RAW 264.7

CTRL

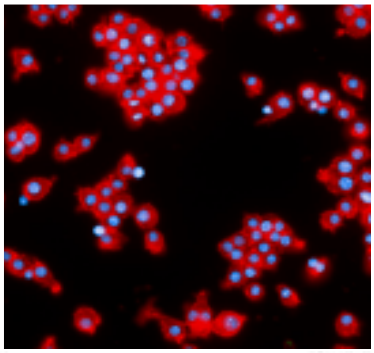

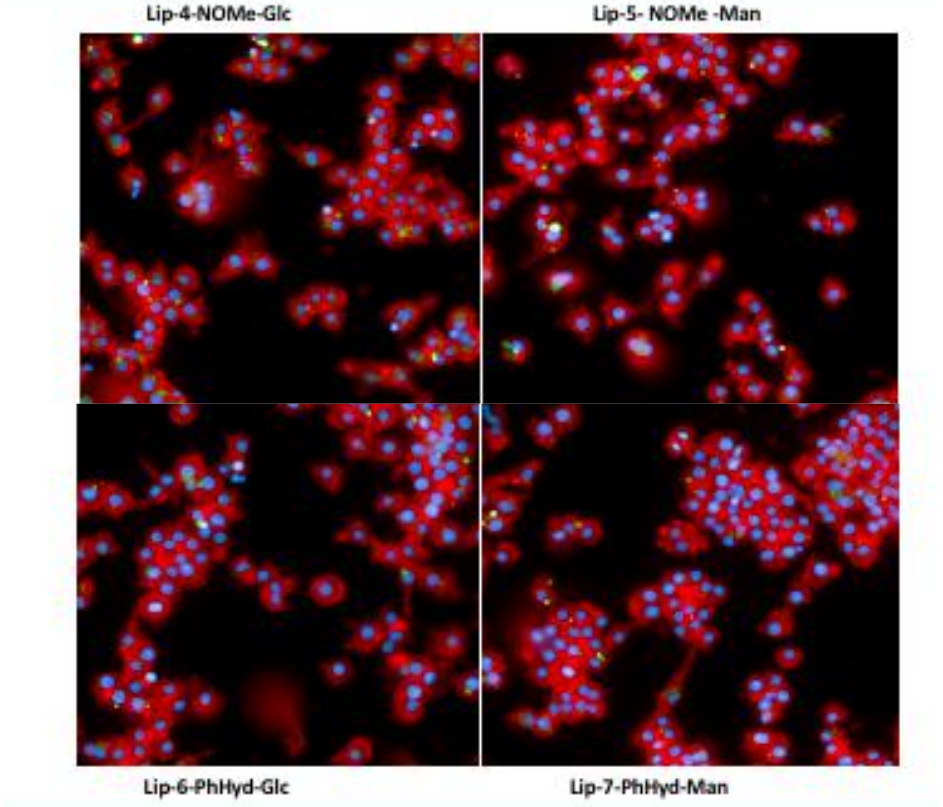

Figure 5: 3 hours Cell uptake study conducted on RAW 264.7 macrophage cell line. The 5 BODIPY fluorescently labeled samples tested are: **Lip1**-Blank, **Lip4**-NOMe-Glucose, **Lip5**-NOMe-Mannose, **Lip6**-PhHyd-Glc, **Lip7**-PhHyd-Man. N=1.

An increase in uptake of Mannosylated liposomes (5 and 7) would be expected due to the overexpression of CD206 receptors (C-type lectin specific for mannose) in macrophages. However, in this study, there was a large non-variable uptake noted in all 5 samples. This could be due to the 3 hours selected time-point that exceeds the receptor based selective active-uptake window of macrophages. Further studies should be conducted using different liposome concentrations and time points to better understand the behavior and variability of this hyper-responsive cell line.

Conclusion

Glucosylated and Mannosylated liposomes functionalized with linkers 1 or 2 displayed similar behaviors when tested with RAW 264.7 macrophages for cytotoxicity and cell uptake. They had low cytotoxicity at 3 hours and 24 hours' time-points, which make them promising candidates for the reduction of the cytotoxic profile of drug-encapsulated liposomes. In the uptake study, even though mannose mediated phagocytosis was observed to some degree, its overall efficiency in specific targeting was minor. These results conform to a similar study conducted by Wattendorff et al. using mannose-based ligands to target phagocytic C-type lectin receptors (CLRs) on human dendritic cells (DCs) and macrophages[103].

[103] Wattendorf, U., Coullerez, G., Vörös, J., Textor, M., & Merkle, H. P. Mannose-based molecular patterns on stealth microspheres for receptor-specific targeting of human antigen-presenting cells. *Langmuir*, 2008, *24*(20), 11790-11802.

Chapter 3

Gadolinium labeled Galactose and Sialyl Lewis X functionalized liposomes for *in-vitro and in-vivo* MRI studies of targeted delivery to Hepatocellular Carcinoma

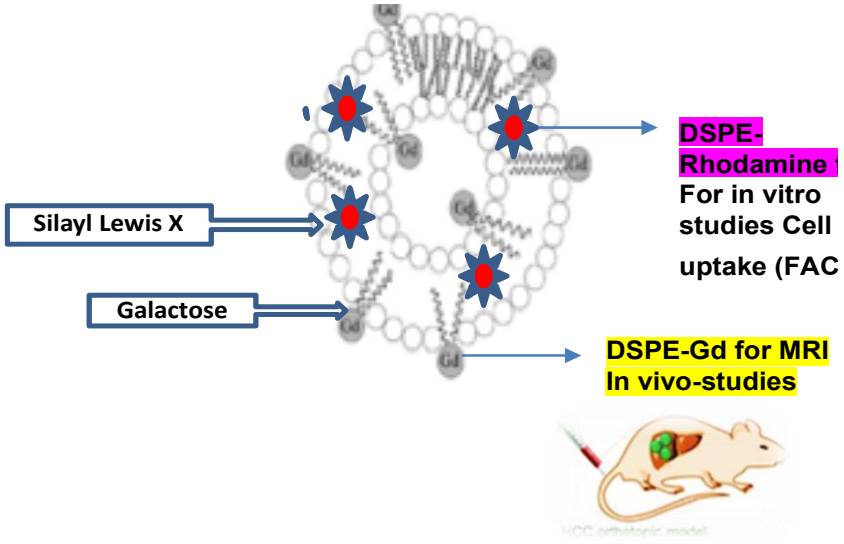

Introduction

Hepatocellular carcinoma (HCC) is an aggressive primary liver cancer, 5th most frequently diagnosed, and 2nd leading cause of death in life-threatening cancer cases worldwide[104]. It primarily affects hepatocytes which represent 80% of the hepatic cells [105]. The main obstacle that faces current therapeutic approaches is the low hepatocytic accumulation that occurs due to the fast onset uptake by Kupffer cells. Therefore, targeted delivery specific to hepatocytes has been a major topic of investigation[106]. Since the functionalization of drug carriers with different types of carbohydrate has been of great interest due to the overexpression of carbohydrate-specific receptors in various pathologies[107], in addition to the low cytotoxic profile of carbohydrates, this study was designed as follows; Asialoglycoprotein receptor (ASGPR), a hepatic lectin specific for D-galactose, and selectin, a sialic acid specific receptor overexpressed in proinflammatory tissues, were used as a target for the delivery of MRI compatible glycoliposomes encapsulated with Sorafenib (a first line defense drug).

---

[104] Torre, L.A., Bray, F., Siegel, R.L., Ferlay, J., Lortet-Tieulent, J., Jemal, A. Global cancer statistics. CA: cancer j clin, **2015,** 65: 87–108.
[105] Poelstra K, Prakash J, Beljaars L. Drug targeting to the diseased liver. J Control Release, **2012**, 161:188–97.
[106] Pranatharthiharan, S. Asialoglycoprotein receptor targeted delivery of doxorubicin nanoparticles for hepatocellular carcinoma. Drug delivery, **2017**; 24(1): 20-29.
[107] Huang, KW. Galactose Derivative-Modified Nanoparticles for efficient SiRNA delivery to hepatocellular carcinoma. Biomacromolecules, **2018;** 19: 2330-2339.

Strategy of Targeted delivery to Hepatocellular Carcinoma

i. Targeted Receptors

1) Asialoglycoprotein Receptor (ASGPR)

The galactose-specific hepatic lectin is expressed in abundance exclusively on hepatocytes (500,000.0 ASGPR per hepatocyte) and hepatoma cells in high density[108]. ASGPR can recognize β- D-galactose residues with high specificity and efficiency, thus enhancing the ligand-receptor mediated endocytosis of galactose decorated nanoparticles that act as diagnostic/therapeutic vehicles[109].

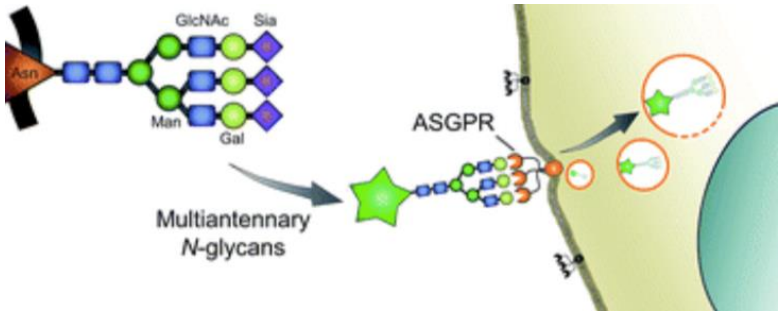

Figure 1: Hepatocyte specific targeting via ASGPR

[108] Huang, X., Leroux, J.C, Castagner, B. Well-defined multivalent ligands for hepatocytes targeting via asialoglycoprotein receptor, Bioconjugate Chem. **2017**, 28: 283–295.
[109] Zhong, Y., Meng, F., Deng,C., Zhong, Z. Ligand-directed active tumor-targeting polymeric nanoparticles for cancer chemotherapy, Biomacromolecules 15 (2014) 1955–1969.

➢ ***Experimental Strategy***

Glycofunctionalization of liposome with D-Galactose using the newly synthesized Phenyl Hydrazine Linker 2, to produce a targeted carrier for drug/contrast agent specific for ASGPRs overexpressed in the mutagenic conditions of advanced Hepatocellular Carcinoma[110].
This strategy has been priorly tested by multiple laboratories, but as far as our knowledge never in combination with encapsulated Sorafenib/Gadolinium[111].

2) Selectins

There are three known types of selectins with similar structural features including a Ca^{+2} dependent lectin domain[112] :

a. L-selectin (leukocyte adhesion molecule-1 [LECAM-1])
b. E-selectin (endothelial-leukocyte adhesion molecule-1 [ELAM-1])
c. P-selectin (GMP-140)

---

[110] Shi, Bin, Marc Abrams, and Laura Sepp-Lorenzino. "Expression of asialoglycoprotein receptor 1 in human hepatocellular carcinoma." *Journal of Histochemistry & Cytochemistry* 61.12 (2013): 901-909.
[111] Oh, H. R., Jo, H. Y., Park, J. S., Kim, D. E., Cho, J. Y., Kim, P. H., & Kim, K. S. Galactosylated liposomes for targeted co-delivery of doxorubicin/vimentin siRNA to hepatocellular carcinoma. *Nanomaterials*, **2016**, *6*(8), 141.
[112] Foxall, C., Watson, S. R., Dowbenko, D., Fennie, C., Lasky, L. A., Kiso, M., ... & Brandley, B. K. The three members of the selectin receptor family recognize a common carbohydrate epitope, the sialyl Lewis (x) oligosaccharide. *The Journal of cell biology*, *117*(4), (1992) 895-902.

These mammalian receptors are identified for their primary role as adhesion molecules between leukocytes and vascular endothelia. In proinflammatory environments; they facilitate the first line of inflammatory defense including lymphocyte homing, platelet binding, and neutrophil extravasation.

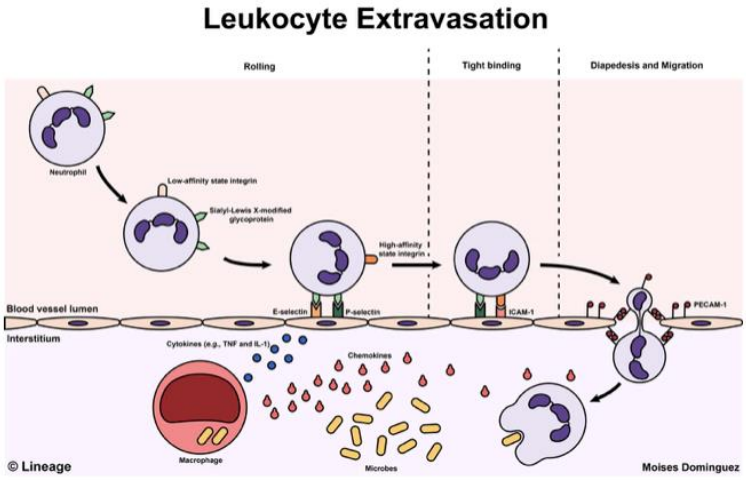

Figure 2: The role of selectin receptors in leukocyte extravasation. They have are essential in for the binding/rolling/internalization effect.

In this context, Sialyl Lewis X, a complex carbohydrate epitope, has been repeatedly reported as a ligand for all of L-, E-, and P-selectins, overly expressed in proinflammatory environments. It has also been directly associated with abnormal glycosylations that are used as a marker for malignant transformations found in the serum of cancer patients, and indicate

a distinct cell behavior related to selectin-mediated adhesion of cancer cells to vascular endothelium[113].

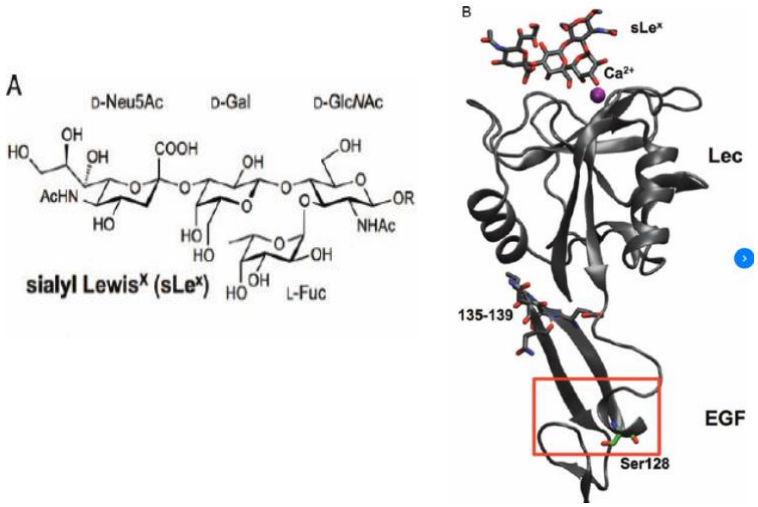

Figure 3: The structure of Sialyl Lewis X and its specificity for the selectin pocket.

- ***Experimental Strategy***

  Glycofunctionalization of liposome with complex glycan, Sialyl Lewis X, using the newly synthesized Phenyl Hydrazine Linker 2 for the targeted delivery to selectins overexpressed in the pro-inflammatory environment of Hepatocellular carcinoma.

ii. Encapsulated Drug

Sorafenib (Nexavar)

[113] Kannagi, R., Izawa, M., Koike, T., Miyazaki, K., & Kimura, N. (2004). Carbohydrate-mediated cell adhesion in cancer metastasis and angiogenesis. *Cancer science*, (2004), *95*(5), 377-384.

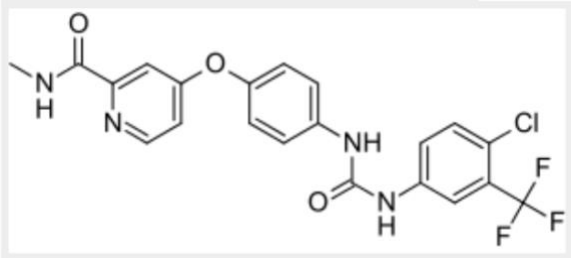

Figure 4: Molecular formula of Sorafenib (Nexavar)

Sorafenib is the only clinically FDA approved molecular targeting drug for advanced hepatocellular carcinoma, and is by default considered the standard treatment for HCC patients[114]. It is a multikinase inhibitor including tyrosine-kinase (PDGF and VEGF receptors). It also blocks the signaling pathway of serine/threonine kinases Raf-1 and B-Raf [115]. Some of the drawbacks of this treatment is that it suffers from low bioavailability (38-49%) and low solubility of approximately 1.7 μg/ml[116,117]. Additionally, as with most small molecules rapidly metabolized in the body, sorafenib causes adverse side effects ranging from hand-foot syndrome, diarrhea, fatigue, rash, and nausea.

[114] Lang, L. FDA approves sorafenib for patients with inoperable liver cancer. Gastroenterology. **2008**, 134(2), 379.
[115] Potenza N, Mosca N, Zappavigna S et al. MicroRNA-125a-5p is a downstream effector of sorafenib in its antiproliferative activity toward human hepatocellular carcinoma cells. J. Cell Physiol. **2017**, 232(7), 1907–1913.
[116] Liu C, Chen Z, Chen Y et al. Improving oral bioavailability of sorafenib by optimizing the 'spring' and 'parachute' based on molecular interaction mechanisms. Mol. Pharm. **2016,** 13(2), 599–608 (2016).
[117] Ranieri G, Goffredo V, Patruno . Sorafenib (BAY 43–9006) in hepatocellular carcinoma patients: from discovery to clinical development. Curr. Med. Chem. **2012,** 19, 938–944.

To address these shortcomings, a strategy entailing the design of a suitable drug carrier has been adopted by many researchers, in a similar approach to doxorubicin/doxil. Doxorubicin is an anthracycline chemotherapy dug approved by the FDA in 1974 and is commonly used in the treatment of various types of cancer including leukemia, breast/stomach/ovaries/thyroid/lung cancer, multiple myeloma, soft tissue sarcoma, and others. It shares a similarly poor biodistribution profile and induces cardiotoxicity especially in combinatorial drug therapy treatments. A pegylated liposome-encapsulated form of doxorubicin (Doxil)[118] was developed and approved by the FDA and a non-pegylated liposome-encapsulated form of doxorubicin (Myocet)[119] was developed and approved in Europe and Canada. The latter form of doxorubicin was found to display a more favorable biodistribution as well as reduced cardiotoxicity/risk of congestive heart failure.

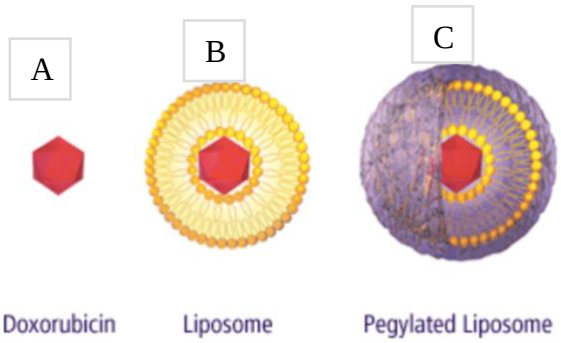

Figure 5: A display of A) Doxorubicin, B) Myocet, and C) Doxil

[118] Liposomal doxorubicin (Caelyx, Myocet) Macillan cancer support. 2009.
[119] Doxorubicin liposomal. Chemocare Cleveland clinic.2010.

➢ ***Experimental Strategy***

Following the same guidelines towards the improvement of Sorafenib's solubility profile and the reduction of small-molecule onset side effects, studies were conducted to encapsulate Sorafenib in the bilipid layer of the glycofunctionalized liposomes.

iii. Encapsulated Diagnostic MRI Contrast Agent

Gadolinium (III) Complex

This family of Gd chelated contrast agents is the most widely used for the enhancement of the body's internal structures in MRI scans to better visualize cranial, spinal, and breast scans in addition to vessels, vasculature, lesions, and tumors. Gadolinium (III) complex is used in the chelated form as displayed in the figure bellow to prevent the toxicity of gadolinium while preserving the contrast agent properties.

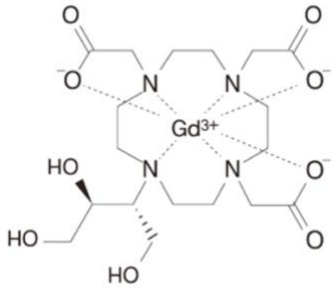

Figure 6: Gadobutrol (Gadovist), a clinically used gadolinium-based MRI chelated contrast agent.

➢ ***Experimental Strategy***

The design of a theragnostic tool by encapsulating 1.25 mM 16:0 PE-DTPA (Gd) 1**,**2-dihexadecanoyl-sn-glycero-3-phosphoethanolamine-N-diethylenetriaminepentaacetic acid (gadolinium salt) into the lipid bilayer. The contrast agent will be tested in-vitro via MRI in comparison to the clinical standard (Gadovist).

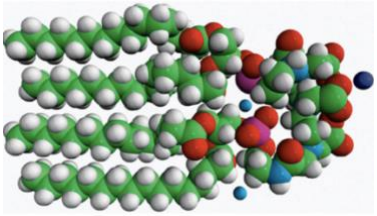

Figure 7: 16:0 PE-DTPA (Gd) embedded in the lipid biayer of the liposome

- **Further Considerations**

Sorafenib (SF) and gadolinium (Gd) co-loaded liposomes for drug delivery and MRI-guided HCC treatment

Beyond Glyco-Receptor-Targeting, the rational of the design of SF/Gd co-loaded liposomes is to test the following properties: (1) The structure of liposome could increase the solubility of SF; (2) SF/Gd-liposome could change the biodistribution of SF after injection. In effect, SF when encapsulated into liposome could be more easily accumulated in the tumor tissue due to the EPR effect; and (3) SF can be slowly released from the liposome because of the reservoir effect and still maintain an effective

therapeutic concentration in the tumor area for a longer period of time because of its prolonged blood circulation time, thus resulting in higher tumor growth inhibition.

This study was conducted at Nerviano Medical Sciences and consisted of three parts: 1) In-vitro HepG2 cell uptake of glycoliposomes, 2) In-vitro MRI analysis of Gd encapsulated liposomes, 3) In-vivo analysis of the Biodistribution of Gd-encapsulated glycoliposomes.

Part I: In vitro HepG2 cell uptake

Materials:

Cell Culture: Murine HCC cells (HepG2) were cultured in medium containing E-MEM + 2mL of L-glutamine +1% non-essential amino acids + 10% FBS. Incubation at 5% CO2 and 37°C.

Briefly, liposomes **Lip1-Blank**, **Lip2-Gal, Lip3-SLX** were added to cells at 0.1 mM concentration (Normalized via Stewart Assay) and incubated for 6 hours and 24 hours at both temperatures of 4°C and 37°C.

Competition assay

Murine HCC cells (HepG2) were preincubated with D-galactose (final concentration 10mM) and liposomes were added to each well following the same cell culture protocol for 6 hours and 24 hours incubation times at 4C and 37C.

Samples Tested

Sample 1: Blank Liposome

Sample 2: Lip- PhHyd-Galactose

Sample 3: Lip- PhHyd-Sialyl Lewis X

Incorporation of 1.5% of PEG-Rhodamine

+ encapsulation of Gd-1.25mM

Liposome Characterization

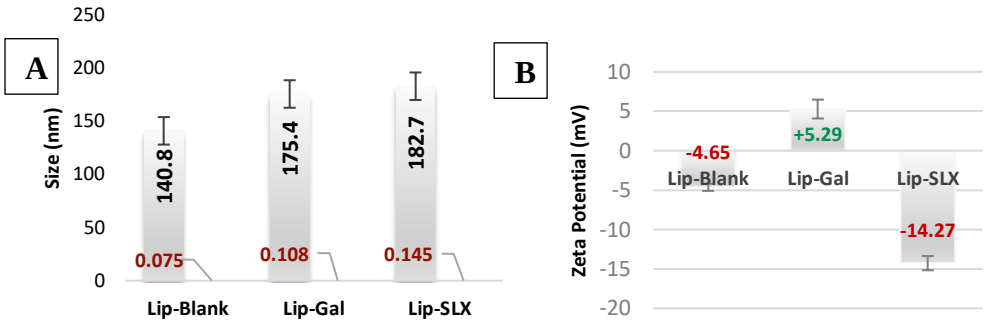

Figure16: A) DLS size in (nm) and B) Zeta Potential of Lip-Blank, Lip-Galactose, and Lip-Sialyl Lewis X.

Three samples of liposomes encapsulated with Gadolinium were prepared: 1) Lip-Blank, 2) Lip-Galactose, 3) Lip Sialyl Lewis X. The size of the liposomes was detected using DLS (nm). The size increased by 30-40nm increments with the addition of galactose and Sialyl Lewis X. The z-potential was in the negative range for the blank liposome, positive range for the

galactose liposome (functionalization with neutral molecule), and negative with Sialyl Lewis X which carries a negative charge at physiological pH, indicative of the occurrence of functionalization.

Part I: In vitro HepG2 cell uptake

FACS 6 Hours at 4C

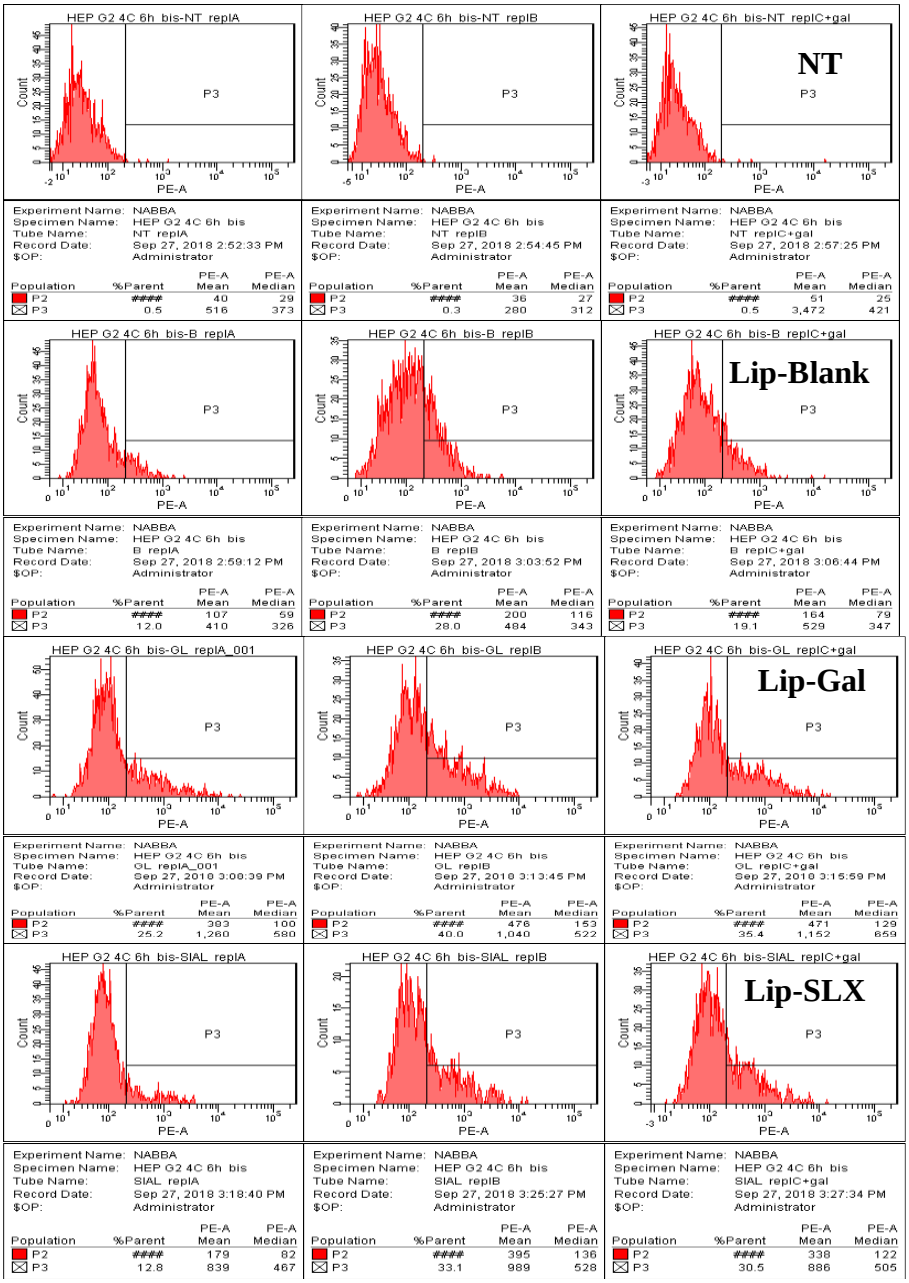

FACS 6 Hours at 37C

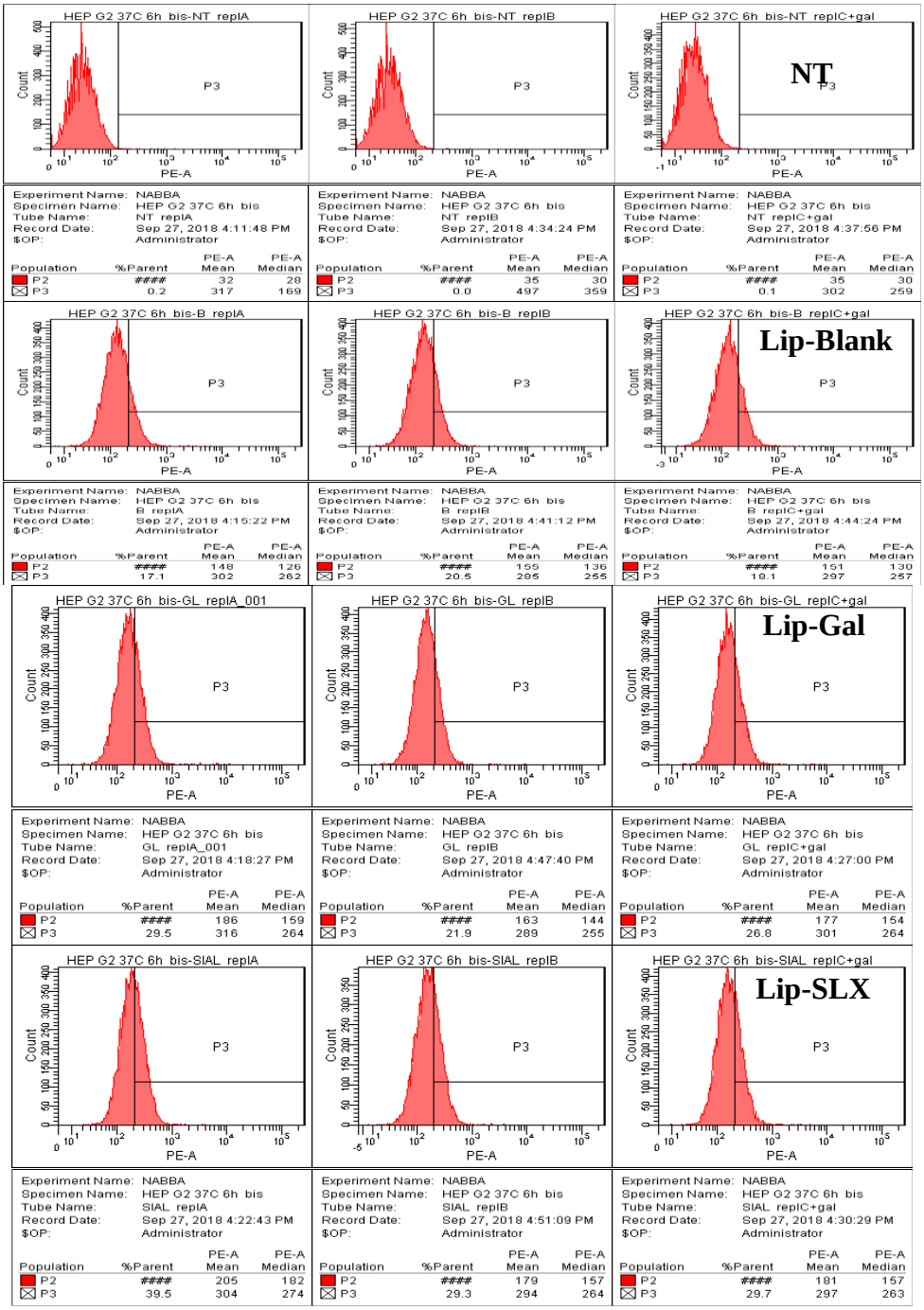

FACS 24 Hours at 37C

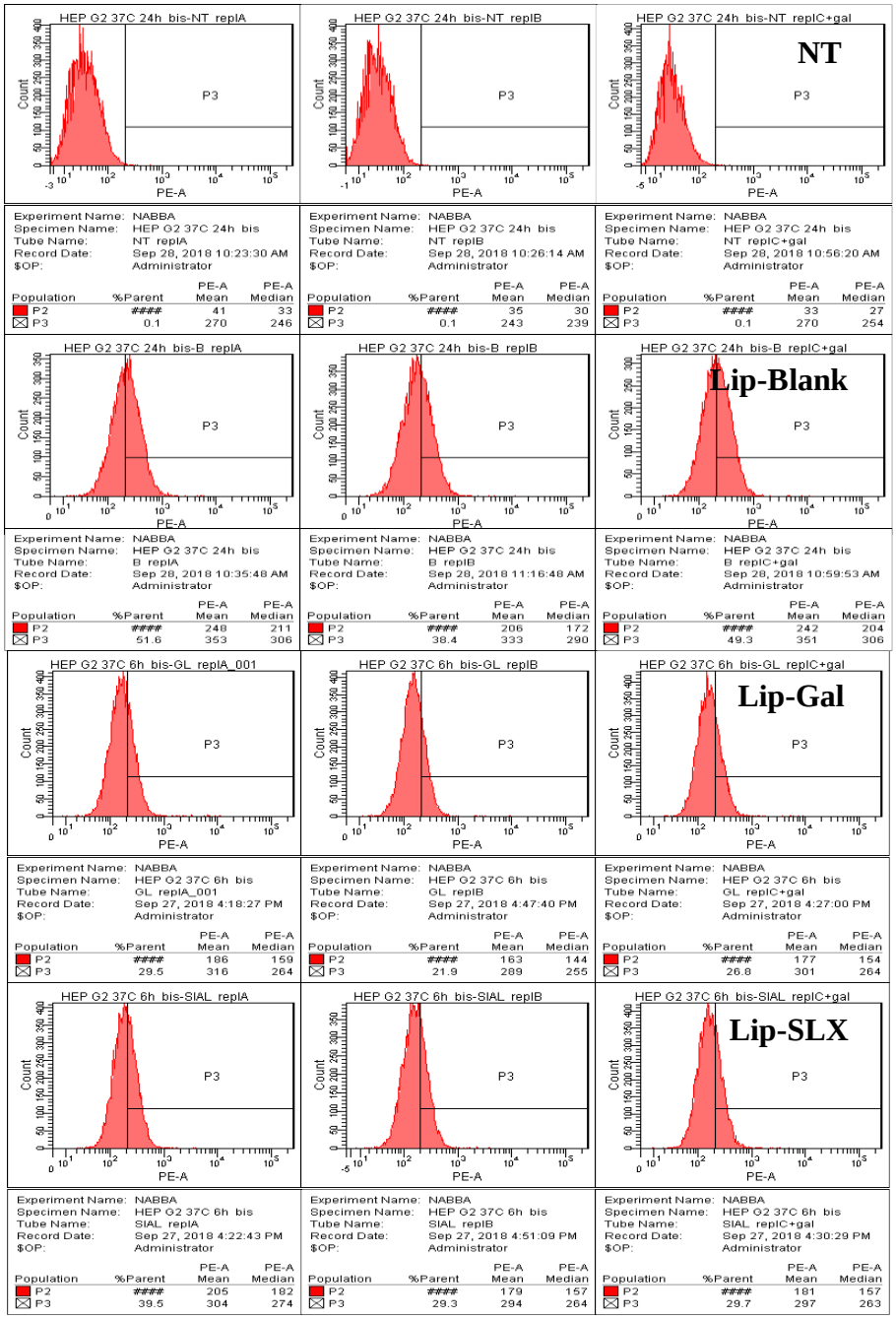

Experiment Name	Specimen Name	Tube Name	Record Date	$OP	Population	%Parent	PE-A Mean	PE-A Median
NABBA	HEP G2 37C 24h bis	NT replA	Sep 28, 2018 10:23:30 AM	Administrator	P2	####	41	33
					P3	0.1	270	246
NABBA	HEP G2 37C 24h bis	NT replB	Sep 28, 2018 10:26:14 AM	Administrator	P2	####	35	30
					P3	0.1	243	239
NABBA	HEP G2 37C 24h bis	NT replC+gal	Sep 28, 2018 10:56:20 AM	Administrator	P2	####	33	27
					P3	0.1	270	254
NABBA	HEP G2 37C 24h bis	B replA	Sep 28, 2018 10:35:48 AM	Administrator	P2	####	248	211
					P3	51.6	353	306
NABBA	HEP G2 37C 24h bis	B replB	Sep 28, 2018 11:16:48 AM	Administrator	P2	####	206	172
					P3	38.4	333	290
NABBA	HEP G2 37C 24h bis	B replC+gal	Sep 28, 2018 10:59:53 AM	Administrator	P2	####	242	204
					P3	49.3	351	306
NABBA	HEP G2 37C 6h bis	GL replA_001	Sep 27, 2018 4:18:27 PM	Administrator	P2	####	186	159
					P3	29.5	316	264
NABBA	HEP G2 37C 6h bis	GL replB	Sep 27, 2018 4:47:40 PM	Administrator	P2	####	163	144
					P3	21.9	289	255
NABBA	HEP G2 37C 6h bis	GL replC+gal	Sep 27, 2018 4:27:00 PM	Administrator	P2	####	177	154
					P3	26.8	301	264
NABBA	HEP G2 37C 6h bis	SIAL replA	Sep 27, 2018 4:22:43 PM	Administrator	P2	####	205	182
					P3	39.5	304	274
NABBA	HEP G2 37C 6h bis	SIAL replB	Sep 27, 2018 4:51:09 PM	Administrator	P2	####	179	157
					P3	29.3	294	264
NABBA	HEP G2 37C 6h bis	SIAL replC+gal	Sep 27, 2018 4:30:29 PM	Administrator	P2	####	181	157
					P3	29.7	297	263

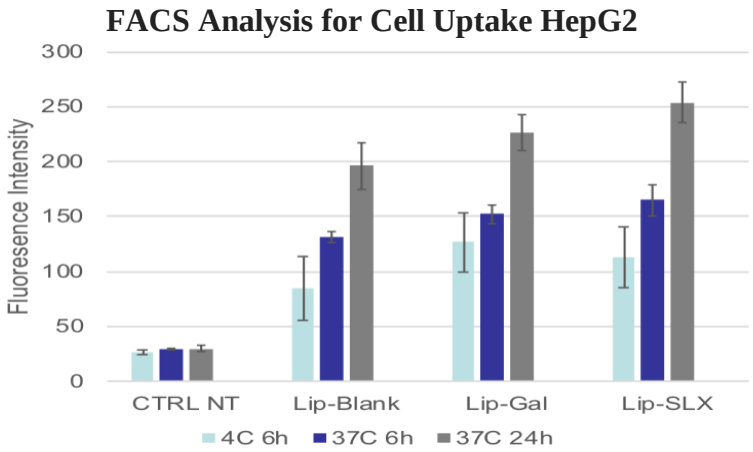

Figure: *FACS in-vitro analysis of fluorescently labeled Liposomes: Blank, Galactose, SLX versus CTRL on HepG2 hepatic cell line at temperatures 4°C at 6 hours, 37°C at 6 hours, and 37°C at 24 hours.*

M.F.I.	4C 6h	37C 6h	37C 24h
NT	29	28	33
	27	30	30
with gal	25	30	27
average	**27**	**29**	**30**
SD	**2**	**1**	**3**
BLANK	59	126	211
	116	136	172
with gal	79	130	204
average	**85**	**131**	**196**
SD	**29**	**5**	**21**
GAL	100	159	225
	153	144	242
with gal	129	154	210
average	**127**	**152**	**226**
SD	**27**	**8**	**16**
SIAL	82	182	268
	136	157	234
with gal	122	157	260
average	**113**	**165**	**254**
SD	**28**	**14**	**18**

Figure 8: FACS data of HepG2 uptake of NT CTRL versus Liposomes Blank, Galactose, Sialyl Lewis X at 4°C (6 hours), 37°C (6 hours), and 37C (24 hours).

Results of HepG2 in-vitro cell Uptake

The uptake of fluorescently labeled liposomes (Blank – Galactose – SLX) by HepG2 cell line was evaluated at 4°C at 6 hours and at 37°C at 6 hours and 24 hours. There was notable increase in uptake SLX > Galactose> Blank liposome at both 6hrs and 24hrs time-points. The blank liposome was also uptaken at 4°C and 37°C in lesser quantity, hypothetically due to the lipidic nature of the liposome that can enter cells via *passive diffusion*. This study confirms that the peak of uptake happens in 24 hours - based on this information the **in-vivo** treatment and analysis frame of time was designed.

Magnetic Resonance Imaging (MRI)

Theory of In-vivo imaging on animal models

The objective of Nanomedicine is the use of nanoparticles for diagnosis or/and therapy. MRI can be used as a non-invasive real time monitoring tool for the validation of efficacy of targeted therapy and ADME evaluations[120]. MRI has an absorption and emission of energy in the FM range (radio and TV frequency), it allows multiplanar 3D visualization of in-vivo through soft tissue contrast with additional applications in flow, diffusion, profusion.

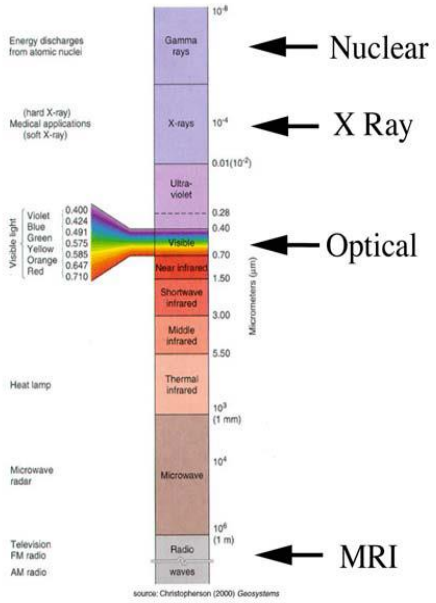

Figure 9: *Absorption and emission range of*

[120] Homer, H..Pien Alan, J.,Fischman, J., Thrall, H., Gregory S. A.. *Using imaging biomarkers to accelerate drug development and clinical trials*. Drug Discovery Today **2005**, 10(4).

NMR and MRI theory

NMR detects the interaction between Rf pulse produced by the oscillating magnetic field and the net magnetization of a sample in presence of a static magnetic field. Similarly, magnetic resonance detects the hydrogen nucleus (proton) in water molecules highly abundant in biological tissues. The most commonly used magnets in MRI are superconducting electromagnets that use helium liquid cooling systems to induce conductivity in the coil. The magnetic field produced is homogenous and ranges between 0.2 – 3.0 Tesla in strength in clinical practice and 4.7 – 11 Tesla in research.

Figure 10: *Bruker Pharmascan 7.0 T MRI instrument at Nerviano Medical Sciences (NMS)*

Parameters for MRI scanning

1) MSME AXIAL → pilot scan (spin echo)
2) MSME CORONAL → pilot scan (spin echo)
3) AXIAL TUMOR → RARE – Inv – Rec
4) AXIAL TUMOR → MSME – ax

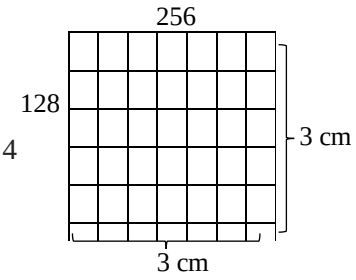

Spin Echo TR/TE = 300/12 ms N.averages = 4

Total acquisition time = 2 min 33 sec

FOV = 3 x 3 cm

Matrix = 256 x 128

Spatial resolution = 0.0117 cm/pixel $Spatial\ resolution = \frac{FOV\ (3\ cm)}{Matrix\ (256)}$

Spatial resolution = 0.0234 cm/pixel

12 slices (1mm thickness)

5) CORONAL LIVER → MSME – cor – liver

Spin Echo TR/TE = 300/12 ms N.averages = 4

Total acquisition time = 2 min 33 sec

FOV = 5 x 5 cm

Matrix = 256 x 128

Spatial resolution = 0.0195 cm/pixel $Spatial\ resolution = \frac{FOV\ (5\ cm)}{Matrix\ (256)}$

Spatial resolution = 0.0391 cm/pixel

*1 & 2 are pilot scans to ensure sample position in the middle of field view

*MSME (multi slide multi echo) – Spin echo

*RARE → inversion recovery susceptible to T1 weighted.

* TR (repetition time) & TE (echo time)

* 3 & 4 & 5 are T1 weighted

$$Gd \rightarrow \downarrow T1 \rightarrow \uparrow signal\ intensity\ in\ T1\ weighted\ images$$

Gadolinium is a positive contrast agent, therefore at a lower T1, the signal intensity of T1 weighted images is magnified.

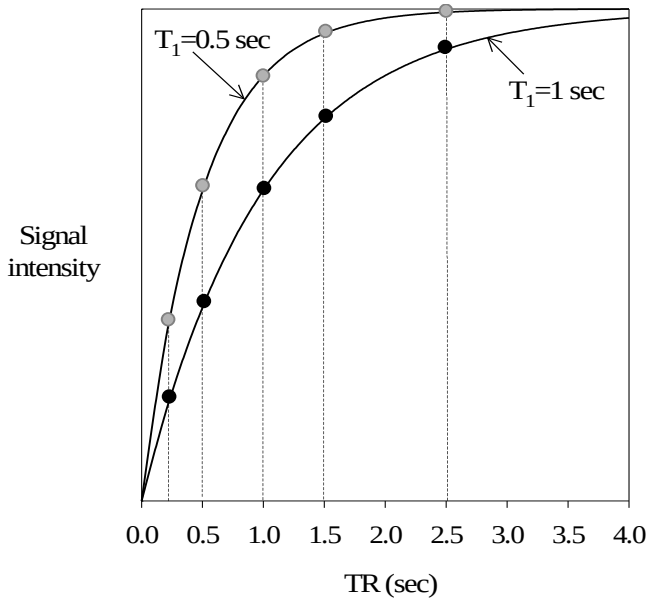

Figure 11: Curve displaying MRI signal intensity using a positive contrast agent

Tissue contrast depends on signal intensity produced due to ΔT1.
Positive contrast agent (T1 agents such as Gd^{+3} or Mn^{+2}) are paramagnetic Induce predominant shortening of T1 while negative contrast agents (SPIO, Iron Oxide) are superparamagnetic T2 agents that have a higher effect on T2. Therefore, at a shorter TR (300) T1 weighted samples should display a higher SI due to the larger difference in T1 as displayed by the graph.

T1-weighted MRI

The effect of the contrast agent (Gd-DSPE) encapsulated within the lipid bilayer of the liposome on the T1 relaxation time was tested in vitro to evaluate the imaging property of the samples. Gadovist, a gadolinium contrast agent used in clinical trials, was used as a standard for the magnetic reasonance signal intensity at concentrations 0.02-0.12mM. Liposome samples of SF/Gd were diluted to the same concentration range, and evaluated in-vitro concurrently at 3.0T using a clinical MRI scanner (Bruker Pharmascan). Both Gadovist and SF/Gd liposomes displayed larger signal enhancement compared to nanopure water, and the increase in Gd concentration corresponded to an increase in signal intensity. The relaxivity was calculated as the slope of the curve between 1/T1 and Gd concentration.

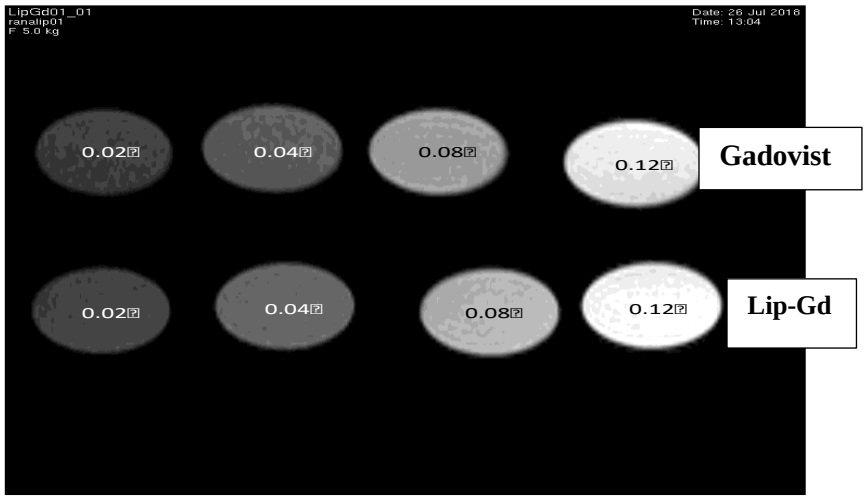

Figure 12: T1-weighted MRI image of SF/Gd-liposomes and Gadovist at different concentrations at 37C. The values represent concentrations in mM.

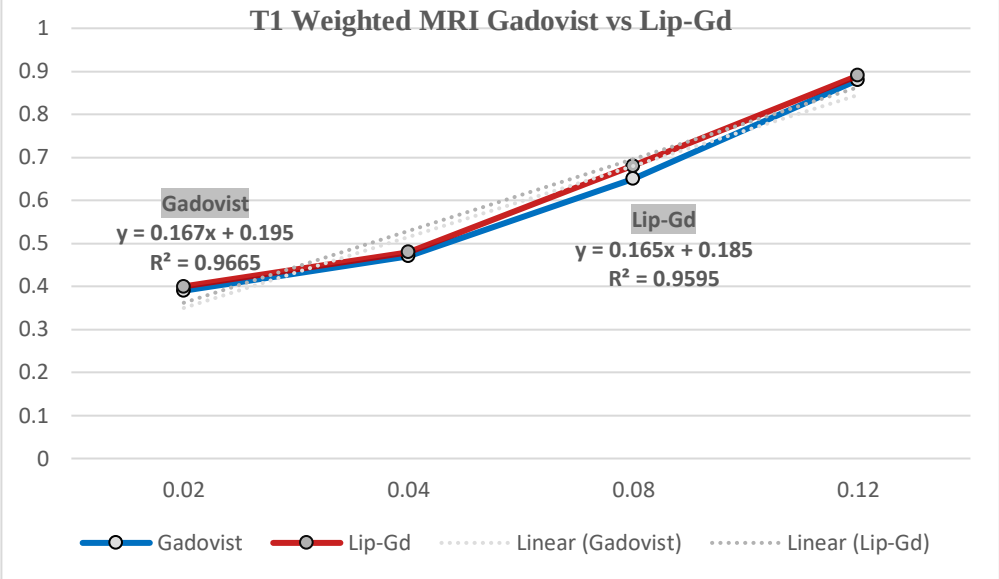

Figure 13: T1 weighted MR images of Gadovist (a clinical standard for positive contrast agents) versus Gd-encapsulated liposomes. Both lines have similar slopes that represent the relaxivity values, indicating that the two contrast agents behave similarly at different concentrations.

T1 measurements (sec)

	0.02 mM	0.04 mM	0.08 mM	0.12 mM
Gadovist	2.55	2.11	1.54	1.14
Lip-Gd	2.46	2.07	1.46	1.12

Figure 14: T1-weighted MRI image of SF/Gd-liposomes and Gadovist at different concentrations at 37C. The values represent T1 different concentrations in mM.

As displayed in the figure, the relaxivity of Gadovist (approximately r1 = 0.167 $mM^{-1}s^{-1}$) was slightly higher than the relaxivity of the Gd-Lip (0.165 $mM^{-1}s^{-1}$). These results indicate the efficiency of encapsulation of DSPE-Gadolinium as an embedded component of the lipid bilayer of the liposome, making it an effective contrast agent tool for T1 imaging.
The slight difference in relaxivity however is due to the exchange rate between Gadolinium and water, which differs in the environment of the liposome versus chelated Gd[121]. The in-vitro study was used to optimize the procedure of the encapsulation of DSPE-Gd at the 0.12 mM for the samples used in the in-vivo study.

In-vivo MRI guided test

MRI is the most powerful non-invasive imaging tool that offers high soft tissue contrast, spatial resolution, and penetration depth[122]. Although soft tissues display a high contrast in MRI images, the diagnosis of certain pathologies can require the use of contrast agents to improve the contrast-to-noise ratio. This ratio can be improved by shortening the spin-lattice T1 and/or spin-spin T2 relaxation times of the water protons at the tissue of interest[123]. The use of liposomes as vehicles to encapsulate paramagnetic ions such as Gadolinium has been widely proposed due to the shielding effect of the liposome that can reduce the toxic property of the contrast agent.

---

[121] Na, K., Lee, S.A., Jung, S.H., Shin, B.C. Colloids Surf. B: Biointerfaces 84 (***2011***) 82.
[122] Nakada, T. Clinical application of high and ultra high-field MRI.
Brain Dev. 2007, 29, 325–335.
[123] Navon, G.; Panigel, R.; Valensin, G. Liposomes containing paramagnetic macromolecules as mri contrast agents. Magn. Reson. Med. 1986, 3, 876–880.

Initial In-Vivo Strategy

Targeted delivery of glycoliposomes co-loaded with Gadolinium and Sorafenib for efficacy treatment and biodistribution MRI studies

HepG2 (human liver cancer cell line) was selected based on the FACS results to be expanded and inoculated into nude mice (Nu/Nu).
60 mice were inoculated with 8 x 106/0.2 mL cells subcutaneously into the abdomen The progression of the tumor was monitored until the initial peak of metastasis. Once tumor size reached the 0.1-gram mark, the mice would be randomized into 5 groups consisting of 8 animals/group
The 5 groups are the following:
1- Control
2- Sorafenib (dissolved in 50:50 CremophorCrEL: 95% Ethanol) IV
3- Liposome-Sorafenib (Lip-SF) IV
4- Liposome- Sorafenib-Galactose (Lip-SF-Gal) IV
5- Liposome-Sorafenib-Sialyl Lewis X (Lip-SF-SLX) IV

Efficacy Treatment:
The treatment to be administered 2 or 3 times/week (depending on the rate of metastasis) at an identical quantity of sorafenib **(**8mg/kg) intravenously.

- The dose to be administered is 10ul/gram of mouse
- Tumor Volume Measurements: twice a week

Sorafenib Calibration Curve at 265nm in Hexane

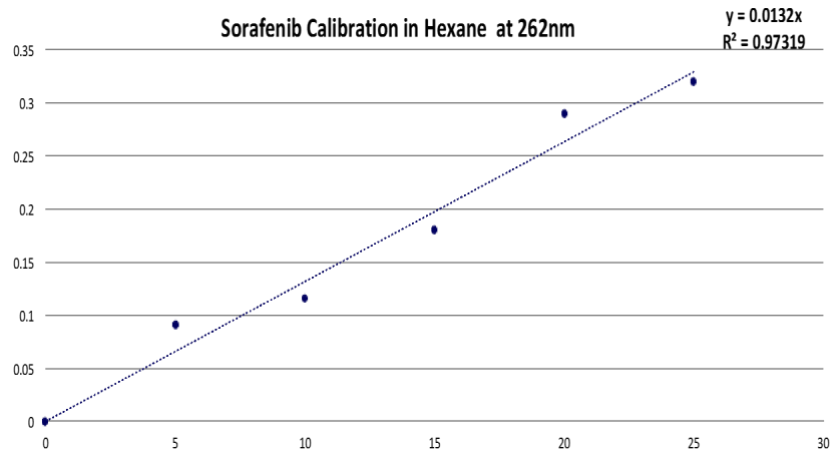

Figure 15: Calibration curve of (0-30µg) of Sorafenib (Hepatocellular carcinoma first line defense drug).

Biodistribution:

Of the randomized mice, 4 groups (n=4) will be used to analyze targeted biodistribution of Lip-Blank/Galactose/Sialyl Lewis X by monitoring the encapsulated MRI contrast agent (DSPE-Gd).

The 3 groups tested are:

1- Liposome-Sorafenib (Lip-SF) IV
3- Liposome- Sorafenib-Galactose (Lip-SF-Gal) IV
4- Liposome-Sorafenib-Sialyl Lewis X (Lip-SF-SLX) IV

The goal of the study is to track the pathway of liposomes in two sites: 1) the liver and 2) the ectopic HCC tumor, and analyze the potential of targeting in extending the half-life and tumor-site accumulation. The MRI images were processed and analyzed for the detection of increase in signal intensity corresponding to the accumulation of Gd encapsulated liposomes at the evaluated site.

Experimentally → Magnetic Resonance imaging detected at 1 hour, 3 hours, 6 hours, 24 hours, and 48 hours.

- Due to discrepancies in tumor growth in-vivo, the two experiments were narrowed down to the MRI guided Biodistribution study as will be elaborated on in the following section.

In-vivo MRI study of the Biodistribution of targeted delivery of Glycoliposomes in hepatocellular carcinoma

Liposome Preparation

The same procedure indicated in pages (91-98) was followed for the assembly, functionalization and characterization of the following liposomes:

Sample 1: Blank Liposome

Sample 2: Lip- PhHyd-Galactose

Sample 3: Lip- PhHyd-Sialyl Lewis X

With the Encapsulation of DSPE-Gd-1.25mM

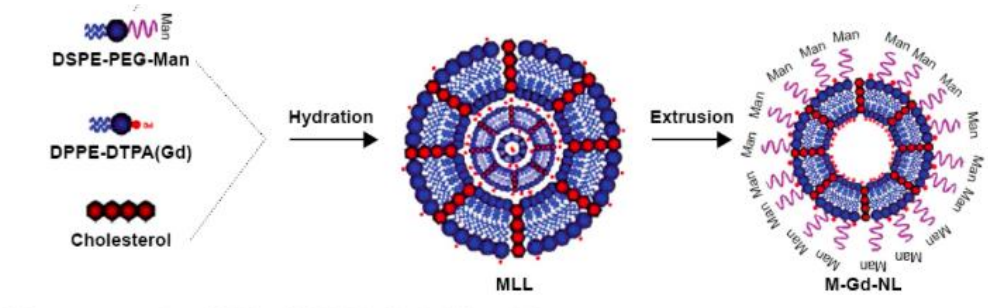

Gadolinium-encapsulated liposome

Animal Studies

All aspects of animal studies have been conducted under the supervision of Dr. A. Degrassi at Nerviano Medical Sciences (NMS) in accordance with rules and regulations of animal handling.

The orthopic HCC mice model and treatments

HepG2 (human liver) was the selected cell line to be inoculated into nude mice (Nu/Nu). The inoculation protocol followed was retrieved from prior studies conducted at Nerviano Medical Sciences. In this study, 60 mice were transplanted with 8 x 106/0.2 mL cells subcutaneously into the abdomen as displayed in the image bellow.

Figure 15: Ectopic inoculation with HepG2 cell line

The progression of the tumor was monitored over the period of 6-8 weeks until the initial peak of metastasis.

The following tables display 1) the time line correlated to the tumor growth in the 60 mice inoculated over the period of 8 weeks, 2) the degree of tumor growth.

Monitoring of mice Post-inoculation

Tumor	1-4 weeks	4-6 weeks	Week 6	Week 7	Week 8
-	60	**51**		**37**	**29**
+/--		**8**	**5**	**1**	**2**
+/-			**4**	**3**	**5**
+			**6**	**4**	**5**
++				**5**	**7**
+++/+				**7**	**9**
Dead		**1**	**+1**	**+1**	**+1**

Table1: *Schedule of mice monitoring post-inoculation over 8 weeks.*

Tumor size Indication Table

-	No tumor
+/--	**Small black dot <0.05 mg**
+/-	**Black dot (0.06-0.09 mg)**
+	**0.1-0.3mg**
++	**0.3-0.6mg**
+++/+	**0.6>**

Table2: Tumor size indication sheet

➢ Tumor Growth Evaluation

At 8 weeks time point → out of 60 mice:

1) 29 mice did not display any tumor growth

2) 2 mice displayed a small black dot indicated by (+/--)

3) Only 16 mice varied between (++) and (+++) and were randomly distributed and used for the Biodistribution study

4) it was not possible to perform the efficacy study due to the great variability in tumor growth.

5) Mice varied in weight between 27g and 34g (randomized)

Tumor growth noted in nearly ¼ of the population. The tumor growth was hemorrhagic (black dot), which was found to be a property of the cell line (HepG2) and made MRI detection at instants more complex. Magnetic Resonance imaging was performed at Pre-treatment, 3 hours, 6 hours, 24 hours. Additionally, 1 mouse of each group was randomly selected for additional testing at 1 hour and 48 hours to cover a larger biodistribution window. Each mouse was used as its own control and monitored against Pre-treatment imaging.

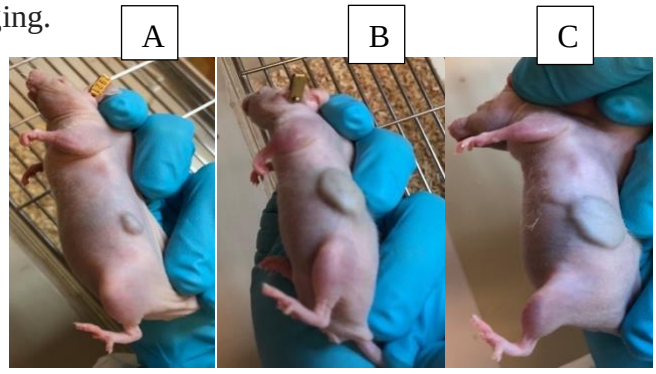

Figure 16: Display of variable tumor sizes represented in Table 2.
a) (+) tumor, b) (++) tumor, c) (+++) tumor

Results of MRI Biodistribution in-vivo

Group 1: Blank Liposome N = 4 mice, [**N 1**, N 2, N 3, N 4]

N 1 -Liver

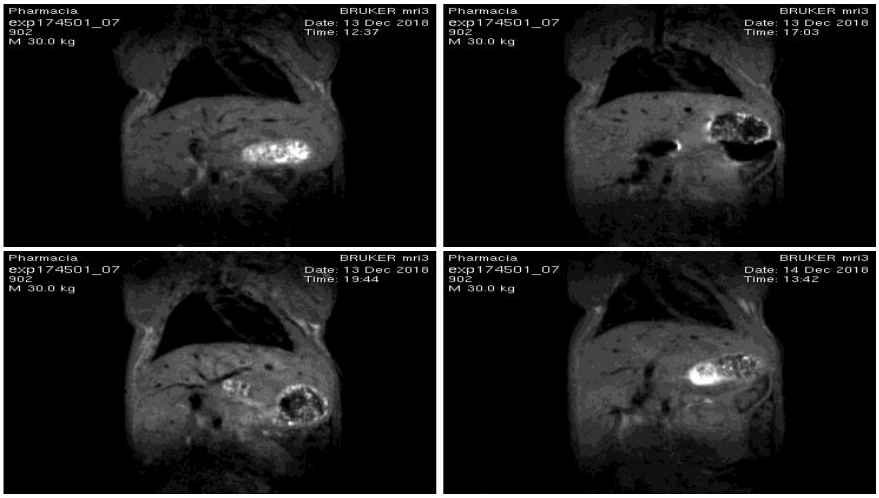

LIVER		Coronal		SI Ratio
N 1		**Liver**	**muscle**	
Lip Blank	**Pre**	2.08	1.6	1.3
	1 hr	2.08	1.35	1.54
	3hrs	2.28	1.46	1.56
	6 hrs	2.3	1.63	1.4
	24 hrs	2.28	1.27	1.795
% SI increase				**38.10%**

Table 3: N 1 MRI Coronal scan of the liver at Pre-treatment, 1 hour, 3 hours, 6 hours, and 24 hours. The signaling intensity of the liver was normalized against SI of muscle tissue in each scan. Signal intensity increased by 38.1% in comparison to Pre-Treatment, which indicates the accumulation of Blank liposomes in the liver over 24-hours time frame.

N 1-Tumor

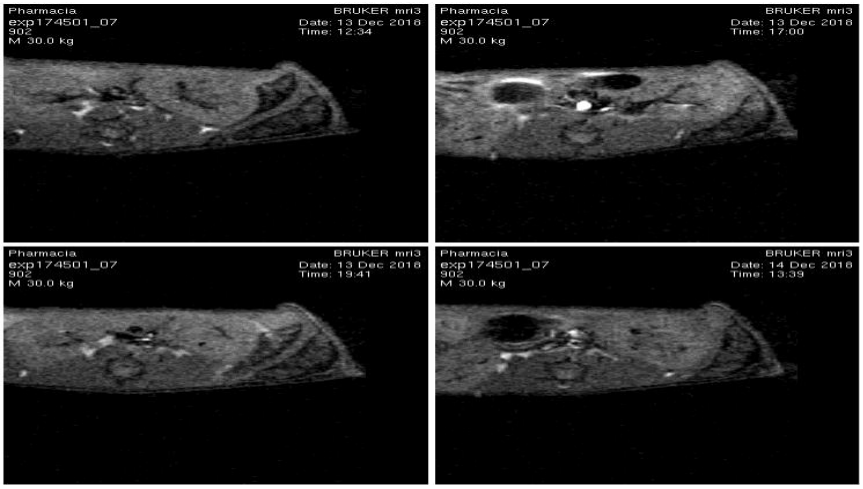

TUMOR		Axial		SI Ratio
N 1		**tumor**	**muscle**	
Lip Blank	**Pre**	4.38	6.01	0.73
	1 hr	4.62	5.96	0.775
	3hrs	4.29	5.83	0.73
	6 hrs	5.2	6.02	0.86
	24 hrs	5.12	5.91	0.87
% SI increase				**19.20%**

Table 4: N 1 MRI Axial scan of the tumor at Pre-treatment, 1 hour, 3 hours, 6 hours, and 24 hours. The signaling intensity of the Tumor tissue was normalized against SI of muscle tissue in each scan. Signal intensity increased by 19.2% in comparison to Pre-Treatment, which indicates the accumulation of Blank liposomes in the tumor over 24-hours time frame. The highest SI increase was equally noted at 6 hours and 24 hours.

In N 1, there was higher accumulation of Blank liposome in the Liver (38.1%) versus Tumor (19.2%).

Group 1: Blank Liposome N = 4 mice, [N 1, **N 2**, N 3, N 4]

N 2-Liver

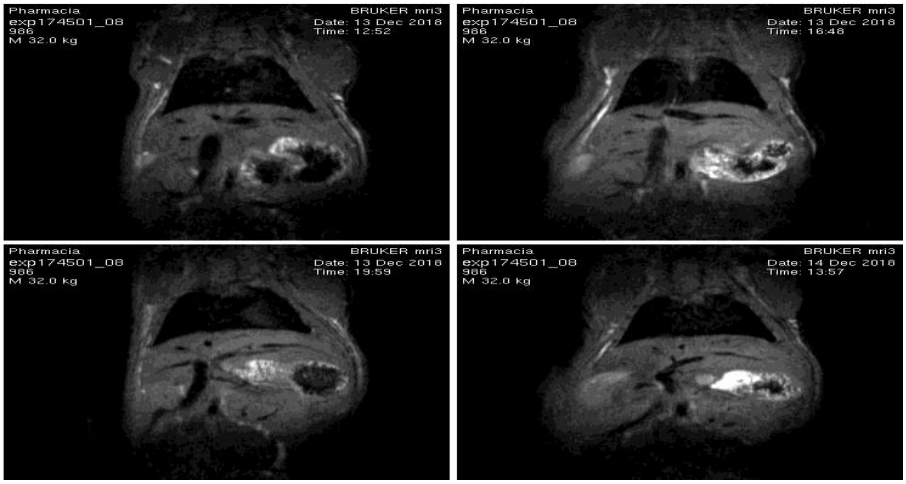

LIVER		**Coronal**		**SI Ratio**
N 2		**Liver**	**muscle**	
Lip Blank	**Pre**	1.51	1.22	1.23
	3hrs	1.84	1.44	1.28
	6 hrs	1.8	1.43	1.26*
	24 hrs	1.84	1.56	1.18
% SI increase				NC

Table 5: N 2 MRI Coronal scan of the liver at Pre-treatment, 3 hours, 6 hours, and 24 hours. The signaling intensity of the liver was normalized against SI of muscle tissue in each scan. There was no visible change in SI noted in comparison to Pre-Treatment over 24-hours. An insignificant SI increase was noted at 3 hours and 6 hours. In this case, there was no visible evidence of the accumulation of Blank liposome in the liver.

N 2-Tumor

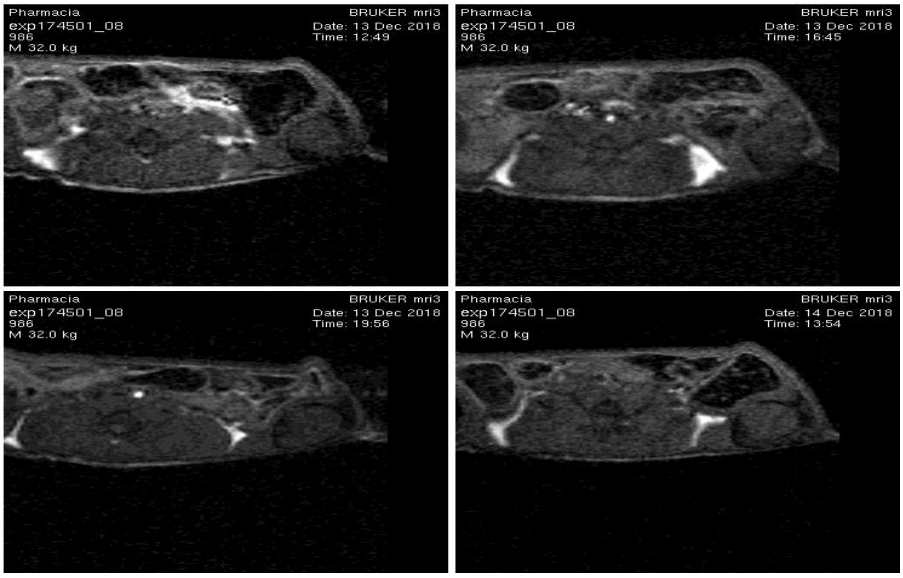

TUMOR		Axial		SI Ratio
N 2		**tumor**	**muscle**	
Lip Blank	**Pre**	4.7	5.31	0.88
	3hrs	6.2	6.39	0.97
	6 hrs	5.33	6.34	0.84
	24 hrs	6.18	5.69	1.08
% SI increase				22.70%

Table 6: N 2 MRI Axial scan of the tumor at Pre-treatment, 1 hr, 6 hrs, and 24 hrs. The signaling intensity of the Tumor tissue was normalized against SI of muscle tissue in each scan. Signal intensity increased by 22.7% in comparison to Pre-Treatment, which indicates the accumulation of Blank liposomes in the tumor at 24 hrs. The highest SI increase was noted at 24 hrs.

In N 2, there was higher accumulation of Blank Liposome in the Tumor (22.7%) versus no accumulation in the Liver.

Group 1: Blank Liposome N = 4 mice, [N 1, N 2**, N 3**, N 4]

N 3-Liver

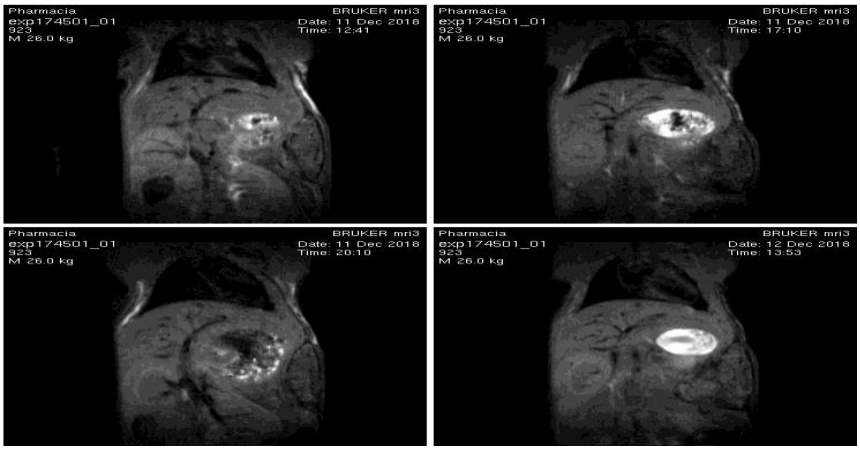

LIVER		**Coronal**		**SI Ratio**
N 3		**Liver**	**muscle**	
Lip Blank	**Pre**	1.81	1.24	1.46
	3 hrs	2.14	1.15	1.86
	6 hrs	1.98	1.55	1.277
	24 hrs	2.49	1.35	1.84
	48 hrs	2.23	1.83	1.21
% SI increase				26.03%

Table 7: N 3 MRI Coronal scan of the liver at Pre-treatment, 3 hrs, 6 hrs, 24 hrs, and 48 hrs. The signaling intensity of the liver was normalized against SI of muscle tissue in each scan. Signal intensity increased by 26.03% at 24hrs in comparison to Pre-Treatment, which indicates the accumulation of Blank liposomes in the liver at the 24-hrs time point. The highest SI increase was noted at 24 hrs, meanwhile, all the Gd-labeled Blank Liposomes were cleared out at 48 hrs.

N 3-Tumor

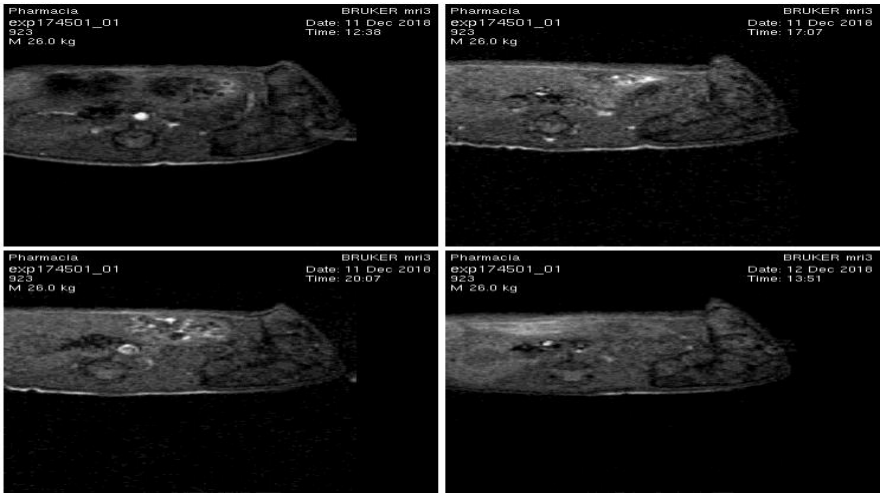

TUMOR		Axial		SI Ratio
N 3		tumor	muscle	
Lip Blank	Pre	5.94	6.67	0.891
	3 hrs	5.47	6.09	0.898
	6 hrs	5.79	6.78	0.85
	24 hrs	7.31	7.94	0.92
	48 hrs	5.33	6.67	0.799
% SI increase				3.25%

Table 8: N 3 MRI Axial scan of the tumor at Pre-treatment, 3 hrs, 6 hrs, 24 hrs, and 48 hrs. The signaling intensity of the Tumor tissue was normalized against SI of muscle tissue in each scan. Signal intensity increased by 3.25% in comparison to Pre-Treatment, which indicates a minor accumulation of Blank liposomes in the tumor at 24-hrs time point. The highest SI increase was noted at 24 hrs, and similarly to the liver scan there was a complete clear out of Gd-Lip-Blank at 48hrs.

In N 3**, there was higher accumulation of Blank liposome in the Liver (26%) versus Tumor (3.25%).**

Group 1: Blank Liposome N = 4 mice [N 1, N 2, N 3, **N 4**]

N 4 -Liver

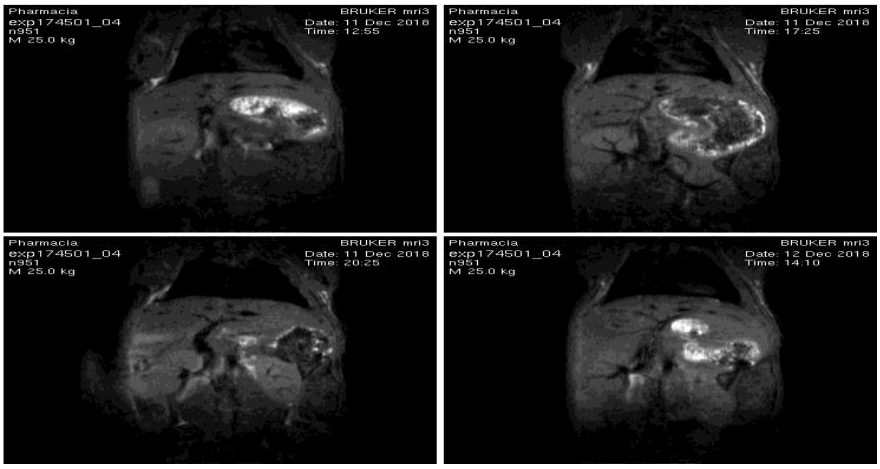

LIVER		**Coronal**		**SI Ratio**
N 4		**Liver**	**muscle**	
Lip Blank	**Pre**	2.02	1.42	1.42
	3hrs	1.87	1.08	1.73
	6 hrs	1.55	0.88	1.76
	24 hrs	1.89	0.83	2.28
% SI increase				60.56%

Table 9: N 4 MRI Coronal scan of the liver at Pre-treatment, 3 hrs, 6 hrs, and 24 hrs. The signaling intensity of the liver was normalized against SI of muscle tissue in each scan. Signal intensity increased by 60.56% at 24hrs in comparison to Pre-Treatment, which indicates a significant accumulation of Blank liposomes in the liver at the 24-hrs time point. The highest SI increase was noted at 24 hrs.

N 4-Tumor

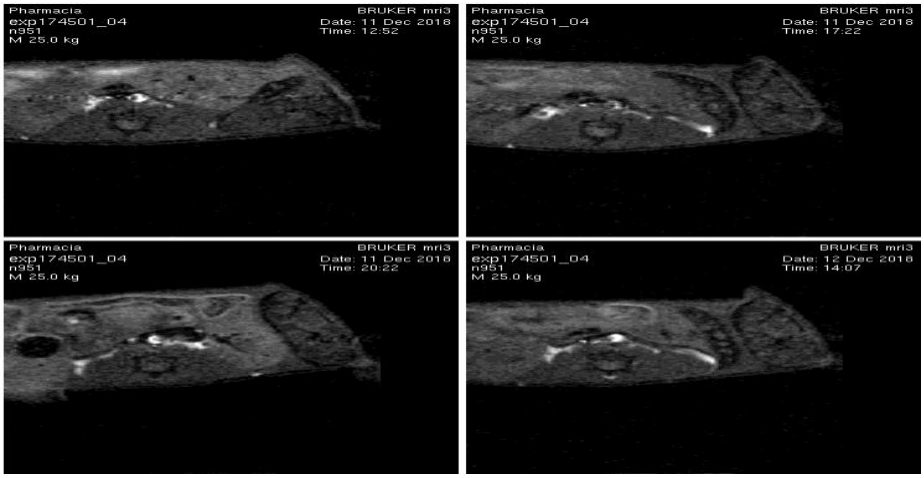

TUMOR		Axial		SI Ratio
N 4		**tumor**	**muscle**	
Lip Blank	**Pre**	5.71	6.17	0.925
	3hrs	6.34	6.15	1.03
	6 hrs	7.41	6.12	1.21*
	24 hrs	7.17	6.84	1.04
% SI increase				30.8%

Table 10: N 4 MRI Axial scan of the tumor at Pre-treatment, 3 hrs, 6 hrs, and 24 hrs. The signaling intensity of the Tumor tissue was normalized against SI of muscle tissue in each scan. The highest SI increase was noted at 6hrs. Signal intensity increased by 30.8% in comparison to Pre-Treatment, which indicates the accumulation of Blank liposomes in the tumor.

In N 4**, there was higher accumulation of Blank liposome in the Liver (60.6%) versus Tumor (30.8%).**

Group 2: Liposome-Galactose N = 4 mice, [**N 5**, N 6, N 7, N 8]

N 5 -Liver

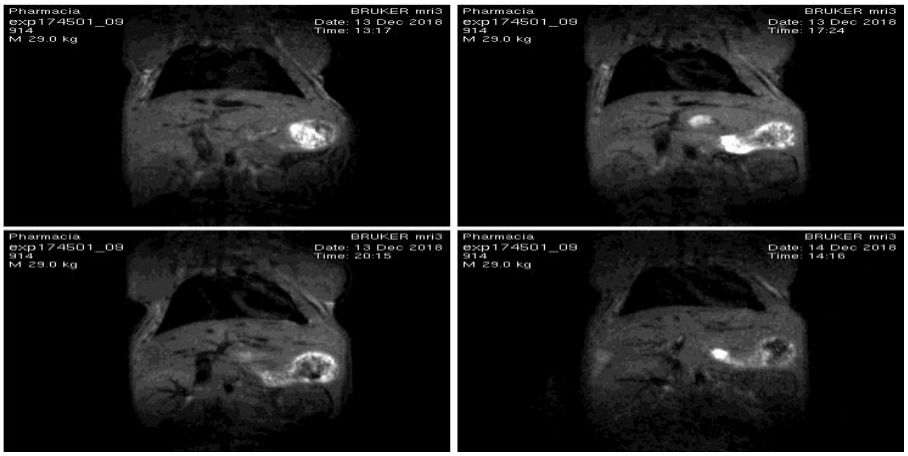

LIVER		**Coronal**		**SI Ratio**
N 5		**Liver**	**muscle**	
Lip Gal	**Pre**	2.2	1.33	1.65
	1 hr	2.24	1.62	1.38
	3hrs	2.2	1.6	1.375
	6 hrs	2.18	1.67	1.31
	24 hrs	1.27	0.7	1.8
% SI increase				9.10%

Table 11: N 5 MRI Coronal scan of the liver at Pre-treatment, 1 hr, 3 hrs, 6 hrs, and 24 hrs. The signaling intensity of the liver was normalized against SI of muscle tissue in each scan. Signal intensity increased by 9.10% at 24hrs versus Pre-Treatment. The highest SI increase was noted at 24 hrs. Meanwhile, scanning at 1 hr showed no Lip-Galactose accumulation, thus offering additional confirmation of the 24hrs time-point accumulation.

N 5 -Tumor

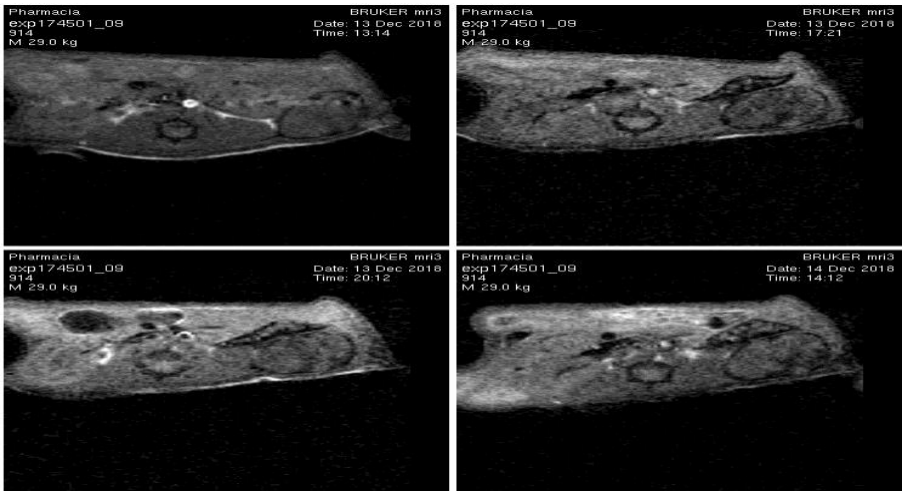

TUMOR		Axial		SI Ratio
N 5		tumor	muscle	
Lip Gal	Pre	7.59	7.27	1.04
	1 hr	5.77	5.86	0.98
	3hrs	4.9	5.95	0.82
	6 hrs	5.73	6.42	0.89
	24 hrs	6.3	5.86	1.07
% SI increase				2.90%

Table 12: N 5 MRI Axial scan of the tumor at Pre-treatment, 1 hr, 3 hrs, 6 hrs, and 24 hrs. The signaling intensity of the tumor was normalized against SI of muscle tissue in each scan. Signal intensity increased by 2.9% at 24hrs versus Pre-Treatment. The highest SI increase was noted at 24 hrs. Meanwhile, scanning at 1 hr also showed no Lip-Galactose accumulation, thus offering additional confirmation of the 24hrs time-point accumulation.

In N 5**, there was higher accumulation of Galactose-liposome in the Liver (9.1%) versus Tumor (2.9%).**

Group 2: Liposome-Galactose N = 4 mice, [N 5, **N 6**, N 7, N 8]

N 6 - Liver

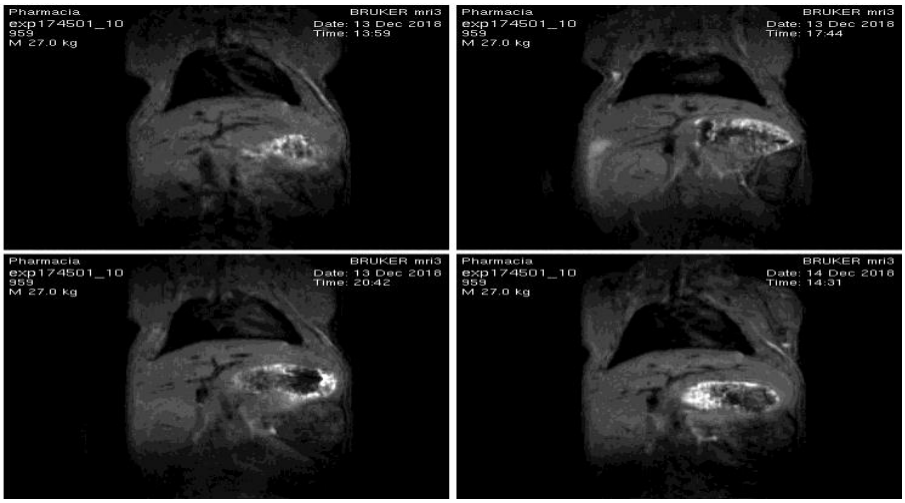

LIVER		Coronal		SI Ratio
N 6		**Liver**	**muscle**	
Lip Gal	**Pre**	2.42	1.71	1.415
	3hrs	2.18	1.42	1.535
	6 hrs	2.14	1.07	2*
	24 hrs	2.57	1.42	1.8
% SI increase				28.6%

Table 13: N 6 MRI Coronal scan of the liver at Pre-treatment, 3 hrs, 6 hrs, and 24 hrs. The signaling intensity of the liver was normalized against SI of muscle tissue in each scan. The highest SI increase was noted at 6 hrs and 24 hrs. Signal intensity increased by 27.2% at 6hrs versus Pre-Treatment.

N 6-Tumor

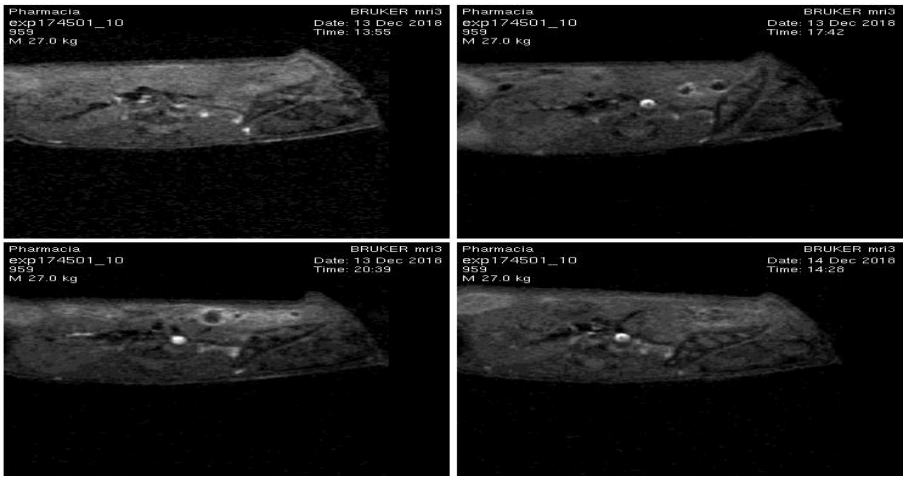

TUMOR		Axial		SI Ratio
N 6		**tumor**	**muscle**	
Lip Gal	**Pre**	5.59	6.52	0.86
	3hrs	5.58	6.52	0.856
	6 hrs	5.47	6.09	0.898
	24 hrs	6.23	6.1	1.02
% SI increase				18.60%

Table 14: N 6 MRI Axial scan of the tumor at Pre-treatment, 3 hrs, 6 hrs, and 24 hrs. The signaling intensity of the tumor was normalized against SI of muscle tissue in each scan. Signal intensity increased by 18.6% at 24hrs versus Pre-Treatment. The highest SI increase was noted at 24 hrs.

In N 6**, there was higher accumulation of Galactose-liposome in the Liver (28.6%) versus Tumor (18.6%).**

Group 2: Liposome-Galactose N = 4 mice, [N 5, N 6, **N 7**, N 8]

N 7-Liver

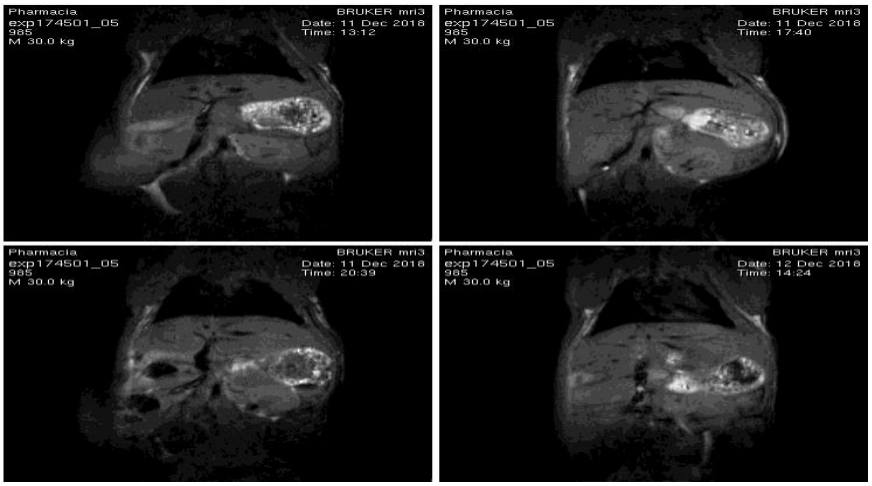

LIVER		**Coronal**		**SI Ratio**
N 7		**Liver**	**muscle**	
Lip Gal	**Pre**	1.58	0.94	1.68
	3hrs	1.92	1.42	1.35
	6 hrs	1.86	0.98	1.9*
	24 hrs	2.08	1.42	1.46
% SI increase				13.1%

Table 15: N 7 MRI Coronal scan of the liver at Pre-treatment, 3 hrs, 6 hrs, and 24 hrs. The signaling intensity of the liver was normalized against SI of muscle tissue in each scan. There was no noticeable change (NC) at 24hrs. The highest SI increase was noted at 6 hrs and 24 hrs. The signal intensity increased by 13.1% at 6hrs versus Pre-Treatment.

N 7-Tumor

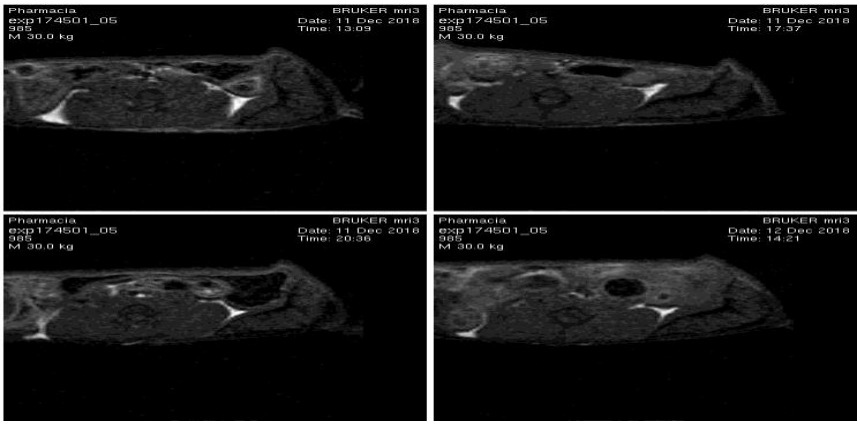

TUMOR		Axial		SI Ratio
985		**tumor**	**muscle**	
Lip Gal	**Pre**	5.23	6.2	0.84
	3hrs	5.61	6.24	0.899
	6 hrs	5.26	5.77	0.915*
	24 hrs	5.29	5.93	0.89
% SI increase				8.9%

Table 16: N 7 MRI Axial scan of the tumor at Pre-treatment, 3 hrs, 6 hrs, and 24 hrs. The signaling intensity of the tumor was normalized against SI of muscle tissue in each scan. The highest SI increase was noted at 6 hrs. Signal intensity increased by 8.9% at 6hrs versus Pre-Treatment.

In N 7**, there was higher accumulation of Galactose-liposome in the Liver (13.1%) versus Tumor (8.9%).**

Group 2: Liposome-Galactose N = 4 mice, [N 5, N 6, N 7, **N 8**]

N 8-Liver

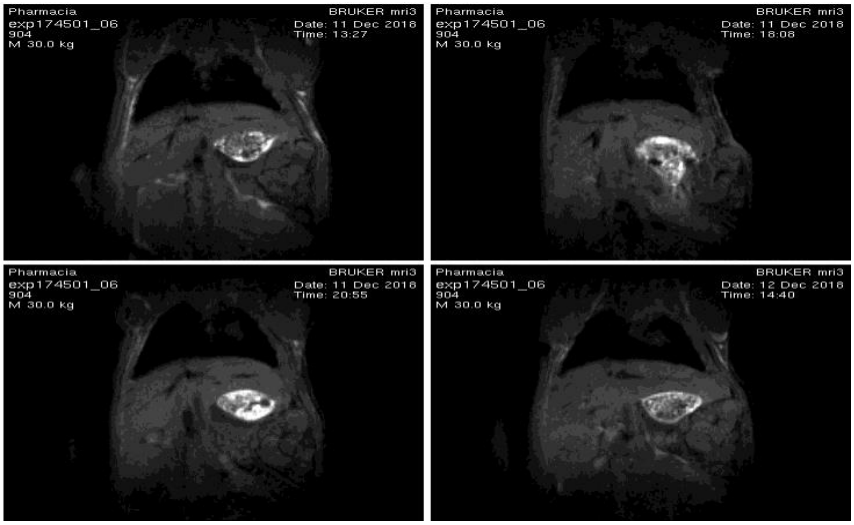

LIVER		**CORONAL**		**SI Ratio**
N 8		**LIVER**	**muscle**	
Lip GAL	**Pre**	2.26	1.44	1.57
	3 hrs	2.01	0.9	2.23
	6 hrs	2.34	1.48	1.58
	24 hrs	2.12	0.95	2.23
	48 hrs	2.17	1.63	1.33
% SI increase				42.04%

Table 17: N 8 MRI Coronal scan of the liver at Pre-treatment, 3 hrs, 6 hrs, 24hrs, and 48hrs. The signaling intensity of the liver was normalized against SI of muscle tissue in each scan. The highest SI increase was noted at 24 hrs. Signal intensity increased by 42.04% at 24hrs versus Pre-Treatment. Meanwhile, at 48hrs, Galactose-Lip were cleared-out.

N 8-Tumor

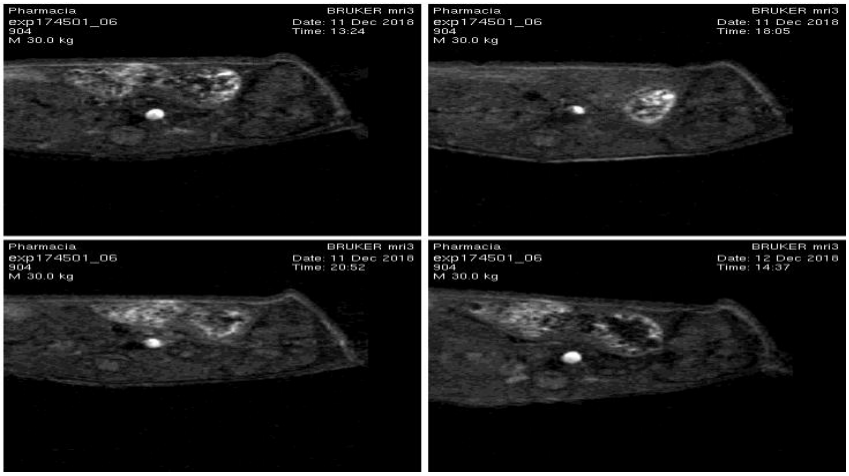

TUMOR		Axial		SI Ratio
N 8		tumor	muscle	
Lip GAL	Pre	6.73	6.26	1.07
	3 hrs	6.03	6.35	0.95
	6 hrs	6.11	6.52	0.93
	24 hrs	6.67	6.18	1.08
	48 hrs	6.28	5.82	1.08
% SI increase				1%

Table 18: N 8 MRI Axial scan of the tumor at Pre-treatment, 3 hrs, 6 hrs, 24 hrs, and 48hrs. The signaling intensity of the tumor was normalized against SI of muscle tissue in each scan. The highest SI increase was noted at 24 hrs and 48hrs. There was no significant change in signal intensity with only a 1% increase at 24hrs versus Pre-Treatment.

In N 8**, there was higher accumulation of Galactose-liposome in the Liver (42%) versus Tumor (1%).**

Group 3:Liposome-Sialyl Lewis X, N = 4 mice, [**N 9**, N 10, N 11, N 12]

N 9-Liver

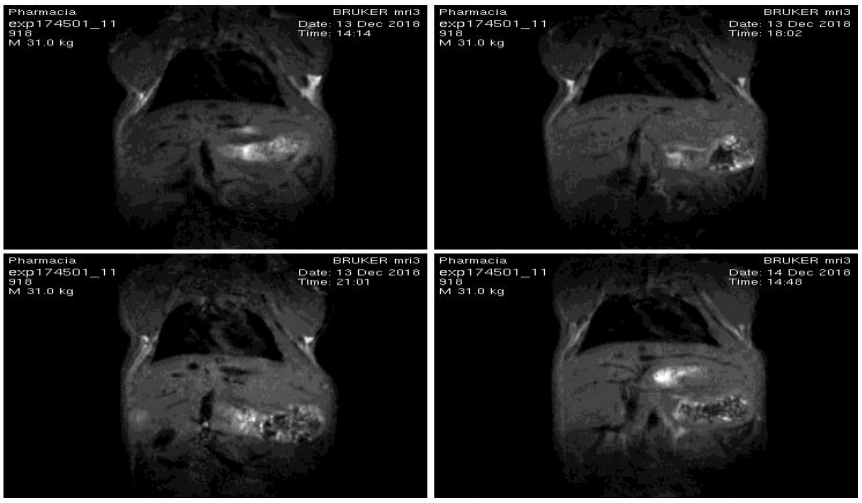

LIVER		**Coronal**		**SI Ratio**
N 9		Liver	muscle	
Lip SLX	Pre	1.71	1.63	1.05
	3hrs	2.09	1.45	1.44
	6 hrs	2.1	1.42	1.47
	24 hrs	2.26	1.43	1.58
% SI increase				50.48%

Table 19: N 9 MRI Coronal scan of the liver at Pre-treatment, 3 hrs, 6 hrs, and 24hrs. The signaling intensity of the liver was normalized against SI of muscle tissue in each scan. The highest SI increase was noted at 24 hrs. Signal intensity increased by 42.04% at 24hrs versus Pre-Treatment.

N 9-Tumor

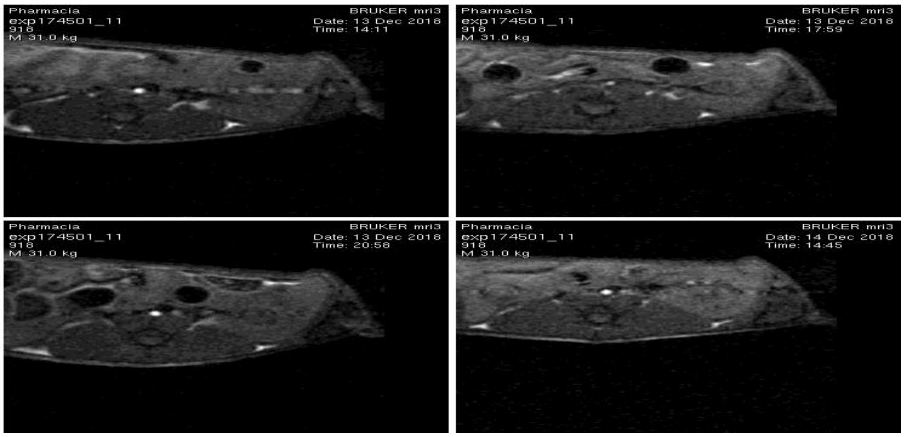

TUMOR		Axial		SI Ratio
N 9		**tumor**	**muscle**	
Lip SLX	**Pre**	4.7	5.43	0.866
	3hrs	5.5	6.26	0.87
	6 hrs	4.75	6.26	0.76
	24 hrs	5.0	6.07	0.82
% SI increase				NC

Table 20: N 9 MRI Axial scan of the tumor at Pre-treatment, 3 hrs, 6 hrs, and 24 hrs. The signaling intensity of the tumor was normalized against SI of muscle tissue in each scan. There was no significant change in signal intensity at 24hrs versus Pre-Treatment.

In N 9**, there was higher accumulation of SLX-liposome in the Liver (50.5%%) versus Tumor (NC)**

Group 3:Liposome-Sialyl Lewis X, N = 4 mice, [N 9, **N 10**, N 11, N 12]

N 10-Liver

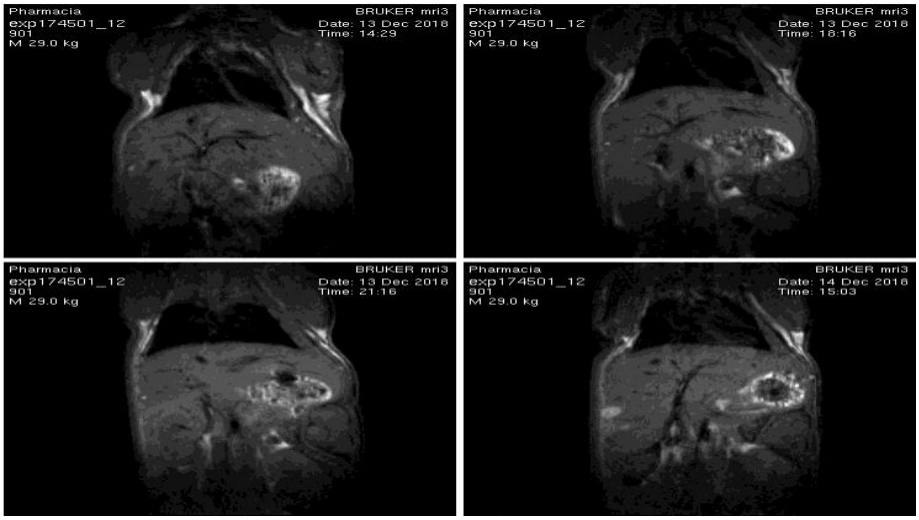

LIVER		CORONAL		SI Ratio
N 10		**LIVER**	**muscle**	
Lip SLX	**Pre**	2.15	1.46	1.47
	3hrs	2.16	1.27	1.7
	6 hrs	2.21	1.19	1.86*
	24 hrs	1.79	1.0	1.79
% SI increase				26.5%

Table 21: N 10 MRI Coronal scan of the liver at Pre-treatment, 3 hrs, 6 hrs, and 24hrs. The signaling intensity of the liver was normalized against SI of muscle tissue in each scan. The highest SI increase was noted at 6 hrs and 24 hrs. Signal intensity increased by 26.5% at 6hrs versus Pre-Treatment.

N 10 -Tumor

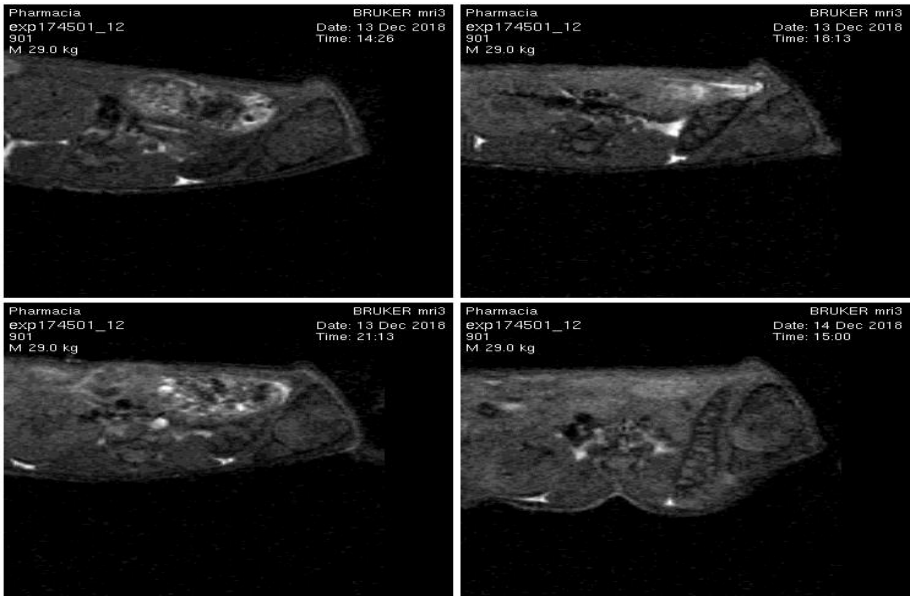

TUMOR		Axial		SI Ratio
N 10		tumor	muscle	
Lip SLX	Pre	6.87	6.32	1.09
	3hrs	5.76	5.56	1.04
	6 hrs	6.83	6.46	1.06
	24 hrs	6.2	6.39	0.97
% SI increase				NC

Table 22: N 10 MRI Axial scan of the tumor at Pre-treatment, 3 hrs, 6 hrs, and 24 hrs. The signaling intensity of the tumor was normalized against SI of muscle tissue in each scan. There was no significant change in signal intensity at 24hrs versus Pre-Treatment.

In N 10**, there was higher accumulation of SLX-liposome in the Liver (26.5%) versus Tumor (NC)**

Group 3:Liposome-Sialyl Lewis X, N = 4 mice, [N 9, N 10, **N 11**, N 12]

N 11-Liver

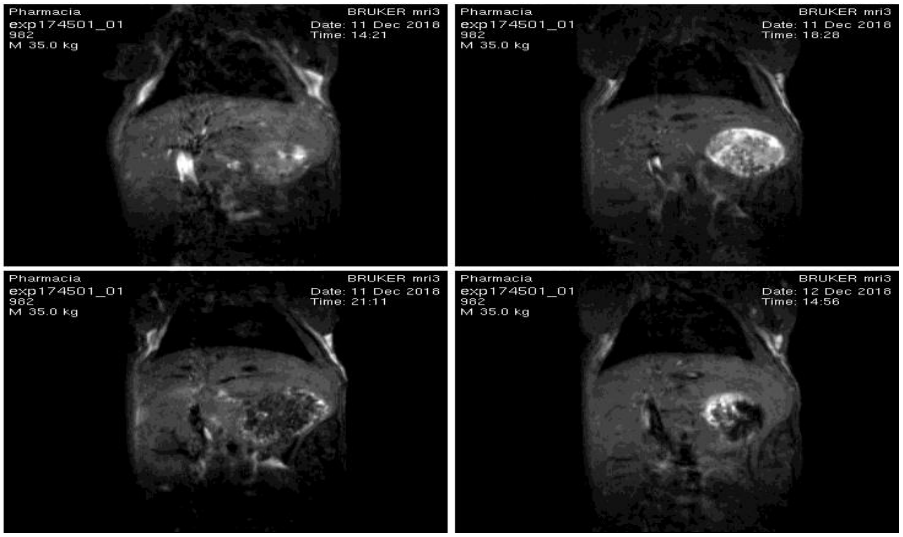

LIVER		**Coronal**		**SI Ratio**
N 11		**Liver**	**muscle**	
Lip SLX	**Pre**	2.01	1.43	1.4
	3hrs	1.95	1.26	1.55
	6 hrs	2.14	1.35	1.59
	24 hrs	2.2	1.09	2.02
% SI increase				44.29%

Table 23: N 11 MRI Coronal scan of the liver at Pre-treatment, 3 hrs, 6 hrs, and 24hrs. The signaling intensity of the liver was normalized against SI of muscle tissue in each scan. The highest SI increase was noted at 24 hrs. Signal intensity increased by 44.29% at 24hrs versus Pre-Treatment.

N 11-Tumor

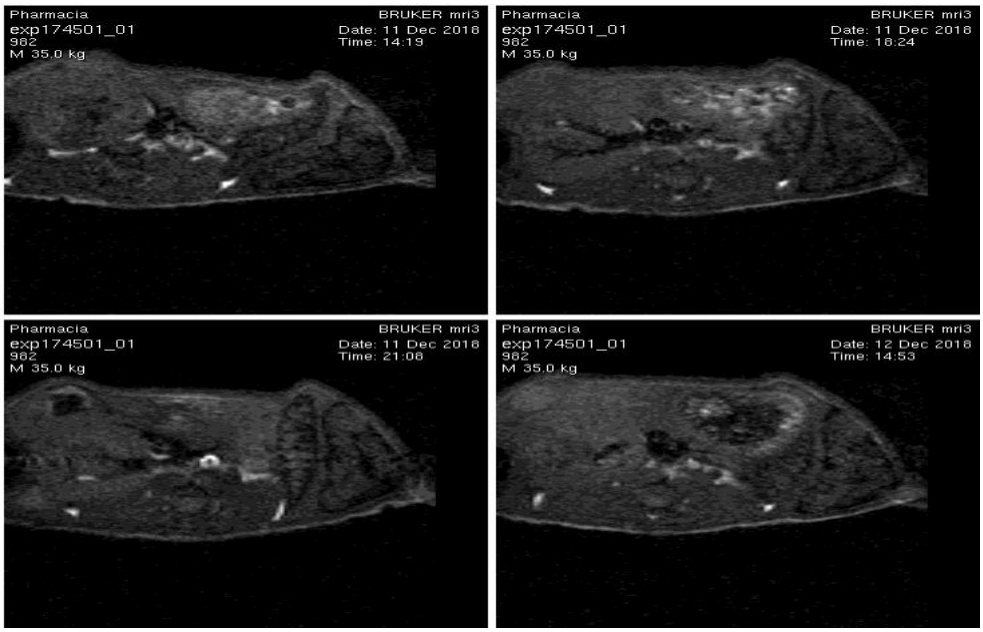

TUMOR		Axial		SI Ratio
N 11		tumor	muscle	
Lip SLX	Pre	4.59	4.13	1.11
	3hrs	4.98	5.67	0.88
	6 hrs	5.98	5.32	1.12
	24 hrs	5.75	5.93	0.97
% SI increase				NC

Table 24: N 11 MRI Axial scan of the tumor at Pre-treatment, 3 hrs, 6 hrs, and 24 hrs. The signaling intensity of the tumor was normalized against SI of muscle tissue in each scan. There was no significant change in signal intensity at 24hrs versus Pre-Treatment.

In N 11**, there was higher accumulation of SLX-liposome in the Liver (44.3%) versus Tumor (NC)**

Group 3:Liposome-Sialyl Lewis X, N = 4 mice, [N 9, N 10, N 11, **N 12**]

N 12-Liver

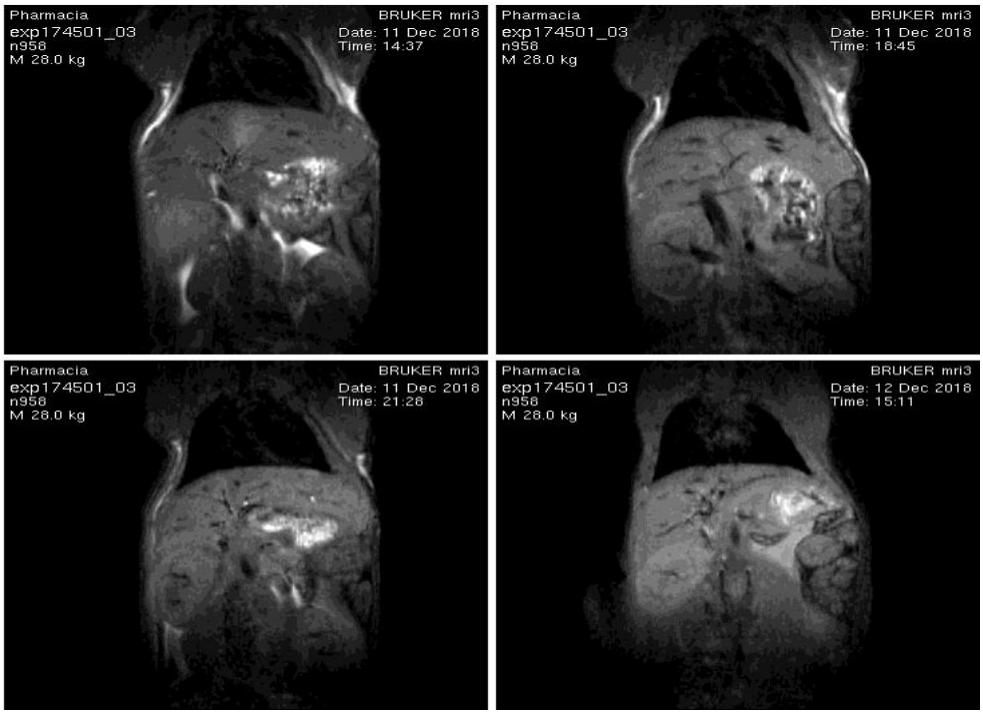

LIVER		**CORONAL**		**SI Ratio**
N 12		**LIVER**	**muscle**	
Lip SLX	**Pre**	2.02	1.15	1.76
	3 hrs	2.28	1.26	1.81
	6 hrs	2.44	1	2.44
	24 hrs	2.84	1.18	2.41
% SI increase				36.9%

Table 25: N 12 MRI Coronal scan of the liver at Pre-treatment, 3 hrs, 6 hrs, and 24hrs. The signaling intensity of the liver was normalized against SI of muscle tissue in each scan. The highest SI increase were noted at 6 hrs and 24 hrs. Signal intensity increased by 36.9% at 24hrs versus Pre-Treatment.

N 12-Tumor

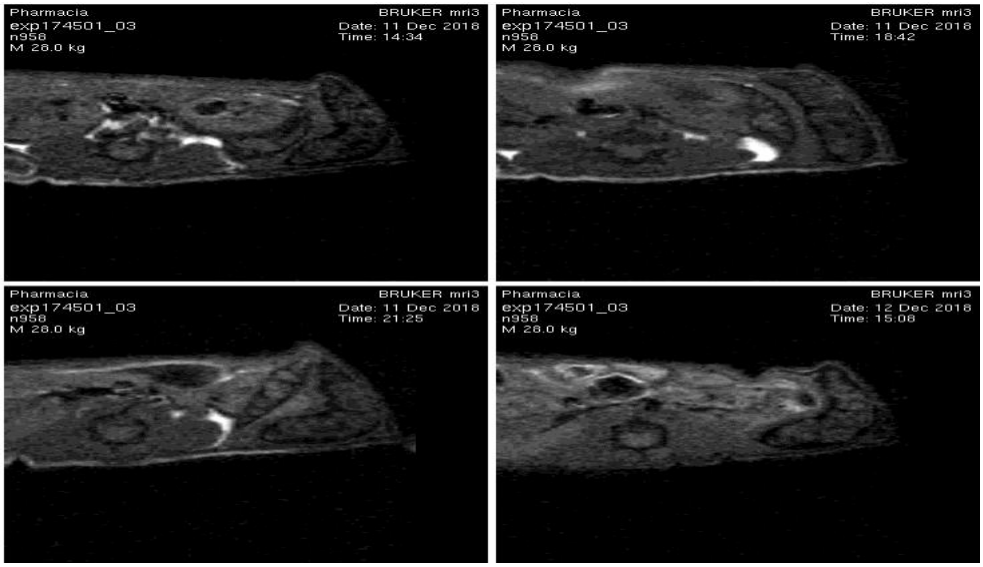

TUMOR		Axial		SI Ratio
N 12		tumor	muscle	
Lip SLX	Pre	5.07	6.24	0.81
	3 hrs	6.07	6.85	0.89
	6 hrs	6.01	7.16	0.85
	24 hrs	6.96	7	0.99
	48 hrs	6.59	8.15	0.81
% SI increase				22.2%

Table 26: N 12 MRI Axial scan of the tumor at Pre-treatment, 3 hrs, 6 hrs,, 24 hrs, and 48hrs. The signaling intensity of the tumor was normalized against SI of muscle tissue in each scan. The highest SI increase was noted at 24 hrs. Signal intensity increased by 22.2% at 24hrs versus Pre-Treatment. At 48hrs, the SLX-liposomes were cleared out.

In N 12**, there was higher accumulation of SLX-liposome in the Liver (36.9%) versus Tumor (22.2%)**

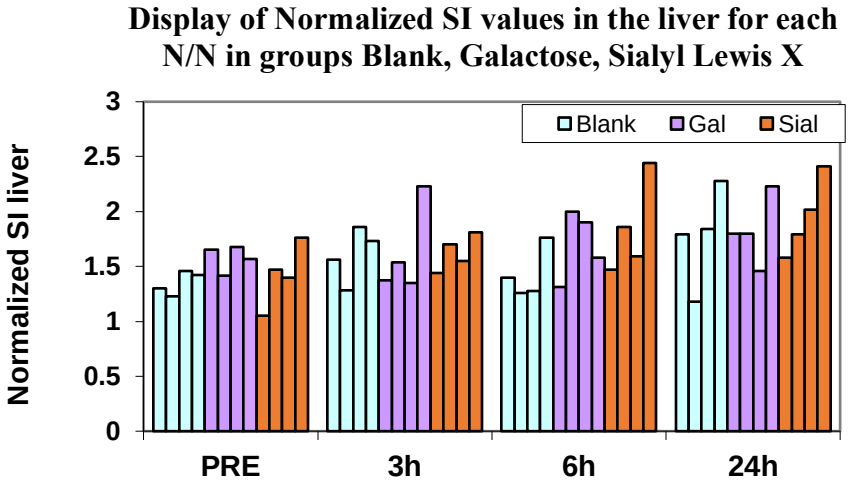

Figure17: Normalized MRI signal intensity values in the Liver of each N/N (n=12) separated into 3 groups (n=4): 1) Lip-Blank (blue), 2) Lip-Galactose (purple), and Lip-Sialyl Lewis X (orange) at Pre-treatment, 3 hrs, 6 hrs, and 24hrs.

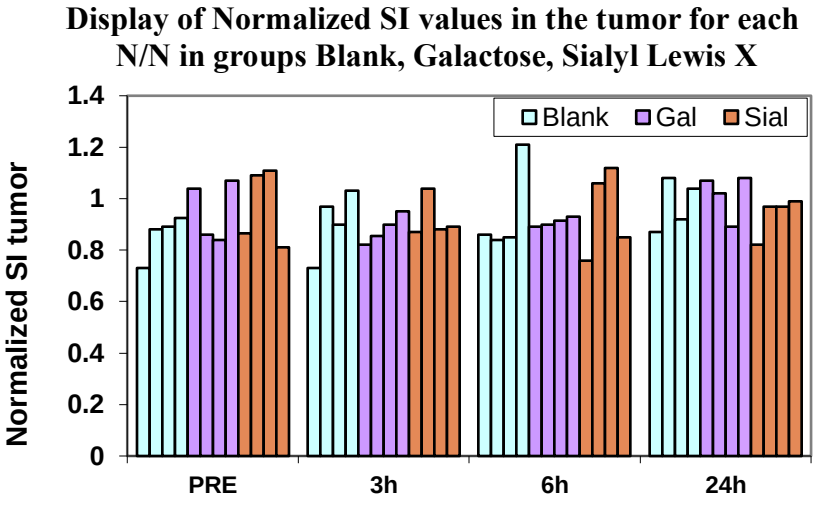

Figure18: Normalized MRI signal intensity values in the tumor

of each N/N (n=12) separated into 3 groups (n=4): 1) Lip-Blank (blue), 2) Lip-Galactose (purple), and Lip-Sialyl Lewis X (orange) at Pre-treatment, 3 hrs, 6 hrs, and 24hrs.

Average of Normalized MRI signal intensities Per Liposome Group

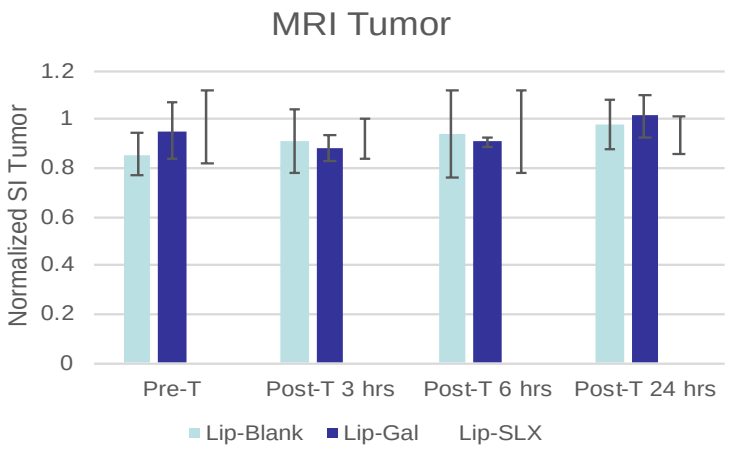

Figure19: The average of Normalized MRI signal intensity values in the tumor of 3 groups (n=4): 1) Lip-Blank (blue), 2) Lip-Galactose (purple), and Lip-Sialyl Lewis X (orange) at Pre-treatment, 3 hrs, 6 hrs, and 24hrs.

$$\%\ SI\ Increase = \frac{Avg\ SI\ 24\ hrs\ Pos\_T - Avg\ SI\ Pre\_T}{Avg\ SI\ Pre\_T} \text{ X } 100$$

AVG	Lip-Blank	Lip-Gal	Lip-SLX
% Inc Tumor	14.13%	6.56%	NC

Table 27: Percent increase of the average of Normalized MRI signal intensity values in the tumor of 3 groups (n=4): 1) Lip-Blank, 2) Lip-Galactos, and Lip-Sialyl Lewis X.

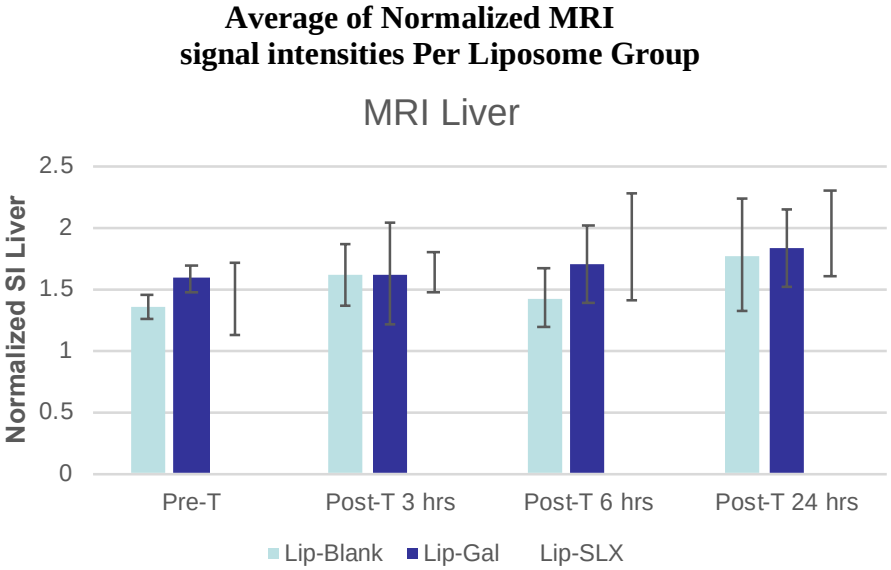

Figure20: The average of Normalized MRI signal intensity values in the Liver of 3 groups (n=4): 1) Lip-Blank (blue), 2) Lip-Galactose (purple), and Lip-Sialyl Lewis X (orange) at Pre-treatment, 3 hrs, 6 hrs, and 24hrs.

$$\%\ SI\ Increase = \frac{Avg\ SI\ 24\ hrs\ Pos\_T - Avg\ SI\ Pre\_T}{Avg\ SI\ Pre\_T} \text{ X } 100$$

AVG	Lip-Blank	Lip-Gal	Lip-SLX
% Inc Liver	31.11%	15.19%	37.32%

Table 28: Percent increase of the average of Normalized MRI signal intensity values in the Liver of 3 groups (n=4): 1) Lip-Blank, 2) Lip-Galactos, and Lip-Sialyl Lewis X.

Discussion

Gadolinium was successfully incorporated into the lipid bilayer of the liposome at 0.12mM concentration as displayed by the MRI in-vitro test **(*Figure 12-14*),** making Gd-encapsulated liposomes an effective diagnostic tool. It was then possible to analyze the biodistribution of liposomes in-vivo Pre-Treatment and Post-injection with liposomes (Blank- Galactose- Sialyl Lewis X) via Magnetic Resonance Imaging (MRI). The discrepancy in growth of HCC tumor in ectopically inoculated mice, as well as the variability of tumor sizes as displayed in tables 1 and 2 lead to the design of a biodistribution experiment with smaller groups (n=4), which made drawing a concrete conclusion on the effect of targeting challenging.

MRI allows for the analysis of biodistribution using the pre-treatment condition as the baseline (control) against post-treatment scanning, thus making each in-vivo scan an entire case study. Tables 3-26 display all 12 N/N divided into 3 groups (n=4 per group) to test the biodistribution of: 1) Liposome-Blank, 2) Lip-Galactose, 3) Lip- Sialyl Lewis X at time points: Pre-treatment and Post-treatment (3 hrs, 6 hrs, 24 hrs). MRI scanning was conducted in two areas, 1) the Liver, 2) the ectopic hepatocellular carcinoma inoculated tumor. Additional randomly selected mice were scanned at the 1 hour and 48 hours time-points to evaluate the half-life of the injected liposome

and the peak of accumulation. At each MRI scan, the signal intensity value (Liver/Tumor) was normalized versus the SI value of a selected muscle of the same scan. As displayed in the previous section, the following results were attained for each category of liposomes:

Blank Liposome N (1, 2, 3, 4)

- In N 1, there was higher accumulation of Blank liposome in the Liver (38.1%) versus Tumor (19.2%).
- In N 2, there was higher accumulation of Blank Liposome in the Tumor (22.7%) versus no accumulation in the Liver.
- In N 3, there was higher accumulation of Blank liposome in the Liver (26%) versus Tumor (3.25%).
- In N 4, there was higher accumulation of Blank liposome in the Liver (60.6%) versus Tumor (12.4%).

Liposome – Galactose N (5, 6, 7, 8)

- In N 5 , here was higher accumulation of Galactose-liposome in the Liver (9.1%) versus Tumor (2.9%).
- In N 6, there was higher accumulation of Galactose-liposome in the Liver (27.2%) versus Tumor (18.6%).
- In N 7 there was higher accumulation of Galactose-liposome in the Liver (13.1%) versus Tumor (8.9%).
- In N 8, there was higher accumulation of Galactose-liposome in the Liver (42%) versus Tumor (1%).

Liposome - Sialyl Lewis X N (9, 10, 11, 12)

- In N 9, there was higher accumulation of SLX-liposome in the Liver (50.5%%) versus Tumor (NC)
- In N 10, there was higher accumulation of SLX-liposome in the Liver (26.5%%) versus Tumor (NC)
- In N 11, there was higher accumulation of SLX-liposome in the Liver (44.3%) versus Tumor (NC)
- In N 12, there was higher accumulation of SLX-liposome in the Liver (36.9%) versus Tumor (22.2%)

Based on individual N analysis (n=4 per group), it was noted that:

1- Peak of accumulation

The 24 hours MRI scan displayed the highest accumulation of Gd-encapsulated liposomes, and can therefore be considered the ideal time-point for the analysis of biodistribution. Hence, it was the reference point for the calculation of percent increase in signal intensity over time.

2- Clearance

The 1 hour and 48 hours scans were analyzed to determine the half-life and clearance of the liposomes. Results have shown that at 1 hour no accumulation was noted, and at 48 hours the liposomes were 100% cleared out consistently in all scans.

3- Targeting

First, efficient targeting to HCC versus normal liver tissues in hepatocellular carcinoma patients remains a challenge[124].

To better evaluate the targeting efficiency, Ectopically inoculated Hepatocellular carcinoma (HCC) were grown distant from the liver *(injection below the left rib as displayed in figure 15)*, and MRI scans of the liver and ectopic tumor were evaluated separately. This strategy gave clear indications of specific targeting of galactose or Sialyl Lewis X moieties to either normal liver tissue or HCC tumor.

The first targeting strategy was based on the use of Galactosylated liposomes specific for Asialoglycoprotein receptors (ASGPR), found predominantly on hepatocytes and HCC cells, and nearly non-existent in non-hepatic cells[125].

In this study, galactose-liposomes were tested on a group (n=4) of HCC inoculated mice. The results showed a higher accumulation of galactose-liposomes in normal hepatic tissue versus HCC tissues. This finding has been confirmed by other studies that tested various galactoside derivatives to achieve higher specificity in targeting ASGPRs in HCC versus normal hepatic tissues. The challenge remains in the absence of an ASGPR oligomer crystal structure to optimize the design of the galactoside ligand. The research direction in targeting these receptors thus far has been focused on the design of multivalent

[124] Huang, K. W., Lai, Y. T., Chern, G. J., Huang, S. F., Tsai, C. L., Sung, Y. C., Shiue, T. Y. Galactose derivative-modified nanoparticles for efficient siRNA delivery to hepatocellular carcinoma. *Biomacromolecules*, **2018,** *19*(6), 2330-2339.

[125] D'Souza, A., Devarajan, P. V. Asialoglycoprotein receptor mediated hepatocyte targeting - strategies and applications. J. Controlled Release 2015, 203, 126−39.

entities, galactoside/aromatic moieties, incorporated on the surface of modified nanoparticles, following a trial and error approach[126]. For example, to improve the affinity of glycan ligands to ASGPR, Finn and Mascitti groups have modified galactosides with various moieties on C-1,C-2,C-5, and C-6 [127].

In this case, the uptake of the Glactose-liposome designed in our lab did not favor targeting the ectopic HCC versus normal Hepatic tissue.

The second targeting strategy was based on the use of Sialyl Lewis C tetrasaccharide-Liposome specific for selectin binding. Selectins are among the initial adhesion molecules which mediate transendothelial migration of leukocytes. They are expressed by leukocytes and endothelial cells in the liver and overexpressed upon inflammation triggered by HCC microenvironment [128]. Therefore, the therapeutic potential of polymer-based selectin binders for the treatment of liver disease has been a great attraction.

Sialyl Lewis X tetrasaccharide is the common structural binding motive for selectins. In this study, SLX was functionalized on the outer surface of liposomes to test its targeting ability in HCC.

---

[126] Zhu, L.; Mahato, R. I. Targeted delivery of siRNA to hepatocytes and hepatic stellate cells by bioconjugation. Bioconjugate Chem. 2010, 21 (11), 2119−27.

[127] Mamidyala, S. K.; Dutta, S.; Chrunyk, B. A.; Preville, C.; Wang, H.; Withka, J. M.; McColl, A.; Subashi, T. A.; Hawrylik, S. J.; Griffor, M. C.; Kim, S.; Pfefferkorn, J. A.; Price, D. A.; Menhaji-Klotz, E.; Mascitti, V.; Finn, M. G. Glycomimetic ligands for the human asialoglycoprotein receptor. J. Am. Chem. Soc. 2012, 134 (4), 1978−81.

[128] McEver, R. P. Selectins: Initiators of Leucocyte Adhesion and Signalling at the Vascular WallCardiovasc. Res. 2015, 107, 331– 9

A study conducted by Tacke et al. demonstrated a similar strategy with compelling evidence that carbohydrate-based selectin-binding polymers (amongst which SLX was tested) accumulate in the liver and impact the inflammatory response. However, the smallest variations in the composition of the SLX-polymers determined the efficacy or toxicity of these compounds in vivo[129].

In our study, the results demonstrated a significantly higher accumulation of the SLX liposomes in the normal hepatic tissue versus in HCC tissue.

Last, a study conducted by Harashima et al. elaborated on the enhanced hepatic uptake of liposomes through opsonic activity versus compliment receptor activation. The evidence show that liposomes were taken up by the liver depending on the extent of opsonization which was directly proportional to the size of the liposomes (larger liposome ~800nm correlated with higher opsonization)[130].

Conclusion

Based on the vitro study using HepG2 cell line, the liposomes displayed an increase in uptake over 24 hours. Liposomes functionalized with Sialyl Lewis X tetrasaccharide demonstrated the highest uptake, followed by Galactose-liposomes, then Blank Liposomes. Based on these results, 60 mice were

[129] Bartneck, M., Schlößer, C. T., Barz, M., Zentel, R., Trautwein, C., Lammers, T., & Tacke, F. Immunomodulatory therapy of inflammatory liver disease using selectin-binding glycopolymers. *ACS nano*, 2017, *11*(10), 9689-9700.

[130] Harashima, H., Sakata, K., Funato, K., & Kiwada, H. Enhanced hepatic uptake of liposomes through complement activation depending on the size of liposomes. *Pharmaceutical research*, *11*(3), 402-406.

inoculated ectopically with HepG2, and the biodistribution of Gd-encapsulated liposomes (Blank, Galactose, Sialyl Lewis X) was studies at 1 hour, 3 hours, 6 hours, 24 hours, and 48 hours post-treatment via MRI.
The MRI results corresponded with the in-vitro FACS results, and the highest accumulation of liposomes was noted at the 24 hours' time-point.
The pre-treatment MRI scans are used as a control to evaluate the signal intensity post-treatment, thus validating the Gd-encapsulated liposomes as a reliable diagnostic tool.
The results displayed higher accumulation of liposomes (Blank, Galactose, Sialyl Lewis X) to the hepatic tissue versus the HCC ectopic tissue.
There could be many factors attributing to such results:

1- Opsonization effect
2- Hepatic Clearance
3- Glycans used require further modifications for specific targeting of HCC (multivalency, cluster effect, glycan-derivatives, etc)

Recommendations for Future experiments:

Hepatocellular carcinoma is a complex experimental setting with only 1 FDA approved first line defense medication (Sorafenib) to this day.
It has been previously tested by Nerviano Medical Sciences in extensive in-vivo studies that lead to non-concrete results due to the following obstacles:

1- Inoculation

According to the literature, HepG2 has been the most widely used HCC cell line but it does have a hemorrhagic property that hinders the quality of MRI scans.

2- Variability

- The discrepancy in tumor size/growth time tends to be difficult to control, making it harder to advance in larger (n) per group (Experiments were initially designed to be n= 8 per group for thorough analysis)

3- Biodistribution

- The peak time of biodistribution was determined to be at 24 hours in all 3 groups tested after extensive MRI scanning at pre-treatment/post treatment at 1hr, 3hrs, 6hrs, 24hrs, 48hrs.

*This information varies depending on the composition and size of the liposome.

Future studies should build off of this information and attempt to execute the experiment over a minimum of 6 months period. With a tumor growth ratio of 20% of mice population, the experiment should be executed in 4 stages with a larger (n) population. MRI scans can be collected in cycles following the tumor growth schedule as indicated in tables 1 and 2.

Conclusion

This project was based on the pivotal role of carbohydrates in biological functions and their potential applications in drug design and crossing biological barriers. In this study, an easy and efficient way was designed to functionalize liposomes with simple and complex glycans (commercial deprotected sugars). Novel characterization methods adapted to the glycofunctionalized liposomes that promote the use of newer instruments such as nanosight as well as modified traditional methods such as the Phenol-

Sulfuric Assay were optimized. As a first in-vitro application, liposomes functionalized with glucose and mannose were tested for cell uptake and cell toxicity using macrophages RAW 264.7 via Operetta. Second, liposomes encapsulated with DSPE- Gadolinium and functionalized with galactose and Sialyl Lewis X tetrasaccharide were tested in-vitro for HepG2 cell uptake (FACS) and in-vivo for targeted biodistribution using MRI. The outcome of this study is the development of a 3D glycomodel variable, efficient, and user-friendly compatible with different types of commercial deprotected sugars.. Additionally, the glycomodel was optimized to become a theranostic tool capable of encapsulating contrast agents such as DSPE-Gd, in addition to hydrophobic insoluble drugs, with added targeting property of the selected glycan functionalized on the outer surface of the liposome. Therefore, offering a complete glycomodel for a multitude of applications in biological and pharmaceutical studies.

Communications

- **XXXVIII National conference of the organic chemistry division of the Italian chemical society- University of Milan**

  09/09/2018 – 13/09/2018 ***Poster Presentation***

- **Biobarriers 2018: 12th international conference and workshop on biological barriers (University of Saarbrucken, Germany)**

25/08/ 2018 – 30/08/2018 ***Oral and Poster Presentations***

- **XII Spanish-Portuguese Conference on controlled Drug Delivery (University of Coimbra, Portugal)**

  14/01/2018 – 19/01/2018 ***Poster Presentation***

- **Nanoinnovation 2017 Conference and Exhibition**

  26/09/2017 – 29/09/2017 ***Poster Presentation***

- **NABBA 2nd Scientific and complementary training meeting**
  Erice, Sicily (Center of Scientific Culture Ettore Majorana)

  06/06/2016 – 10/06/2016 Network Presentation

- **NABBA 1st Scientific and complementary training meeting Gif-sur-Yvette (University of Paris Sud)**

  25/11/2015-27/11/2015 *Network Presentation*

- **BtBs Day UNIMIB** 15/12/2015 Poster Presentation

- **BtBs Day UNIMIB** 13/12/2017 Poster Presentation

- **BtBs Day UNIMIB** 21/11/2018 Poster Presentation

- **Doctorate Day Chemistry, Geology, and environmental Sciences**
  18/05/2018 Poster Presentation.

Coursework Certifications

- **Scanning and Transmission electron microscopy, principles and applications** (22/05/2018)
- **Introduction to Photochemistry** (18/06/2018)
- **HorizonChem2018 Workshop** (06/03/2018)
- **Operetta CLS Basic Training** (25/10/2017)
- **Chemistry and Nanomedicine** (05/10/2016)

Interdisciplinary Coursework

- Productivity Tools for young Researchers
- Surfing the academic job market: how to publish in high impact international journals.

Secondment

Nerviano Medical Sciences 25/09/2018 – 25/12/2018

Publication

Mattia Vacchini, Rana Edwards, Roberto Guizzardi, Alessandro Palmioli, Carlotta Ciaramelli, Alice Paiotta, Cristina Airoldi, Barbara La Ferla and Laura Cipolla*, "Glycan Carriers As Glycotools For Medicinal Chemistry Applications", Current Medicinal Chemistry (2019) 26:1